The Pennsylvania State University
The Graduate School

THE CONVECTIVE BOUNDARY LAYER IN THE AMAZON RAINFOREST

A Thesis in
Meteorology
by
Vanessa C. Monteiro

Submitted in Partial Fulfillment
of the Requirements
for the Degree of

Master of Science

December 2018

The thesis of Vanessa C. Monteiro was reviewed and approved* by the following:

Jose D. Fuentes
Professor of Meteorology
Thesis Advisor

Gregory S. Jenkins
Professor of Meteorology

Jerry Y. Harrington
Professor of Meteorology

David J. Stensrud
Professor of Meteorology
Head of the Department of Meteorology and Atmospheric Science

*Signatures are on file in the Graduate School.

Abstract

Among all the interactions in nature - between water, soil, atmosphere, and living beings - this work will be focused on quantifying a very specific one: the thermodynamics of the convective boundary layer preceding and following the passage of mesoscale convective systems (MCSs) in the Amazon rainforest. Over the Amazon basin, the warm and moist conditions favor the formation of mesoscale convective systems, which are constantly modifying the atmospheric features, such as the thermodynamics (e.g., temperature and humidity) and dynamics (e.g., wind shear). Then, the objectives of this work are: quantify the thermodynamic features of the convective boundary layer (e.g., temperature, humidity, convective available potential energy, and energy fluxes) before and after the passage of mesoscale convective systems over the Amazon rainforest; determine the convective boundary layer growth rates before and after such events (MCSs); and, determine the mixed-layer depth using a numerical model. Using the data set provided by the most recent experiment - GoAmazon 2014/15 - this study will address its objectives through the evaluation of case studies and an ensemble of days when there was the passage of mesoscale convective systems. The variables evaluated, such as equivalent potential temperature, specific humidity, and energy fluxes are estimated based on the surface measurements, and the convective boundary layer depth is estimated using the virtual potential temperature profile, obtained from the soundings launched during the experiment. The results show that the convective boundary layer experiences reductions in the equivalent potential temperature within 2 to 8 K and in the specific humidity up to 2 g/kg after the passage of a MCS, due to the cold and dry air brought to the surface by storms downdrafts. These two variables in addition to others (e.g., energy fluxes) are responsible for the low growth rates of the convective boundary layer, that were reduced by 100 m h^{-1} in the following two hours after the rainfall ceases - when compared to undisturbed conditions. Also, the mixed-layer model applied to predict the convective boundary layer growth during disturbed conditions showed a poor performance, that can be linked to the absence of the dynamic features that impact the CBL growth, such as subsidence. Nonetheless, this work provides a better quantitative evaluation of the thermodynamic features of the convective boundary layer under the passage of mesoscale convective systems in the Amazon rainforest, and proposes a set of different perspectives for future studies.

Table of Contents

Chapter 3

Why does it matter?   **45**

Appendix A

Complementary equations   **55**

Appendix B

Complementary case studies   **57**

Appendix C

The performance of exponential and hyperbolic models of wind speed profile within an Amazon forest canopy   **64**

Bibliography   **73**

List of Figures

List of Tables

Acknowledgments

"Orbiting this [...] is an utterly insignificant little blue-green planet whose ape-descended life forms are so amazingly primitive that they still think digital watches are a pretty neat idea.
This planet has - or rather had - a problem, which was this: most of the people living on it were unhappy for pretty much all the time. Many solutions were suggested for this problem, but most of these were largely concerned with the movements of small green pieces of paper, which is odd because on the whole it wasn't the small green pieces of paper that were unhappy."

- Hitchhiker's Guide to the Galaxy – Douglas Adams

Chapter 1

Atmospheric features in the Amazon rainforest

1.1 Introduction to the Amazon rainforest and its atmosphere

The Amazon rainforest is a unique place in the world hiding many mysteries and, sometimes, it is considered a mystical place. And there are many reasons for that. The Amazon rainforest is the largest tropical forest in the world, and has more than 2,500 animal species among mammals, birds, reptiles and amphibians, 40,000 plants species, and up to 128,840 invertebrates, only in the Brazilian Amazon, according to data from World Wildlife Fund (WWF-Brasil) [1]. Due to its diversity and size, we still do not know all the secrets hidden in such an ecosystem (Figure 1.1).

Figure 1.1: Amazon - trees, clouds, amphibians, snakes, birds, and insects: a sample of the jungle. Pictures taken during the GoAmazon 14/2015 from personal archive.

---

[1] https://www.wwf.org.br/natureza_brasileira/areas_prioritarias/amazonia1/bioma_amazonia/

The Amazon rainforest has an important role in climate regulation due to its complex interaction among forest, water resources, and the atmosphere. In simple words, the forest transports the water from the soil and groundwater to the atmosphere through the evapotranspiration. It brings humidity to the air and allows the formation of clouds. In the sequence, it rains and the rivers will be supplied with water. And the processes keep going. It sounds very simple, but there are many details to be explored in each one of these interactions.

Focusing on the atmospheric processes there are many research possibilities, and the ongoing of science allowed scientists to discover many important interactions, processes, and features of the atmosphere. For example, having a little background in cloud formation, one can ask: if the Amazon rainforest has a pristine atmosphere, similar to the ocean's atmosphere (Roberts et al., 2001) - free of pollutants, what are the drivers to produce such amount of precipitation over this region? And where does the cloud condensation nuclei (CCN) come from? And this is one question that has been largely studied. A study from 1997 (Andreae and Crutzen, 1997), explores the importance of understanding and quantifying atmospheric aerosols, and highlight how variable the concentration of biogenic hydrocarbons, as isoprenes and terpenes, are in space and time. These compounds, the BVOCs (biogenic volatile organic compounds), are largely emitted by trees in the Amazon, and the secondary aerosols formed by oxidation will serve as cloud condensation nuclei, leading to cloud formation. Also, as presented by Martin et al. (2010) in an article review, the Amazon basin has the influence of additional sources of atmospheric aerosols. Long-range sources, relevant during the wet season, are the Atlantic ocean (sea spray and sulfate) and the Saharan desert (mineral dust). Also, biomass burning emission, either natural and anthropogenic, added to southern and eastern Brazil and South America countries contribute to the aerosol composition of the Amazon basin atmosphere (Martin et al., 2010). In addition, the contribution of anthropogenic pollutants to cloud formation are being questioned, (e.g., Roberts et al., 2001; Martin et al., 2010), and being investigated in the GoAmazon 2014/15 experiment (Martin et al., 2017).

Another relevant finding is the biotic pump (Poveda et al., 2014), which helps to explain the large amount of precipitation over the forest. The biotic pump is a mechanism that works as following: the amount of precipitation over the forest is higher compared to the precipitation over the Atlantic Ocean; so the atmospheric pressure over the forest is lower than over the ocean, which makes the wind blows from the ocean to the forest, and as a consequence, there will be even more moisture in the forest atmosphere. It also reinforces the fact that the predominant winds in the Amazon basin blow from east to west. Also, studying a little about Amazon's geography, one will see that the forest is limited by the Andes, which is one more contributor to make the clouds rain over the forest.

Besides the atmospheric composition and cloud formation, there is also the precipitation itself. Rainfall is a remarkable characteristic of the Amazon basin for its large total annual accumulated precipitation. Different types of storms (e.g., mesoscale convective systems and unorganized systems), lead to different atmospheric thermodynamic and dynamic conditions, impacting the atmospheric boundary layer (the layer of the atmosphere closest to the surface), and also in the weather regulation, and society (e.g., flooding event).

Studying the precipitation processes within the atmospheric boundary layer (ABL) is a more specific subject that can lead to research on atmospheric thermodynamics, among others as atmospheric chemistry

and turbulence. The ABL is the region closest to the Earth's surface and it will be explored in this document with more details and within the Amazon rainforest context.

Why to study the Atmospheric Boundary Layer (ABL)?

People are interested in the atmospheric boundary layer because it is the part of the atmosphere where pollutants dispersion, mixing, deposition occurs; where the interaction between Earth's surface and the atmosphere happens - where there is turbulence; is the layer of air we directly breathe.

The mean atmospheric boundary layer (ABL) grows from the surface to up to 3 km, and within this layer, many important processes are happening simultaneously. Regarding the thermodynamic processes, the ABL is where part of the solar radiation is absorbed by the ground, for example, and emitted back to the atmosphere in the form of longwave radiation. It keeps the surface warm during the day, with a characteristic adiabatic virtual potential temperature profile. Overnight the ABL stops receiving solar radiation but keeps emitting longwave radiation, cooling down this layer. All the vegetation is within the ABL and it is responsible for important gas exchanges and for evapotranspiration, also being a crucial component in terms of land-surface cover, altering the surface albedo. Biogenic volatile organic compounds are emitted by vegetation and interact in the ABL as part of the cloud condensation nuclei, for example. The evapotranspiration drives the amount of water vapor present in the atmosphere. In addition, there is the photosynthesis which is important for carbon sequestration. Health concerns are also associated with air quality and linked to the atmospheric boundary layer. The ABL can keep the pollutants trapped in the layers close to the surface, degrading the safe conditions for human health. Along with these few examples, the turbulent transport in the ABL is one of the most distinguished characteristics of this layer, being responsible for the transport of water vapor, oxygen, aerosols, particles, pollutants from the surface to the free atmosphere and vice versa. The turbulence is a remarkable process in the ABL because it is generated from the interactions between atmosphere and land-surface, through solar heating, frictional drag, and obstacles, for example (Stull, 1988).

Then, the study of the ABL is integrated with multiple variables, including human actions. There are all the interactions between all the life's forms and its role in the atmospheric motion; which makes the ABL such an important, interesting and complicated subject of study.

What is different in the Amazon rainforest's ABL?

As seen briefly above, the ABL is driven by several forcings that under the context of the specific characteristics (e.g., surface cover, high humidity and temperature) of a tropical forest will change the mean characteristics of this layer. First, the Amazon rainforest is covered by tall trees - 35 meters or even more -, the humidity is high - which can change how fast the ABL can grow -, the Amazon's sky is usually covered by clouds - which reduces the amount of radiation at the surface, also decreasing the ABL

growth rates -, and there is a frequent passage of storms - which keep changing the whole structure of the ABL. So, to have a full understanding of atmospheric processes, it is necessary to know the behavior of the ABL, which includes knowing how the atmospheric thermodynamic, and also dynamic, evolves over the day in different conditions in the Amazon.

But, a lot is already known about the ABL in the Amazon rainforest. Many experiments were conducted to explore as many as possible features of this environment. Since 1980's, when the first experiment related to the Amazon ABL started, scientists are interested in land-atmosphere interactions and cloud formation (e.g., Martin et al., 1988; Dias et al., 2002; Betts and Jakob, 2002; Betts and Viterbo, 2005; Strong et al., 2005; Fitzjarrald et al., 1990; Fuentes et al., 2016), deforestation impacts on atmospheric processes (e.g., Gash and Nobre, 1997; Wang et al., 2009; Nobre et al., 1991), in different seasons (e.g., Betts et al., 2002a; Harriss et al., 1990), and different surfaces (e.g., Fisch et al., 2004), the atmospheric chemistry (e.g., Culf et al., 1997; Zimmerman et al., 1988; Betts et al., 2002c), and large-scale processes (e.g., Betts et al., 2009a; Fu et al., 1999).

Despite that, there are still many details not well explored yet. Then, a new experiment was set up in 2014 and 2015, the GoAmazon (Green Ocean Amazon) experiment (Martin et al., 2017) to measure meteorological variables at the surface and the atmospheric column (e.g., temperature, relative humidity, air pressure, wind speed), and chemicals mixing ratios, e.g., ozone, isoprene, monoterpenes, to help to understand better the cloud formation in pristine and polluted environments. Since this experiment started, many results were already reported, in atmospheric chemistry and aerosol particles (e.g., Liu et al., 2018; Fraund et al., 2017; Sá et al., 2017; Gu et al., 2017; Freire et al., 2017; Thalman et al., 2017; Cecchini et al., 2017; Fuentes et al., 2016; Pöhlker et al., 2016; Martin et al., 2017; Gerken et al., 2016); convective parameterizations (e.g., Schiro et al., 2018; Song and Zhang, 2017); buoyancy was deeply investigated (e.g., Ahmed and Neelin, 2018; Zhuang et al., 2018), as well precipitation processes (e.g., Machado et al., 2018; Ahmed and Neelin, 2018; Kuo et al., 2018; Schiro and Neelin, 2018; Giangrande et al., 2017; Marengo et al., 2017; Dias-Junior et al., 2017; Collow et al., 2016).

Even after so many new reports about the ABL, there are still some knowledge gaps to fill out, which can help to better model the Amazonian atmosphere. Mesoscale convective systems, for example, are not well represented in climate models (Schiro et al., 2018). A study derived from GoAmazon 2014/15 campaign (Schiro and Neelin, 2018) showed the variations of the thermodynamics before and after the passage of mesoscale convective storms, but studies showing the convective boundary layer evolution after and before such events are not found in the literature. Then, this work will explore this topic, bringing some background on thermodynamics, case studies for the Amazon rainforest - based on the data collection of the GoAmazon 2014/15 project, CBL modeling based on the case studies, and some perspectives for future works. Also, this work is concluded with some comments and thoughts about the interaction of society and forest and its impacts on climate change, and the environmental impacts.

> What are the goals in this work?

This work intends to examine the thermodynamic features of the ABL, such as temperature and humidity, to characterize the ABL growth in the Amazon rainforest - before and after precipitation events, specifically mesoscale convective systems.

The investigation will be done using the data set provided on GoAmazon 2014/15 experiment (Martin et al., 2017). Case studies representing the precipitation events, called disturbed days, will be explored. The ABL growth will be estimated based on the virtual potential temperature profiles, and thermodynamic variables - e.g., equivalent potential temperature and specific humidity - will be characterized according to the time of precipitation event and diurnal basis. A thermodynamic atmospheric boundary layer model will be applied to the results to demonstrate how the models' performance is compared to the observations for disturbed days. Thus, this work aims to provide a deeper understanding of the unique features resulting from the passage of convective systems over a forested area.

1.2   Area and Population

The Amazon basin, is a forested area of approximately 7,500,000 km^2, inhabited by an estimated 28 million people [2], at least 40,000 plant species, 427 mammals, 1,300 birds, 378 reptiles, more than 400 amphibians and around 3,000 freshwater fishes, according data from World Wildlife Fund (WWF-Brasil) [3], and it is the world's largest tropical rainforest.

The Amazon basin is located within 50°W and 80°W longitude and 5°N and 17°S latitude and has significant area in 6 countries: Brazil (70%), Peru (12%), Bolivia (12%), Colombia (8%), Ecuador (3%), Venezuela (2%), and Guiana (1%) [4]. Its main geographical limits are the Guianese Plateau (North), Central Plateau (South) and Andean Mountain Range (West), and it is horseshoe-shaped towards the Atlantic Ocean. The Amazon basin has a low population density, which is mainly distributed in areas near the Amazon river and its tributaries, and these regions suffer from low investments and infrastructure (Figure 1.2) [5]. Hundreds of indigenous communities (e.g., Guarani, Yanomami, Awa, and Guajajara) also characterize the Amazon scenario, being the estimated population greater than 300,000 people who declared as indigenous in 2010 [6]. The largest city in the Amazon basin is Manaus (Brazil), also one of the biggest cities in Brazil, with an estimated population of more than 2 million inhabitants in 2017 (IBGE, 2010). It also concentrates an industrial polo with more than 500 industries of high technology (Suframa, 2003).

The Amazon basin comprises thousands of small rivers (Salati and Marques, 1984), and has the world's largest river in discharge, the Amazon river, which is also the first or second longest river - competing with Nilo river (Goulding et al., 2003).

---

[2] http://www.fao.org/nr/water/aquastat/basins/amazon/index.stm
[3] https://www.wwf.org.br/natureza_brasileira/areas_prioritarias/amazonia1/bioma_amazonia/
[4] Approximated values.
[5] https://www.worldwildlife.org/pages/conservation-science-data-and-tools
[6] Only within Brazil; https://censo2010.ibge.gov.br/
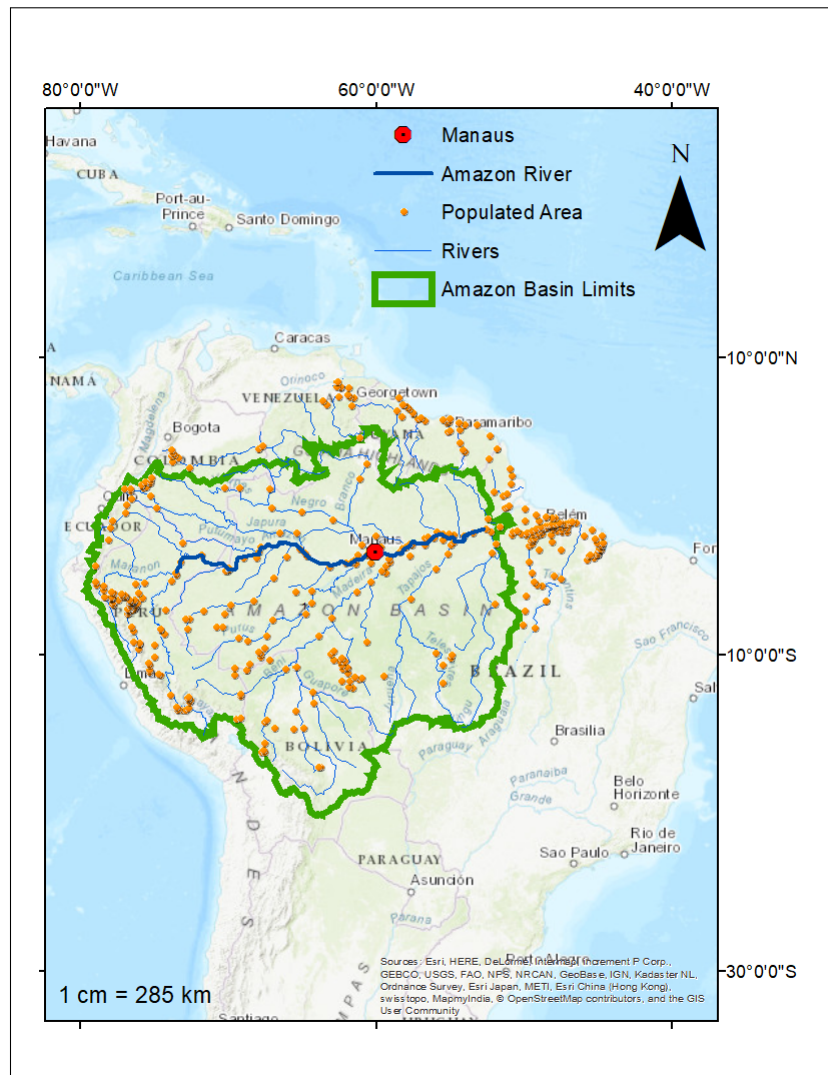
Figure 1.2: Amazon basin: populated areas. Map created on ArcGis using data from: World Wildlife (WWF)

"The Amazon River runs almost 4,000 miles from the Andes Mountains in the west to the Atlantic Ocean in the east. The river basin plays a key role in heat, moisture, and carbon cycles both regionally and globally. The region is also the most biologically diverse location on Earth, supporting perhaps half of all species on the planet." - *NASA Earth Observatory* [a]

[a]https://earthobservatory.nasa.gov/Features/LBA

1.3 Climate

The humid tropical climate [7] of the Amazon rainforest suffers very small variation of temperature over the year, ranging from 24°C to 28°C, and sunshine hours varying from 11h 36min to 12h 38min (Salati and Marques, 1984). The annual precipitation is, approximately, 2300 mm year^{-1} (Salati and Marques, 1984), with a variable monthly precipitation. The Figure 1.3 shows the monthly averaged accumulated precipitation and temperature from 2000 to 2010 distributed over the Amazon basin [8]. The spatial distribution of precipitation is considerably variable in the Amazon basin (20-29°C), and can be as low as 190 mm/month in the borders of the basin towards the ocean, and as high as 480 mm towards the Andean Mountains. The averaged temperature is more spatially distributed, however with noticeable low temperatures in the southwest, near the Andean Mountain range (5°C).
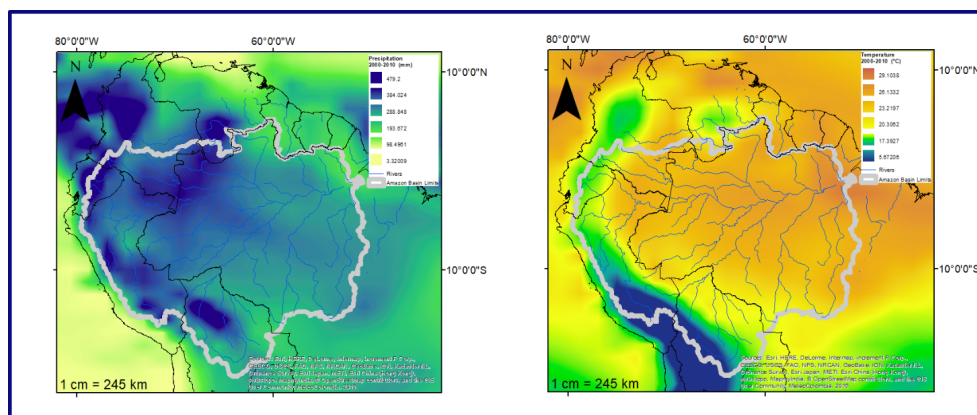
Figure 1.3: Amazon basin precipitation (left) and temperature (right): average from 2000 to 2010. Map created on ArcGis using data from: World Wildlife (WWF)

The different amount of rain in each month determine two distinct seasons: the dry and the wet season, characteristic of Tropical weather. The dry season has less accumulated rainfall, but with an accumulated precipitation greater than the wet season (Giangrande et al., 2017), and presenting organized synoptic systems in lower frequency when compared to wet season (Garstang and Fitzjarrald, 1999). Also, it is the season when more burning events happen - either natural and anthropogenic -, which deteriorate the air quality in the Amazon basin. The seasons' onset is dependent on the location, but typically, the wet season starts in October and ends in April, and the dry season takes over into the remaining months. The months of October and May are usually considered months of transition. Nonetheless, recent studies are showing how the land cover changes can cause shifts on the onset and length of seasons in Amazon (e.g. Wright et al., 2017), and also that the Amazon basin suffered a temperature increase of 0.7°C in the past three decades (Gloor et al., 2015). Deforestation is the main concern and possible cause of these changes.

Looking to 30 years of weather model simulations for precipitation and temperature in Manaus city

---

[7]The majority of the Amazon rainforest is classified as Af (Tropical rainforest) according to Köppen Climate Classification, meaning minimum temperatures of 18°C and minimum precipitation larger than 60 mm per month. The regions on the border of the Amazon basin are classified as Am (Tropical Monsoon), due to its slightly different amount of precipitation. Details on Köppen classification can be found here: http://hanschen.org/koppen/#classification

[8]https://www.worldwildlife.org/pages/conservation-science-data-and-tools

(Figure 1.4)[9] located in the middle of the rainforest, as a representation of monthly averaged precipitation and temperature variability, the month with the highest mean precipitation is March (326 mm), gradually transitioning to a drier period from June to October, meeting a minimum mean precipitation of 35 mm in August. The highest temperatures are between September and October (35°C).
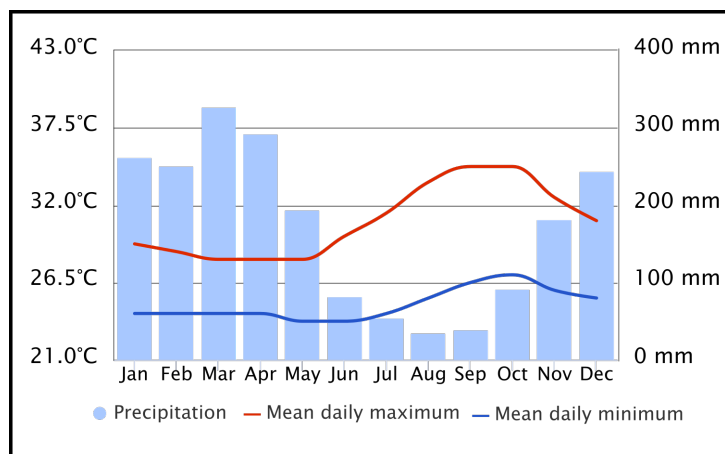
Figure 1.4: Manaus: precipitation and temperature (30 years average). Source: Meteoblue weather

Regarding synoptic features affecting the Amazon rainforest, Machado et al. (2018) highlighted:

- Intertropical Convergence Zone;

- Easterly waves;

- Upper tropospheric cyclonic vortices;

- South Atlantic Convergence Zone;

- Northward propagation of convective clouds.

However, an interesting feature about the Amazon rainforest climate is that it does not follow the "rules" that govern most of the tropical regions (Wright et al., 2017). Both the monsoon winds and the Intertropical Convergence Zone (ITCZ) are experienced in Amazon, but it is not coincident with the onset of the rainy season - as expected in tropical regions. The Amazon rainforest is, actually, highly dependent on the evapotranspiration from the trees at the end of the dry season to initiate the processes that lead to the rainy season (Wright et al., 2017).

1.3.1 Precipitation

The need to understand the precipitation processes in the Amazon rainforest brought researchers to know how the clouds are seeded in the Amazon. It was found that biogenic salts (potassium-salt-rich particles from biota in the rainforest) seed the clouds, by initiating the condensation of BVOC (biogenic volatile

---

[9]https://www.meteoblue.com

organic compounds) products (Pöhlker et al., 2012). BVOCs are largely emitted by trees (Fuentes et al., 2016). Measurements indicate an increased emission of isoprene and monoterpene, both BVOCs , in late morning simultaneously to the increase in cloud condensation nuclei concentration (see Fuentes et al., 2016).

> *"[...] aerosol radiative forcing and cloud formation depend on the individual particle composition, it is important to know how atmospheric components are mixed within a population of aerosols. [...]" - Fraund et al. (2017)*

The location of the site studies in the GoAmazon 2014/15 experiment (Martin et al., 2017) provided a unique opportunity to study aerosol particles in a pristine environment and the influence of a polluted plume over the forest. The anthropogenic emissions had shown an influence in air quality over the rainforest, increasing the nitrogen oxides (NOx) - which concentrations were found larger than the sulfate concentrations (Sá et al., 2017) - and hydroxyl (OH) concentrations, changing the atmospheric oxidation capacity (Liu et al., 2018).

During the dry season, there is also a higher concentration of carbon monoxide and aerosol particles due to fires (in-basin) and, emissions from Manaus are frequently impacting the downwind regions (Fraund et al., 2017). However, even pristine sites can be under the influence of long-range transport as showed in Fraund et al. (2017), who found significant amounts of black carbon in a site 150 km upwind of Manaus. Case studies during the wet season have shown that the pollution can enhance the ozone concentration in 3 times, particle concentration more than 10 times, increase oxides of nitrogen, from less than 1 ppb to more than 1 ppb (Sá et al., 2017).

Gu et al. (2017) shows an important comparison among results obtained by airborne eddy covariance measurements, satellite top-down, and model predictions for isoprene emissions, where the airborne measurements surpassed either satellite measurements and model predictions. But, the most relevant finding in this paper is the correlation between isoprene emissions, terrain elevation and plant species (Gu et al., 2017).

Regarding the precipitation itself, the GoAmazon 2014/15 project along with the ACRIDICON-CHUVA experiment - detailed later in this chapter - provided more observations to help the characterization of the precipitation in the Amazon rainforest, showing that the wet season, despite the higher accumulated precipitation, has a smaller rainfall rates compared to the dry season and the typical precipitation is monsoon-type (Machado et al., 2018).

The higher intensity of rainfall is also observed in the dry season CAPE (convective available potential energy) - which exceeded 2000 J kg^{-1} more often than during the wet season, added to events registering more frequent rainfall rates exceeding 20 mm h^{-1} (Machado et al., 2018). The precipitation over the rainforest caused by COS (Coastal Occurring systems) also showed high rainfall rates, exceeding 30 mm h^{-1}, in up to 70% of the cases presented by Garstang et al. (1990).

The occurrence of mesoscale convective systems (MCSs) is very often in the rainforest, where high convective available potential energy (CAPE >2000 J kg^{-1}) and statically unstable atmosphere, condi-

tions that lead to formation of MCSs (Trapp, 2013) are found. The wet season, typically, does not favor such conditions, presenting lower CAPE values and high relative humidity (Giangrande et al., 2017).

> *" Mesoscale convective systems (MCSs) are the largest of the convective storms. They form when clouds occurring in response to convective instability amalgamate and organize upscale into a single cloud system with a very large upper cirriform cloud structure and rainfall covering large contiguous rain areas. They account for a large proportion of precipitation in both the tropics and warmer midlatitudes."* - *Houze Jr (2004)*

The overall diurnal distribution of precipitation shows the prevailing events happen between 12:00 LT (local time) and 17:00 LT (Tanaka et al., 2014), when the convective activity is large. During the dry season, the precipitation is shown more concentrated between 14:00 LT and 16:00 LT (Tanaka et al., 2014). During the dry season, organized mesoscale systems show a peak at 14:00 LT, while locally originated precipitation is found later, 18:00 LT (Garstang and Fitzjarrald, 1999).

Under different wind regimes, westerly or easterly, the diurnal cycle of precipitation suffer some changes. A study made during two months of the wet season of 1999 (January and February) (Marengo et al., 2004), observed that for the easterly regime the peak of precipitation intensity is 5 hours earlier than the average rainfall (07:00 LT), from measurements obtained from 4 rain gauge networks; the westerly winds, however, presented a peak of rainfall intensity at 21:00 LT, different than the average or the easterly winds. Despite those differences, both regimes and the average have a preferred intensity observed between 12:00 and 16:00 LT. Marengo et al. (2004) suggests that the easterly regimes are associated with the development of large-scale circulation and convection, which is the reason for the high rainfall intensity in such regime; the westerly regimes seems to be associated more to *"large-scale stratiform clouds coexisting with convective clouds"* (Marengo et al., 2004).

Rainfall modifies the amount of solar radiation reaching the surface, which implies in changes in the photochemical processes, as the oxidation of BVOCs (Fuentes et al., 2016). In addition, storms downdrafts play an important role in bringing tropospheric ozone from upper levels to the surface, which also implies in increases in hydrocarbons oxidation (Gerken et al., 2016). Regarding the atmospheric boundary layer, the occurrence of early morning precipitation was shown as an inhibitor of convective cloud growth, preventing the mixed layer growth as well (Garstang et al., 1990). During the GoAmazon 2014/15 experiment, for example, were recorded more than 200 days with rainfall, which justify the interest in studying disturbed days are fundamental to understand the atmospheric boundary layer processes.

1.4 Atmospheric Boundary Layer

The atmosphere is divided into several layers according to the characteristics that each one of the layers present. The atmospheric layers from the Earth's surface to the top of the atmosphere are: troposphere, mesosphere, stratosphere, thermosphere, exosphere. The distinction between each layer results of differ-

ent temperature profiles observed throughout the atmosphere, as seen in Figure 1.5.
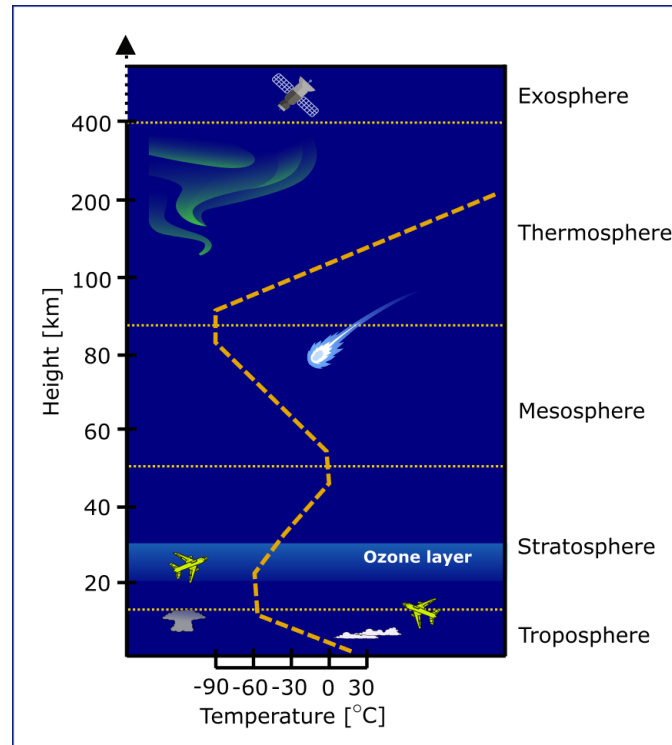
Figure 1.5: Atmospheric layers and thermal stratification

Different temperature profiles from one layer to the other is the result of the composition of each layer (different chemical species) in response to the incoming solar radiation and, at the troposphere, is mainly due to the interactions with the Earth's surface. Then, in the troposphere interesting features are observed. There is a layer, extending from the surface to typically 1 to 3 km: the atmospheric boundary layer (ABL). The ABL responds to forcings as heat transfer, evaporation, transpiration, and pollutant emissions. Turbulence, for example, is an important transport process, which is remarkable in the ABL.

In the ABL, turbulence is driven by mechanical (e.g. wind shear) and buoyant processes (e.g., turbulence production by statically unstable thermal stratification) (Stull, 1988). The thermodynamic states of the ABL govern the turbulent transport of heat, water vapor, gases, and particles from the surface to the free atmosphere. Knowledge of turbulent transport in the ABL is directly relevant to understanding and quantifying cloud formation processes, for example. During the daytime, the surface-atmosphere exchanges of sensible heat create thermodynamic conditions that promote statically unstable conditions, when thermal plumes rise and reach the upper regions of the ABL. A manifestation of the intense turbulence is the formation of a uniform mixed layer where the virtual potential temperature is nearly invariant with altitude. Under such conditions, the boundary layer is known as the convective boundary layer (CBL) or mixed layer (Stull, 1988). Above the CBL, there is a region characterized by a strong temperature inversion, known as the entrainment zone (EZ) , where the air exhibits attributes (e.g., moisture content, warmth, etc.) from the mixed layer and the free atmosphere: it is the layer that allows the air from the

free atmosphere to enter the CBL and vice versa. There is, also, a thin layer, typically 10% of the total depth of the ABL, which is in direct contact with the ground. For this layer is given the specific name of the surface layer (SL), and it is where changes at the molecular level happen.

After sunset, the surface sensible heat flux becomes negative in response to the cooling of the lower air layers, and a stable boundary layer (SBL) develops from the surface up, decreasing the turbulence intensity due to the statically stable conditions, known also as the nocturnal boundary layer (NBL) for the nighttime. The remaining layer between the SBL and the EZ is known as the residual layer (RL) and preserves the thermodynamic characteristics of the previous CBL.
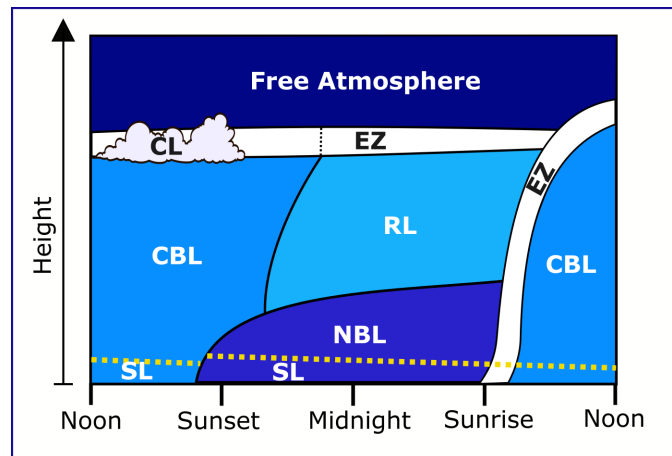
Figure 1.6: Atmospheric layers and thermal stratification in a high pressure region. CL: cloud layer, EZ: entrainment zone, CBL: convective boundary layer, RL: residual layer, NBL: nocturnal boundary layer, SL: surface layer. Figure adapted from Stull (1988)

However, over the tropics, the content of water vapor in the lower atmosphere is an important factor that drives the thermodynamic features of the ABL that produce distinct growth rates of the mixed layer over the course of the dry and the wet seasons. Due to the lack of instruments and the peculiar environmental conditions found in Amazon, it is always a challenge for researchers to set experiments over there. Then, measurements in such environments took a longer time to start than experiments in mid-latitudes.

But, before exploring the peculiarities of the ABL in Amazon, a summary of experiments and projects that were done about ABL in the Amazon rainforest is provided in the following subsection. Such studies helped to design what we know, nowadays, about the ABL in the tropical regions.

1.4.1 ABL experiments

Back in 60's, there was a lack of measurements, on a regional level, of parameters/variables that regulate the cycles of water, nutrients, carbon and energy (Salati and Marques, 1984). Between 60's and 80's, some experiments were set up but only for mid-latitudes. Then, the first meteorological experiment in the Amazon basin is from 1983 to 1985, which started the studies in the structure and growth of the convective boundary layer, trace gas exchanges, and convective transports in the Amazon rainforest (Garstang, 1987).

In 1985, the Amazon Boundary Layer Experiment (ABLE II(a)) [10], during the Amazon basin dry season - July and August 1985 -, characterized the chemistry and meteorology in and over the rainforest (Harriss et al., 1990). Regarding the atmospheric boundary layer, it was found that the mixed layer grows up to a maximum height of 1800 m, registered at 13:00 LT (local time), after the fast growth rate of 180-290 m h^{-1} (Martin et al., 1988). Undisturbed conditions presented deep mixed layers also in the morning, sometimes surpassing 1000 m (Martin et al., 1988). Two years later, in 1987, the ABLE II(b) repeated the previous experiment but for the wet season - April and May 1987 (Garstang et al., 1990). Regarding precipitation processes, one of the conclusions found in ABLE II(b) are the three modes of precipitation identified as: Coastal occurring systems (COS) - large meso to synoptic-scale systems -, basin occurring systems (BOS) - meso to synoptic systems, and locally occurring systems (LOS) - smaller convective systems (Garstang et al., 1990).

Due to the increasing need to determine the effects of deforestation, in 1990, ABRACOS (Anglo-Brazilian Amazonian Climate Observation Study), was remarkable by determining the differences in the ABL for deforested and forested areas. A significant difference was found in the CBL growth over a deforested area: it can reach depths between 700 to 1000 meters higher than over forested areas, during the dry season (Gash and Nobre, 1997). Increase in sensible heat flux added to reduced evaporation rates during the dry season also plays an important role in how the ABL develops, being showed that over the pastures (deforested areas) these effects are even stronger (Gash and Nobre, 1997).

Later, in 1998, the Large-Scale Biosphere Atmosphere (LBA) experiment in Amazonia, aimed to build the connections among land use, climate, biology, physics and chemistry over the humid tropics (Nobre et al., 1996a). Studies using the LBA dataset show different scenarios (e.g., different wind regimes and different conditions of precipitation) for the atmospheric boundary layer structure (Betts et al., 2002b); the experiment also led to studies of convective moist processes in the wet season of 1999 (e.g., Dias et al., 2002); integrating data from the European Studies on Trace Gases and Atmospheric Chemistry in Amazonia (EUSTACH), results showed a large uptake flux of carbon dioxide in the forest, large photochemical activity during the dry season - high concentration of hydrocarbons, and the different concentrations of cloud condensation nuclei in dry and wet season (Andreae et al., 2002).

Then, one of the most recent projects is the GoAmazon (Green Ocean Amazon) experiment (Martin et al., 2017), held from 2014 to 2015, provided one of the largest recorded meteorological data set, which is adding to more knowledge about the atmospheric precipitation processes, mainly regarding cloud formation in pristine and polluted environments. Other experiments took place simultaneously to the GoAmazon, for example, the ACRIDICON (Aerosol, Cloud, Precipitation, and Radiation Interactions and Dynamics of Convective Cloud Systems) and CHUVA (Cloud Processes of the Main Precipitation Systems in Brazil: A Contribution to Cloud Resolving Modeling and to the GPM (Global Precipitation Measurement)), which were combined experiments conducted in Manaus, to address the influence of aerosols in cloud formation processes (Wendisch et al., 2016). The GoAmazon 2014/15 will be explored in more details on Chapter 2.

---

[10]The ABLE I was held in 1984 in the W. Atlantic to characterize the "atmospheric chemistry of maritime lower troposphere" (Garstang and Fitzjarrald, 1999)

1.4.2 Convective Boundary Layer

Different land-surfaces (e.g., changes in albedo and roughness), incoming solar radiation, air composition (e.g., particles, aerosols, water vapor concentration) can lead to different growth rates of the atmospheric boundary layer. The land-surface interactions with the atmosphere are influenced by the clouds, but also the ground cover will determine the amount of evapotranspiration, the most representative variable of land-atmosphere interactions (de Arellano et al., 2015).

In the daytime, the ABL is unstable stratified, which means its temperature and, also, humidity decrease with height. Along with this, the ABL is driven by wind shear, that is the variation of wind speed and direction with height.

The passage of storms, for example, will change the dynamic and thermodynamic features of the ABL and lead to a smaller ABL growth rate when compared to a cloudless day. The storms downdrafts bring dry and cold air from the free atmosphere to the CBL and, after the storm passage, this air will take a while to configure similar conditions as the CBL previously to the storm passage (Figure 1.7). This process of disrupting the CBL due to precipitation events is constantly found in the Amazon rainforest. Due to that, when modeling the atmosphere processes in the tropical region, specifically in the Amazon rainforest, the ABL features have to be described taking into account such events.

"The presence of clouds in the atmosphere brings three additional physical processes that impact the atmospheric boundary growth. The first is the diminishing of shortwave radiation that reaches the surface; the second is the divergence of longwave radiation caused by different temperatures and emissivities between the cloud layer and the cloudless layer; and third, the phase changes of water due the process of condensation" - de Arellano et al. (2015)
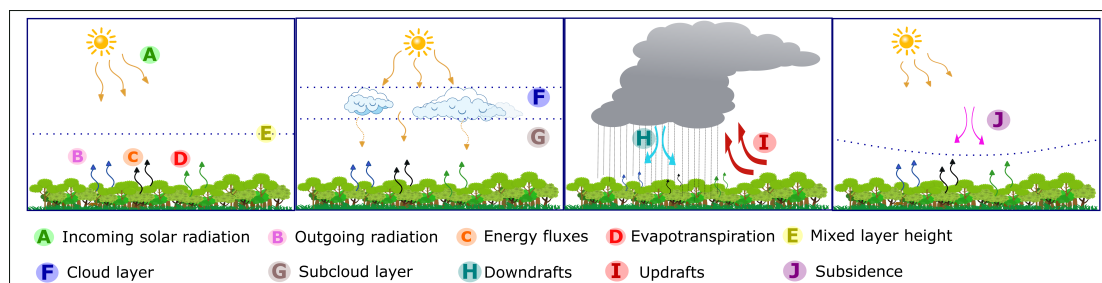
Figure 1.7: Representation of four conditions over the Amazon rainforest. From left to right: Cloudless conditions; the presence of cumulus; passage of storm; after the passage of storm - ABL recovery

As mentioned previously, the land-surface characteristics - e.g., vegetation - is one of the important features that will drive the surface fluxes. To highlight the differences found in different surface coverage and the CBL growth, Fisch et al. (2004) compared two sites of study in the Amazon region: a pasture site and a forested site. These comparisons were made for both dry and wet season and, cases of study, for disturbed (a day with precipitation) and undisturbed (no precipitation) days, and also, a case of *friagem*.

According to the results found by Fisch et al. (2004), the forested and deforested sites revealed a significant difference in the CBL depth mainly during the dry season: the forest had a CBL of, on average, 1100 m and the pasture overcome this value in 500 m. One explanation is the difference in the energy partition. The forest has similar energy partition over the year round. Maximum values of, approximately, 340-397 W m^{-2} for latent heat flux and 110-150 W m^{-2} for sensible heat flux, at 13:00 LT, were found by da Costa Galvão and Fisch (2000), using observations from ABRACOS experiment, for both seasons. In contrast, a pasture site had more variation in the energy partition during the dry season: a 36% smaller latent heat flux and 60% higher sensible heat flux (da Costa Galvão and Fisch, 2000). The main reason that forest keep the same energy partition in both seasons is that the soil moisture is very high even during the dry season, which allows the vegetation to withdraw the water from the soil, not affecting drastically the vegetation evapotranspiration. It corroborates the observed CBL depths found by Fisch et al. (2004), where the forest has the lowest variation in convective boundary layer depths (Figure 1.8(a)), the lowest variation in temperature within the CBL (Figure 1.8(b)), and specific humidity (Figure 1.8(c)). These results are also in agreement with those found by Martin et al. (1988) for the dry season, when a sample of 7 days where analyzed, and showed the CBL growing from 340 m in the morning (07:30 LT) up to 1200 m in the afternoon (17:00 LT).
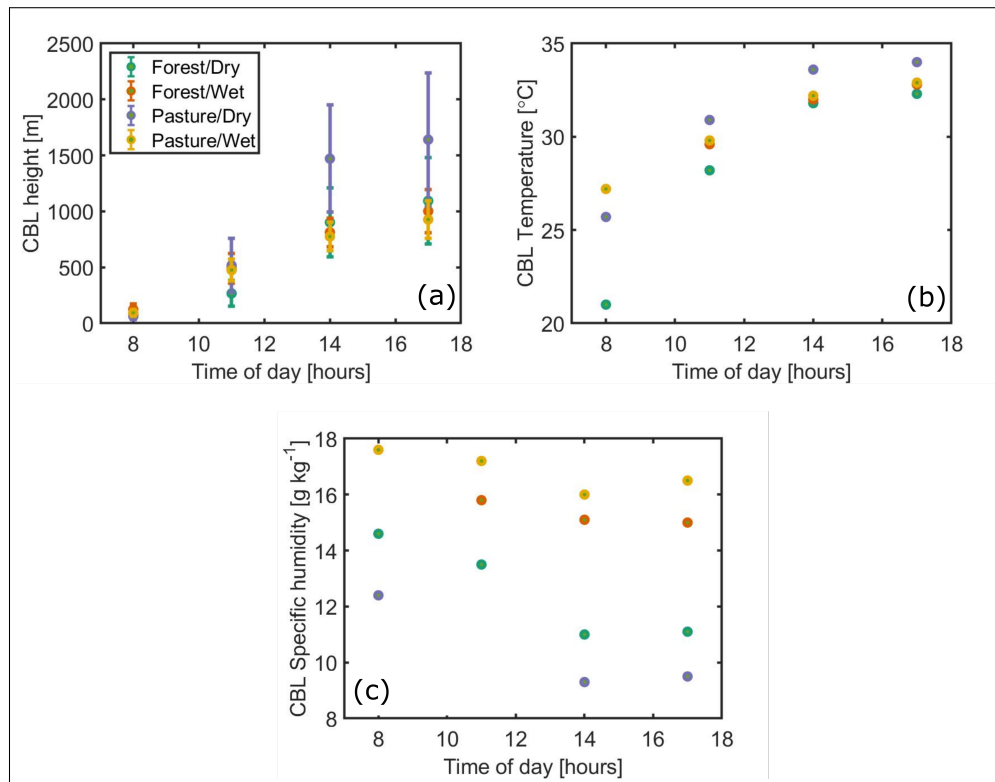
Figure 1.8: CBL features in the Amazon rainforest. Diurnal variation of (a) CBL height, (b) CBL temperature, and (c) CBL specific humidity, for forested and pasture sites. Figures created using data from Fisch et al. (2004)

During the dry season, the Amazonian ABL can undergo sufficient warming rates to establish a deep CBL. Maximum values of sensible heat fluxes measurements range from 100 W m^{-2} to 200 W m^{-2} between 10:00 LT and 12:00 LT (Fisch et al., 2004; Randow et al., 2004) due to surface heating. Heat fluxes are reduced after this period, but an active entrainment at the top of the mixed layer keep the CBL growing (Fisch et al., 2004). Latent heat fluxes ranging from 350 to 450 W m^{-2} in the same period (Randow et al., 2004). The maximum warming rate of the ABL is, on average, 2.4 K h^{-1} in the morning (08:00 to 11:00 LT). After this period, the warming rate decrease to 1.2 K $^{-1}$ (11:00 to 14:00 LT) and 0.2 K h^{-1} (14:00 to 17:00 LT) (Fisch et al., 2004). The specific humidity, on average, varies in a range of 11 to about 14 g kg^{-1} over the day (Fisch et al., 2004). There is a large transport of moisture out of the CBL during the morning in a rate of 0.5 g kg^{-1} h^{-1} (08:00 to 11:00 LT). During the afternoon, however, there is a period of humidification (0.1 g kg^{-1} h^{-1} from 14:00 to 17:00 LT) (Fisch et al., 2004). Nobre et al. (1996b) showed that the temperature gradient above the top of the CBL varies from 1.8 to 3.3 K km^{-1} from 08:00 to 17:00 LT and, for the same period the average virtual potential temperature in the mixed layer increases from 298.8 to 307.2 K. Under these averaged conditions, previous studies (e.g., Fisch et al., 2004; Fitzjarrald et al., 1990; Strong et al., 2005) indicated that the CBL attains its maximum depth in the afternoon, reaching up to 1500 m as shown previously.

In the wet season, the CBL exhibits shallower mixed layer depths due to the reduced solar radiation reaching the ground surface in response to enhanced cloudiness. As a result, the surface-atmosphere exchanges of energy are reduced. Typical sensible heat fluxes, in this season, attains up to 100 W m^{-2} between 11:00 and 13:00 LT (Fisch et al., 2004; Randow et al., 2004). The latent heat fluxes reach a maximum value at noon, with averaged values of 400 W m^{-2} (Randow et al., 2004). The specific humidity levels, on average, do not exhibit much temporal variability whose values range from 12 to 16 g kg^{-1} over the course of the day (Fisch et al., 2004). The warming rates are, on average, 0.8 K h^{-1} between 11:00 and 14:00 LT. This warming rate is 67% slower than during the dry season for the same period of the day. In contrast, from 14:00 to 17:00 LT, the warming rate is 50% higher than during the dry season, with averaged values of about 0.3 K h^{-1}. Under these conditions, the CBL maximum depth can reach up to 1200 m (Garstang et al., 1990) ascribed the shallower depth of the CBL, during the wet season, to the more frequent early morning precipitation that can inhibit the growth rates of the CBL, as seen in the Figure 1.8.

1.5   Summary

This wonderful gift of nature, the Amazon rainforest, is home of a variety of plants and animal species that excels other Earth's ecosystems. Such incredible place has been suffering from human's presence for several years. Big cities are, nowadays, the main source of pollution in this region. In addition, deforestation is also deteriorating the rainforest. A deep understanding of the interactions among land, atmosphere, hydrology, fauna, flora, and human beings are increasing the capacity of models to predict the weather and, even more, climate changes.

Regarding the atmospheric aspects of the Amazon rainforest, many investigations have been conducted since the 80's. Nowadays, many experiments provided a better understanding of, for example,

cloud formation, air pollution, synoptic systems, atmospheric boundary layer processes, thermodynamics, and dynamics features. However, every study brings new questions and, perhaps, unexpected results. It helps to keep the motivation for even deeper or more specific observations and analysis. Then, to add to the atmospheric research in the tropics, the next chapter will evaluate thermodynamic features of the Amazon atmospheric boundary layer in terms of the passage of mesoscale convective systems and unorganized systems, using the data set provided in the GoAmazon 2014/15 experiment (Martin et al., 2017). Cases of study will elucidate the modifications suffered in the ABL when precipitating systems disrupt the development of a mixed layer.

This kind of study is relevant to provide inputs for physical models that aim to simulate atmospheric boundary layer conditions, as for weather predictions and climate models.

Chapter 2

Characterization of the thermodynamic variables of the Convective Boundary Layer in the Amazon Rainforest

2.1 Introduction

After being somehow familiar with the Amazon rainforest and its atmospheric boundary layer, this chapter will provide a deeper insight into the thermodynamic features observed during the GoAmazon 2014/15 experiment (Martin et al., 2017). The goal of this chapter is to apply the thermodynamic concepts to a real case and perform a model to compare the results observed for the convective boundary layer growth and the results obtained through modeling. However, as seen in the previous chapter, there are plenty of researches regarding the CBL growth, but very few are closely related to the passage of storms. Also, models do not describe properly the convective boundary layer growth when there is a passage of a mesoscale convective system, which happens very often in the Amazon rainforest.

The GoAmazon 2014/15 experiment is a good opportunity for this investigation. The extensive data set provided during the 2 years observations allow the identification of several cases of organized systems passing over the site of studies. Despite similar results have already been presented in the literature (e.g., Schiro and Neelin, 2018), complementary investigations are provided in this chapter, in order to explore the convective boundary layer growth rates. As shown in Figure 1.7, the cloud formation over the forest will inhibit the amount of solar radiation, and the presence of a storm will disrupt the CBL growth. What is not well-known is how the CBL starts to re-develop after the passage of these storms and how, for example, subsidence is preventing its growth (Figure 2.1).
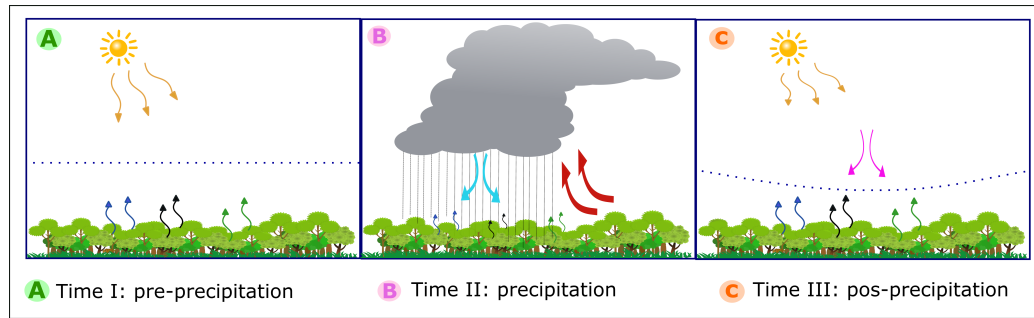
Figure 2.1: Conceptual idea for the investigated cases. (a) Time I: before the precipitation, (b) Time II: passage of precipitation, (c) Time II: after precipitation. The symbols are described in Figure 1.7

The Figure 2.1 shows, first, in the time I the incoming solar radiation (yellow arrows) arriving at the surface. The blue arrows are the outgoing longwave radiation, the black arrows are the latent and sensible heat fluxes, and green arrows represent the exchange of gases, for example. The dotted lines in the middle of the figures are the representation of the top of CBL. Second, the change of the depth of the CBL is represented in time III, after the passage of a storm (time II, where blue arrows are the storm's downdrafts and the red lines, the storm's updrafts). To accomplish the aimed evaluations and to understand better the scenario showed in Figure 2.1, the investigated variables will be: equivalent potential temperature, specific humidity, convective available potential energy, sensible and latent heat fluxes, and height of the convective boundary layer.

Then, in order to provide new insights on this research field, the goals here are: (i) identify case studies to represent the passage of mesoscale convective systems, (ii) evaluate the thermodynamic features of the CBL for the case studies, (iii) study the CBL behavior under the passage of convective systems, (iv) use a thermodynamic model to compare observations and modeling. It is also an effort to answer the following research questions:

1. What are the thermodynamic conditions (e.g., temperature and humidity) in the convective boundary layer preceding a mesoscale convective system?

2. What are the thermodynamic conditions (e.g., temperature and humidity) in the convective boundary layer after the passage of a mesoscale convective system?

3. How do the thermodynamic changes in the convective boundary layer after the passage of a mesoscale convective system relates to the convective boundary layer growth rate?

4. How do an atmospheric boundary layer model perform for disturbed days conditions, such as the days when there is a passage of mesoscale convective systems?

It will be explored in more details over this chapter that is organized as follows: (i) review of the GoAmazon 2014/15 experiment; (ii) site of study used as reference for this part; (ii) measurements of

interest; (iv) derived variables; (v) climatology of 2014 and 2015; (vi) case studies; (vii) results and discussion; and (vii) summary.

2.2 GoAmazon 2014/15

The Green Ocean Amazon (GoAmazon) was an experiment set up to obtain data sets to better understand the coupled atmosphere-cloud-terrestrial tropical systems (Martin et al., 2017). From January 2014 to December 2015, comprising both seasons in the Amazon rainforest, the Office of Biological and Environmental Research's Climate and Environmental Sciences Division in collaboration with Brazilian and German organizations, collected datasets to study the interactions and impacts of pollutants coming from megacities into the pristine forest, and to try to understand how it can interfere in cloud formation (Martin et al., 2017) [1].
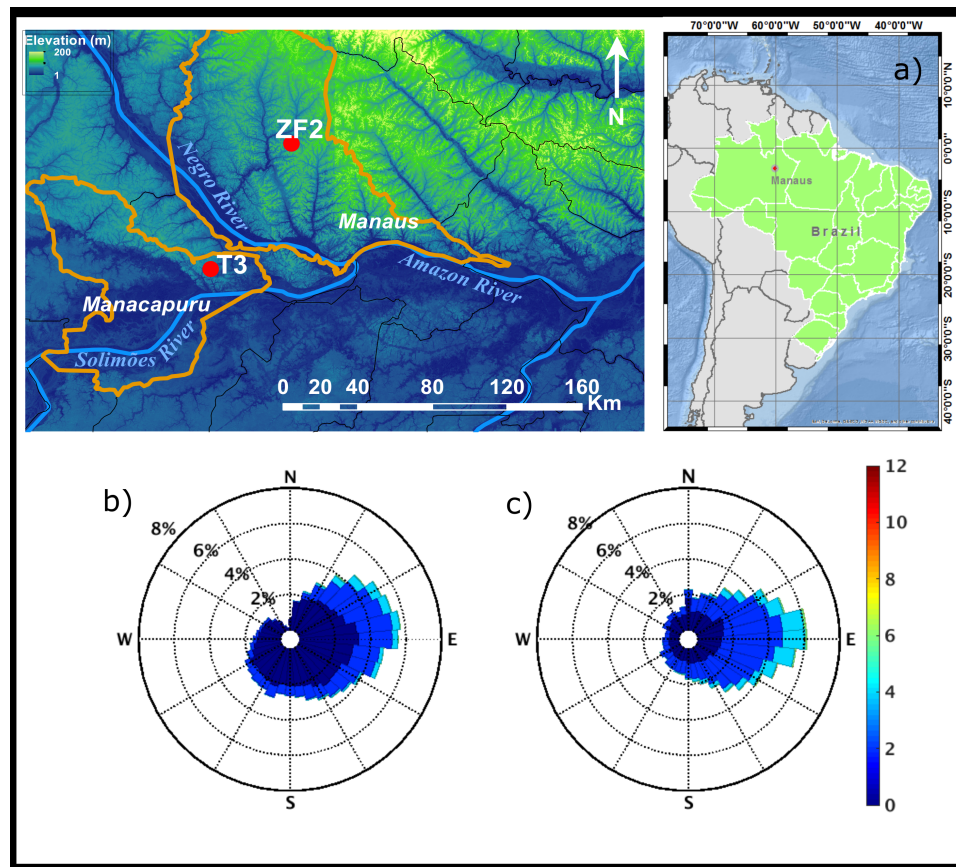
Figure 2.2: Location of two sites from GoAmazon 2014/15 experiment: (a) T3 and ZF2 (left), and Brazil's map showing Manaus location (right). The solid lines (left map) are the delimitation of Manacapuru and Manaus County. Wind rose for (b) T3 site and (c) ZF2 site. Maps created on ArcGIS.

---

[1]The experiment website provides more details and contact information about the campaign: `http://campaign.arm.gov/goamazon2014/`

To set up the experiment, nine ground sites, and two onboard aircraft (Martin et al., 2017). Only two sites are relevant for the analysis of interest in this chapter (Figure 2.2)[2]. The first site is the main ground measurement site, T3. It is located downwind Manaus, it receives the pollutants transported from a big city. More details about this site will be given in section 2.2.1. The second site, ZF2 (Biological Reserve of Cuieiras), is used as a reference of a pristine environment, the site ZF2 does not receives pollution coming from Manaus.

2.2.1   T3 and ZF2 sites of study

The main site of study chosen to represent the thermodynamic features of the Amazon rainforest atmosphere, for this work, is the T3 site. It is situated at geographical coordinates 3° 12' 46.70" S and 60° 35' 53.0" W, 10 km distant from Manacapuru (Brazil) and 70 km southeast (downwind) from the city of Manaus (Brazil) (Figure 2.3); located in the intersection of Negro and Solimões rivers (Figure 2.2). The site is pasture field surrounded by the rainforest and represents a region of the rainforest which is impacted by the pollution plume that comes from Manaus.

During the period between 1 January 2014 and 31 November 2015, the Atmospheric Radiation Measurement (ARM) Climate Research Facility of the United States Department of Energy (Martin et al., 2017; Mather and Voyles, 2013) operated a set of equipment to measure energy fluxes, wind speed and direction, radiation components, humidity, temperature, and chemical fluxes. The reason to choose this site is the data availability that makes possible to conduct the aimed study.

The ZF2 site is located within Manaus County, but upwind to the industrial center and the populated area. It is inside the Biological Cuieiras Reserve, at coordinates 02° 36' 17.1" S and 60° 12' 24.4" W. It is a densely forested area, 60 km northeast of Manaus and 120 km from Manacapuru. This site has a 50 meters tower, from where profiles of ozone, biogenic volatile organic compounds profiles were obtained, in addition to profiles of meteorological variables, e.g., wind speed and direction, temperature, humidity, and radiation components. The ZF2 site will be used in order to complement precipitation data when it is missing in the T3 site (Figure 2.3).

---

[2]Wind rose obtained from the GoAmazon 2014/15 data set

Figure 2.3: GoAmazon sites of study. Left picture: Set of containers with instruments at the T3 site, located in Manacapuru. Right picture: 50 meters tower with instruments at the ZF2 site, located in the Biological Cuieiras Reserve

2.2.2 Measurements

Both sites, T3 and ZF2, had a broad set of measurements. However, only the relevant measurements for this study will be described. The surface meteorological measurements at the T3 site were obtained by in-site sensors, providing 1-minute statistics of surface wind speed and wind direction (propeller anemometer and wind vane, R. M. Young Model 05106 Wind Monitor), air temperature and relative humidity (Platinum RTD and RH, Vaisala Model HMP45D Temperature and Relative Humidity Probe), barometric pressure (digital barometer, Vaisala Model PTB220), and precipitation (Optical Rain Gauge: Optical Scientific, Inc. Model ORG-815-DA MiniOrg) [3].

Due to technical issues, the precipitation data at T3 was collected only between 14 October 2014 an 31 November 2015. To compensate for the period without precipitation data at T3, and to provide an overview of the prevailing conditions in this specific region of central Amazon basin, the rainfall data from the ZF2 site of study, measured between 1 January 2014 and 14 October 2014 is also used (Figure 2.5). The precipitation at ZF2 site was measured by a pluviometer (model ARG-100).

The kinematic sensible and latent heat fluxes were obtained every 30-minutes by an eddy covariance (ECOR) system. Measurements of broadband shortwave radiation for the downwelling component were collected from multifilter radiometers, in a frequency of one minute.

Upper air measurements, such as air pressure, temperature, relative humidity, wind speed and direction, were obtained through radiosondes launched over the T3 site at 6-hours intervals (01:30, 07:30, 13:30 and 19:30 LT) and occasionally 10:30 LT over the wet season. A microwave radiometer profiler [4] was used to obtain the convective available potential energy (CAPE), at a sampling rate of 1 Hz.

---

[3]Instruments details: https://www.arm.gov/

[4]For more information on the microwave radiometer profiler visit: https://www.arm.gov/publications/tech_reports/handbooks/mwrp_handbook.pdf

Satellite images from the GOES-13 (Geostationary Operational Environmental 90 Satellites 13), operated by the National Oceanic and Atmospheric Administration (NOAA) and National Aeronautics and Space Administration (NASA), were used to assess the periods with storms. The satellite images were provided by the Brazilian National Institute for Space Research (INPE), which uses the GOES's system for meteorological forecast and monitoring.

2.2.3 Climatology over the project period

From the data set obtained during the GoAmazon 2014/15 experiment, it is observed that the mean monthly temperature does not vary more than 5°C between the wet and the dry seasons. In 2015 higher temperatures were registered along with lower specific humidity and lower amounts of precipitation when compared to 2014. This behavior is coincident with a strong El Niño observed in 2015, which affected the Amazon basin with record-breaking temperatures and drought (Jiménez-Muñoz et al., 2016). Between the seasons is noticed a relevant difference in the total precipitation (Figure 2.4a), also observed in the high values of the specific humidity, which has the highest monthly average specific humidity, up to 20.0 g kg^{-1}, in the wet season and the lowest, in the dry season, about 18.0 g kg^{-1}, in 2015 (Figure 2.4b). This difference between the amount of rain over the tropics, that distinguishes the dry and the wet season, is attributed to the frequent organized synoptic systems that produce rainfall in large areas during the wet season, in contrast with the dry season (Garstang and Fitzjarrald, 1999). The high amount of water vapor in the atmosphere during the wet season leads to low atmospheric pressure, as seen in Figure 2.4c. Also, the intense cloudy periods during the wet season reduces the amount of incoming solar radiation, which can be more than 65% larger in the dry season.
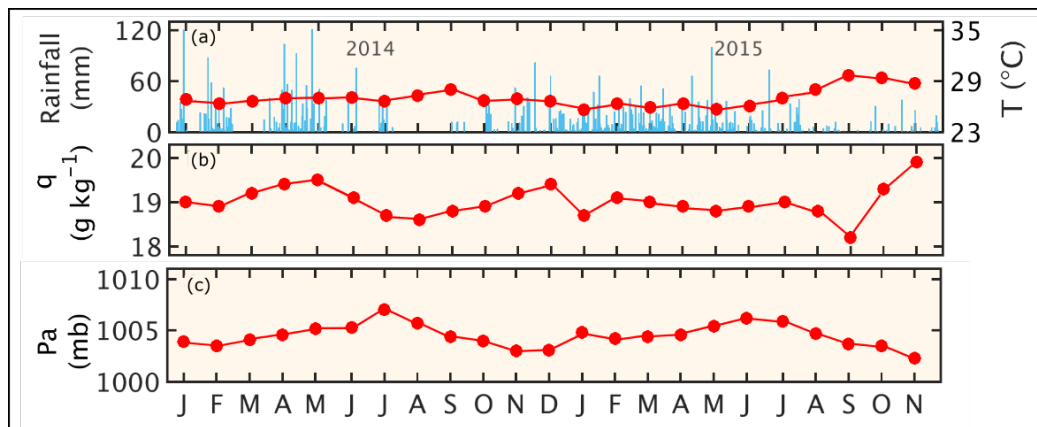
Figure 2.4: Climatology 2014/15. (a) Monthly averaged temperature (T) and total daily rainfall, (b) monthly averaged specific humidity (q), (c) monthly averaged atmospheric pressure (Pa)

A daytime precipitation and temperature pattern are also identified during the period of study. For both the wet and dry seasons, on average, the lowest temperature is about 23°C, and its maximum is reached near noon, when the averaged temperature reaches up to 32°C, in the dry season. The pattern of precipitation reveals a typical precipitation occurring about 04:00 LT (Figure 2.5). This pattern is possibly

related to the penetration of convective systems coming from the east into the Amazon basin (Fuentes et al., 2016). The recurrent afternoon precipitation is more likely due to local convection (Fuentes et al., 2016).
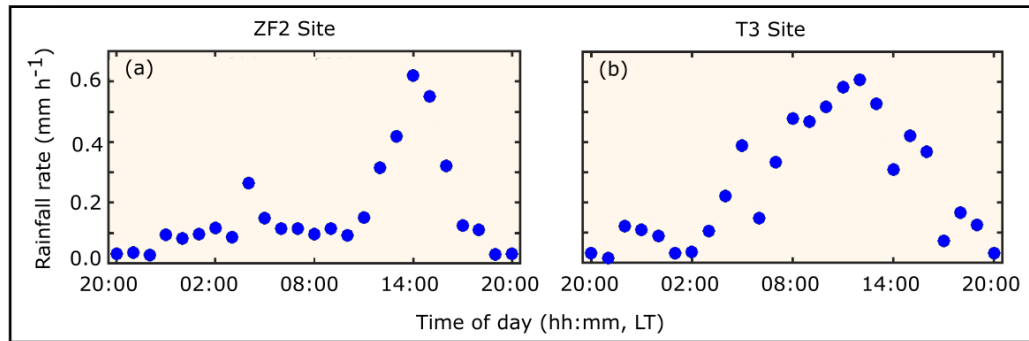
Figure 2.5: Diurnal rainfall rates. (a) ZF2 site: 14 January 2014 to 14 October 2014. (b) T3 site: 15 October 2014 to 31 November 2015

This diurnal pattern can be attributed to three different systems: LOS (local occurring system) , BOS (basin occurring system) , and COS (coastal occurring system) (Garstang et al., 1990; Greco et al., 1990). The LOS is more likely to occur between 14:00 to 18:00 LT and are very small systems formed locally, with precipitation usually no longer than 1 hour. The BOS is more likely to happen between 06:00 to 10:00 LT and are the systems formed in the Amazon basin. The COS is more likely to occur early morning and is the largest systems, formed in the coast.

Mesoscale convective systems (MCSs) are important features at the Amazon rainforest. A study shows the occurrence of, an average, 7181 continental MCSs over the Amazon basin, and March is the month with the largest occurrence of MCSs (Rehbein et al., 2018). During 2014/15 the most frequent MCSs occurred in the afternoon and an around 00:00 LT (Figure 2.6a). A study using 14-years (2000 to 2013) of satellite images showed that the number of occurrences of MCSs during the day is prevailing from 12:00 to 20:00 LT, and a second peak around 00:00 LT (Rehbein et al., 2018), which is in agreement with the frequency found for the current years of study. Also, MCSs that occur late night seems to be stronger (higher accumulated rainfall) in shorter periods of time, when compared to MCSs registered during the daytime (Figure 2.6b,c). Downbursts associated with convective rain over the Amazon basin were also characterized by sharp decreases in the equivalent potential temperature and an increase in the surface pressure (Garstang and Fitzjarrald, 1999).
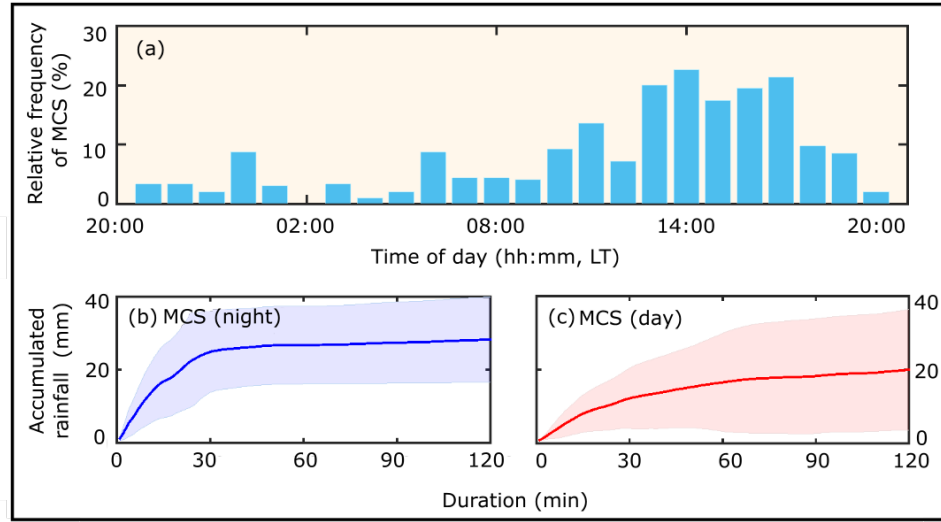
Figure 2.6: (a) Mesoscale convective systems: daily distribution, (b) accumulated rainfall of MCSs occurring during nighttime, (c) accumulated rainfall of MCSs occurring during daytime

Regarding some features found within the atmospheric boundary layer, the surface measurements for the period of the study suggest a small difference between the energy partition from dry to wet season. The daily average sensible heat flux ($\overline{H}$) and (H_{max}) for the wet season is 25.1 W m^{-2}, and 98.5 W m^{-2}, respectively, while for the dry season, 27.6 W m^{-2} and 110.4 W m^{-2} (Fig. 2.7a,f); the daily average latent heat flux ($\overline{LE}$) and maximum latent heat flux (LE_{max}) for the wet season is 75.3 W m^{-2} and 257.8 W m^{-2}, while for the dry season, 80.8 W m^{-2} and 268.0 W m^{-2} (Fig. 2.7b,g). This almost constant energy partition over the year is attributed to the fact that, even during the dry season, the soil has enough moisture, which allows trees to withdraw the water from the ground and keep similar evapotranspiration rates the year round. In contrast, pasture sites show larger differences in the energy partition (da Costa Galvão and Fisch, 2000), which undergoes different CBL growth rates in different seasons.

The daily mean equivalent potential temperature ($\overline{\theta_e}$) and maximum ($\theta_e max$) for the wet season is 348.2 K (352.7 K) and for the dry season, 347.8 K (353.2 K) (Fig. 2.7c,h). The daily mean specific humidity ($\overline{q}$) and its maximum (q_{max}) for the wet season 19.5 g kg^{-1} (20.4 kg^{-1}), and for the dry season 19.1 g kg^{-1} (20.4 g kg^{-1}) (Fig. 2.7d,i). Variation in the equivalent potential temperature and the specific humidity confirm the daily pattern of intense surface warming and evapotranspiration from the morning throughout the day. The small difference in these averaged variables between the seasons shows how the rainforest is capable to keep the diurnal cycles almost constant year-round. However, observing the specific humidity for the dry season is noticeable that in the middle of the afternoon an abruptly decrease in the water vapor content at the surface and it is likely that condensation is occurring faster than evaporation. It also seems to corroborate a cloud formation processes in the middle of the afternoon during the dry season, which may occur more often than during the wet season, due to an elevated presence of cloud condensation nuclei over this season, e.g., more frequent anthropogenic and natural biomass burning.

And, lastly, the daily mean convective available potential energy ($\overline{CAPE}$) and maximum ($CAPE_{max}$)

for the wet season are 1046 J kg^{-1} (1591 J kg^{-1}), and for the dry season 2137 J kg^{-1} (1299 J kg^{-1}) (Fig. 2.7e,j). The higher values for the convective available potential energy reinforces the predisposition for convective clouds form in the dry season, which also agrees with the decrease in the specific humidity in the middle afternoon.
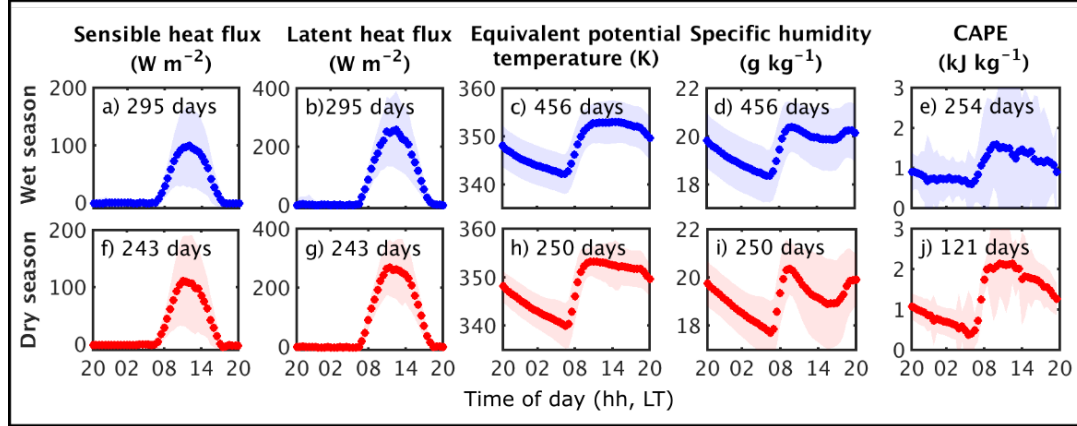
Figure 2.7: Thermodynamic features of the ABL at the surface. First row represents the wet season and second row the dry season. (a),(f) Sensible heat flux (b),(g) Latent heat flux, (c),(h) Equivalent potential temperature, (d),(i) Specific humidity, (e),(j) convective available potential energy. The shadow represents the standard deviation. The number of days highlighted represent the number of days with measurements available to determine the thermodynamic variable. Time of day is local time.

The Amazon rainforest is huge in spatial dimension and results and observations made based on a unique site of study may not reflect the conditions over the whole forest. Also, divergence in results found here and in the literature may reflect either the different location of measurements or time/period of measurements. The alterations in the Amazon rainforest due to the increase of big cities surrounding or within the forest, logging and deforestation are dynamic changes and are responsible for altering temperature and moisture content in the forest.

2.3 Derived variables

To describe the mixed-layer growth it is necessary to relate the changes in the mixed-layer depth with some known boundary-layer attributes. Many studies show different formulations for the entrainment rate, some of them using only thermodynamic attributes (e.g., Rayner and Watson, 1991; Tennekes and Driedonks, 1981). A simple model based on the kinematic heat flux at the surface, the potential virtual temperature lapse rate above the entrainment zone and the mixed-layer depth to predict the heat entrainment rates was developed by McNaughton and Spriggs (1986). One limitation of this model involves neglecting the contribution of moisture to buoyancy. This simple model does not appropriately represent the mixed-layer growth for some situations, as seen later in this chapter. Another limitation related to models is that they are not designed to describe specific conditions as the growth of the mixed layer following storms conditions, such as squall lines and mesoscale convective systems. Thus, the first approach

to develop new models is to describe the thermodynamic attributes that may characterize the precedent conditions of storms and the recovery-phase after the passage of storms.

All the thermodynamic variables were obtained from the measurements of air pressure, relative humidity, and temperature. To first evaluate the thermodynamic attributes of the convective boundary layer, the mixed layer depth will be obtained based on the upper air soundings measurements. The mixed-layer depth (h_{ML}) was obtained from the maximum value of the second derivative of the virtual potential temperature $\left(\partial^2 \theta_v / \partial z^2\right)$ (e.g., Strong et al., 2005). Subsequently, averaged mixed-layer specific humidity ($\langle q \rangle_{ML}$) and virtual potential temperature ($\langle \theta_v \rangle_{ML}$) were obtained by integrating the quantities from the surface to the top of the mixed layer (h_{ML}) as

$$\langle \theta_v \rangle_{ML} = \frac{1}{h_{ML}} \int_0^{h_{ML}} \theta_v(z)dz, \tag{2.1}$$

$$\langle q \rangle_{ML} = \frac{1}{h_{ML}} \int_0^{h_{ML}} q(z)dz. \tag{2.2}$$

The virtual potential temperature is a convenient variable used to describe the static stability of the atmospheric layers, allowing the identification of the convective boundary layer. It is a conserved variable, which also considers the amount of water vapor present in the atmosphere. The specific humidity, which is the ratio of the mass of water vapor to the mass of air (dry air + water vapor). The importance to account the specific humidity is because the water vapor content in the atmosphere regulates the evaporation rate. Also, it is the variable that can determine the limit of cloud formation and the height of the cloud base (de Arellano et al., 2015).

The strength of virtual potential temperature ($\Delta \theta_v$) and specific humidity (Δq) inversions above the mixed layer ($\Delta \theta_v = \theta_{v(h_{ML}+\partial h)} - \theta_{v(h_{ML})}$, and $\Delta q = q_{(h_{ML}+\partial h)} - q_{(h_{ML})}$) were estimated to determine how boundary layer attributes changed over the course of the day. These quantities were calculated based on the measurements observed at the top of the mixed-layer (h_{ML}) and at height $h_{ML} + \partial h$, where ∂h is the thickness of the entrainment zone. Above the mixed layer (e.g., $z > h_{ML} + \partial h$), variations of θ_v and q with altitude were also estimated:

$$\gamma_{\theta v} = \frac{\partial \theta_v}{\partial z} \tag{2.3}$$

$$\gamma_q = \frac{\partial q}{\partial z}. \tag{2.4}$$

Warming rates of the convective boundary layer result from exchanges of heat between surface and atmosphere, and at the top of the mixed layer via entrainment. At the surface, sensible (H_v) and latent (LE) heat fluxes densities were obtained from kinematic quantities $\overline{(w'\theta_v')}_0$ and $\overline{(w'q')}_0$ computed from eddy covariance measurements (see equations (2.5) and (2.6)). For humid environments is defined the virtual sensible flux (Eq. 2.7) (Betts, 1992).

$$H = \left(\overline{w'\theta_v'}\right)_0 \rho c_p, \tag{2.5}$$

$$LE = \left(\overline{w'q'}\right)_0 \rho L_v, \tag{2.6}$$

$$H_v = H + 0.07LE \tag{2.7}$$

where ρ is the air density, c_p is the specific heat capacity of air at constant pressure, L_v is the latent heat of vaporization, w is the vertical velocity, and q is the specific humidity. Primed quantities are deviations from the mean values and the overbar denotes the temporal averaging performed over 30-minute periods. The entrainment fluxes can also be estimated, using the variables obtained at the top of the convective boundary layer. However, the kinematic heat flux is only obtained at the surface, and when this is a variable of interest, a closure method is often adopted to estimate the kinematic heat fluxes at the top of the mixed layer, assuming that this value is twenty percent of the kinematic heat fluxes at the surface (e.g., Stull, 1988).

For the case studies, when the CAPE (convective available potential energy) is missing it is estimated for the specific times when the soundings were launched, according:

$$CAPE = \int_{LFC}^{EL} \frac{(T_p(z) - T_e(z))}{T_e(z)} g dz \tag{2.8}$$

where T_e is the environment temperature, T_p is the parcel temperature, z is the height, LFC is the level of free convection, EL is the equilibrium level, and g is the acceleration due to the gravity.

The equivalent potential temperature (Eq. 2.9) at the surface was also derived because it is a conserved variable that is conserved even if water vapor condenses, and can be used to evaluate both temperature and moisture content. Relative high equivalent potential temperatures in a region with instability is an ingredient to induce mesoscale convective systems.

$$\theta_e \cong \theta + \frac{L_v}{c_p r} \tag{2.9}$$

In the equivalent potential temperature equation, θ is the potential temperature, L_v is the latent heat of vaporization, c_p is the specific heat capacity of the air at constant pressure, and r is the water vapor mixing ratio. All these variables are described in Appendix B.

2.4 Case Studies

2.4.1 Undisturbed days in Amazon for 2014/15: wet and dry season

During the dry season, the subsidence suppresses deep convection and results in a large difference in the relative humidity of the troposphere (Betts et al., 2009b), and the presence of shallow cumulus is observed only if the surface heating is strong enough to create some convection (Betts et al., 2009b). In this case, the absence of deep convection leads to reduced rainfall events, but the presence of more particles, due to biomass burning, for example, will enhance cloud formation.

A clear sunny day was chosen to represent typical conditions of an undisturbed day during the dry season over the site of study, 15 June 2014. The satellite images, not presented here, show that 13, 14 and 15 June 2014 were all non-precipitating days in the Amazon basin. A low-pressure system over the south region of Brazil, along with the subsidence generated due to the high-pressure system over the site of the study was persistent, allowing these consecutive days of clear sky in the northern region of the country.

The 15 June 2014 had a maximum incoming solar radiation at 13:00 LT of 956 W m^{-2} (Figure 2.8a). The increase of the surface temperature allowed the maximum virtual sensible heat flux and the latent heat flux to attain 163.6 (13:00 LT) W m^{-2} and 329.4 W m^{-2} (09:30 LT), respectively (Fig. 2.8c), warming which is also shown in the increase of the mean virtual potential temperature of the mixed-layer ($\langle\theta_v\rangle_{ML}$), which varied from 301.2 K (07:00 LT) to 305.5 K (13:00 LT). The surface warming also generated some convection, and an increase of the wind speed near the surface is observed in the afternoon, which attained its maximum (4.03 m s^{-1}) at 14:00 LT (Figure 2.8d).

The layer-averaged specific humidity ($\langle q\rangle_{ML}$) decreased from 17.7 g kg^{-1} at 07:00 LT to 11.8 g kg^{-1} at 13:00 LT, as the layer was getting drier. With the increase in the mixing of the dry air from the free atmosphere into the CBL, the strength of the virtual potential temperature inversion became weaker, reduced in 50%, which allowed large CBL growth rates. Also, virtual potential temperature lapse rate (γ_{θ_v}) increased from 2.4 K km^{-1} (07:00 LT) to 6.7 K km^{-1} (13:00 LT). The surface equivalent potential temperature for this day was on average 343.8 K and the average specific humidity was 17.6 g kg^{-1} (Figure 2.8b). The estimated CAPE values were high in the afternoon, reaching up to 3151 J kg^{-1} (Figure 2.8e).

Table 2.1: Thermodynamic attributes for 15 June 2014, derived from the measurements at T3 site

t (LT)	07:00	13:00
h_{ML} (m)	64	1807
$\langle\theta_v\rangle_{ML}$ (K)	301.2	305.5
$\langle q\rangle_{ML}$ (g kg^{-1})	17.7	11.8
Δq (g kg^{-1})	-0.9	-7.1
$\Delta\theta_v$ (K)	1.2	0.6
γ_{θ_v} (K km^{-1})	2.4	6.7
γ_q (g kg^{-1} km^{-1})	-1.1	-5.8

Because of the diurnal variation of the incoming solar radiation and the energy fluxes, the shallow CBL in the early morning had a rapid growth rate during the late morning and early afternoon (290 m h^{-1}), allowing the mixed layer to grow from 64 m (07:00 LT) to 1807 m (13:00 LT) (Figure 2.8e). Some studies (e.g., Fisch et al., 2004; Fitzjarrald and Garstang, 1981; Strong et al., 2005) reported maximum mixed layer depth between 710 to 1480 m, and growth rates of 210 m h^{-1} at 14:00 LT (Fisch et al., 2004) up to 360 m h^{-1} (Martin et al., 1988), for undisturbed days, which corroborates the presented results.

Figure 2.8: Case study of an undisturbed day in the dry season: 15 June 2014. Diurnal cycle of: (a) incoming solar radiation, (b) equivalent potential temperature (θ_e) and specific humidity (q), (c) virtual sensible heat flux (H_v) and latent heat flux (LE), (d) wind speed, (e) convective available potential energy (derived from soundings), (f) precipitation, and profiles of (g) virtual potential temperature (θ_v).

In contrast, the wet season has the diurnal variation of the CBL mainly dominated by large-scale convection (Fisch et al., 2004) and the mixed layer growth is usually slower, a fact that can be attributed to eventual early morning precipitation (Garstang et al., 1990). The wet season presents a boundary layer close to moist neutrality (Betts et al., 2009b) and organized synoptic scale systems produce large rainfall in wide areas, more often than during the dry season (Garstang and Fitzjarrald, 1999). Then, the wet season is characterized for more cloud cover due to the presence of convective cloud systems (Betts et al., 2009b). However, for the purpose of characterization of the CBL, a non-precipitating day for the season was identified, 31 October 2014. Similarly to 15 June 2014, it is

Table 2.2: Thermodynamic attributes for 31 October 2014, derived from the measurements at T3 site

t (LT)	07:00	13:00
h_{ML} (m)	145	1541
$\langle\theta_v\rangle_{ML}$ (K)	305.5	307.2
$\langle q\rangle_{ML}$ (g kg^{-1})	18.5	13.7
Δq (g kg^{-1})	-3.8	-0.5
$\Delta\theta_v$ (K)	2.1	0.2
γ_{θ_v} (K km^{-1})	3.8	3.8
γ_q (g kg^{-1} km^{-1})	-2.3	-2.0

found that the previous days (28, 29, and 30 October) were also non-precipitating days. On 31 October 2014, an area under the influence of high pressure is observed, through satellite images (not shown here), over the Amazon basin; and, an area of low pressure in the south and southeast of Brazil, due to a cold front approaching the region. The high-pressure system suppressed the cloud formation and allowed more incoming solar radiation to reach the surface, warming up the air in the lower levels of the troposphere, and creating conditions to a rapid growth of the mixed layer. For this day, the high surface evaporation (latent heat flux equals to 432.9 W m^{-2} at 15:00 LT; Figure 2.9c) generates convective instability, and the formation of some clouds are identified after this time, as observed through the reduction of the incoming solar radiation (Figure 2.9a). The virtual sensible heat flux did not exceed 87.7 W m^{-2} for this day (Fig-

ure 2.9c). The equivalent potential temperature had the average value of 351.4 K and specific humidity of 19.8 g kg^{-1} (Figure 2.9b). Maximum wind speed at the surface was registered in the middle of the afternoon, 5.3 m s^{-1} at 13:00 LT, (Figure 2.9d), when convection is also more intense. The convective available potential energy did not surpassed 2110 J kg^{-1} (Figure 2.9e). Under these conditions, the mixed layer could grow from 145 m, at 07:00 LT, to 1541 m, at 13:00 LT (Fig. 2.9e).

The mean virtual potential temperature of the mixed-layer ($\langle\theta_v\rangle_{ML}$) varied from 305.5 K (07:00 LT) to 307.2 K (14:00 LT), according the available soundings. The mean specific humidity ($\langle q\rangle_{ML}$) was 18.5 g kg^{-1} at 07:00 LT and 13.7 g kg^{-1} at 13:00 LT. Similar to the conditions found in the previous case study for the dry season. The virtual potential temperature lapse rate above the mixed layer was 3.8 K m^{-1} (both times). The strength of the virtual potential temperature inversion was 2.1 K at 07:00 LT and 0.2 K at 14:00 LT.All these conditions favored the formation of a deep mixed layer ($>$1500 m) that exceeded previous depths found in the literature, of approximated 1200 m for this season (e.g., Garstang et al. (1990); Fisch et al. (2004)).
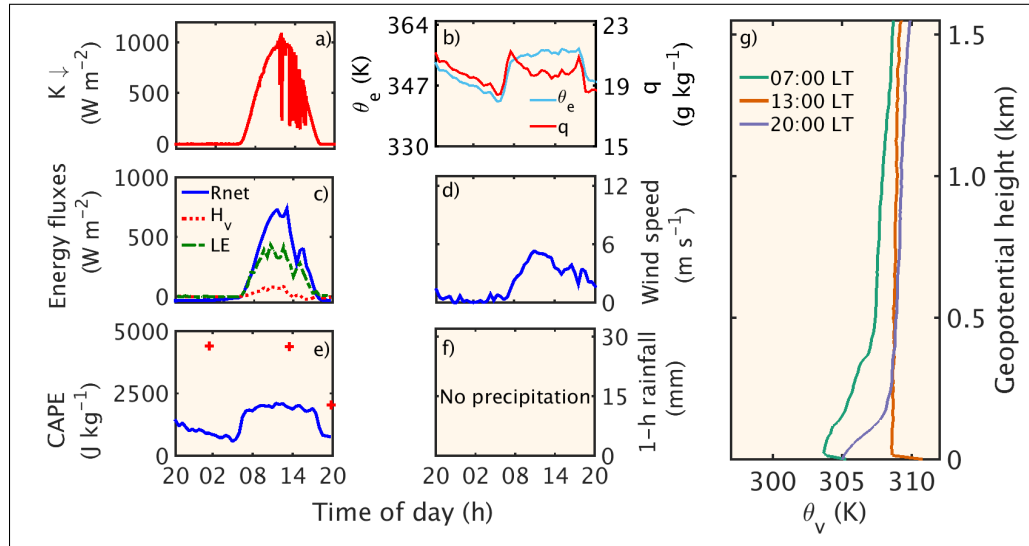
Figure 2.9: Case study of an undisturbed day in the wet season, 31 October 2014. Diurnal cycle of: (a) incoming solar radiation, (b)equivalent potential temperature (θ_e) and specific humidity (q), (c) net radiation (R_net), virtual sensible heat flux(H_v) and latent heat flux (LE), (d) wind speed, (e) convective available potential energy (red symbols: estimated from soundings, solid line: measured), (f) precipitation, and profiles of (g) virtual potential temperature (θ_v).

In addition, to complement the characterization of undisturbed days, and in an effort to start understanding better the dynamic features of the CBL, the Appendix C is a study that evaluates the performance of exponential and hyperbolic models of wind speed profile within the Amazon forest canopy. In the Appendix C, five wind speed models are compared to the measurements, and it is a starter point to amplify the knowledge in this field. It can be used integrated with future studies related to the surface and the convective boundary layer.

2.4.2 Mesoscale convective system and the mixed-layer growth

On 15 October 2014 was identified an isolated mesoscale convective system (MCS) moving westward over the site of study at 04:00 LT. The MCS passage resulted in a total rainfall of 30.8 mm within 6 hours of continuous precipitation, being the first three hours with the most intense rainfall (Figure 2.10f).

As the air is advected due to the storm formation, the wind speed at the surface increased by 6 m s^{-1} (Figure 2.10d). In addition, the cold and dry air from the storm downdrafts reduced the equivalent potential temperature by approximately 7 K and the specific humidity by 2.12 g kg^{-1} (Figure 2.10b). As the surface started warming up after the sunrise and the evapotranspiration started taking place, the air warmed up at a rate of 1.47 K h^{-1} and humidified at a rate of 0.74 g kg^{-1} h^{-1}.

High incoming solar radiation characterized this day, reaching maximum of 1208.6 W m^{-2} at 13:30 LT (Figure 2.10a). This incoming solar radiation contributed to a high virtual sensible heat flux, which maximum reached 87.7 W m^{-2} (13:30 LT), and to a high latent heat flux, with a maximum of 433.0 W m^{-2} (13:00 LT) (Figure 2.10c). The convective potential available energy attained the maximum of 2578 J kg^{-1} (Figure 2.10e). The high incoming energy warms the air parcels increasing its buoyancy, therefore producing thermal turbulence, which will contribute to the formation of a deep CBL. These conditions led to a mixed-layer growth rate of 155 m h^{-1} between 08:00 LT and 14:00 LT. The growth rates for the case studies for undisturbed days are 1.5 to more than 2 times larger than for this presented case.

Table 2.3: Thermodynamic attributes for 15 October 2014, derived from the measurements at T3 site

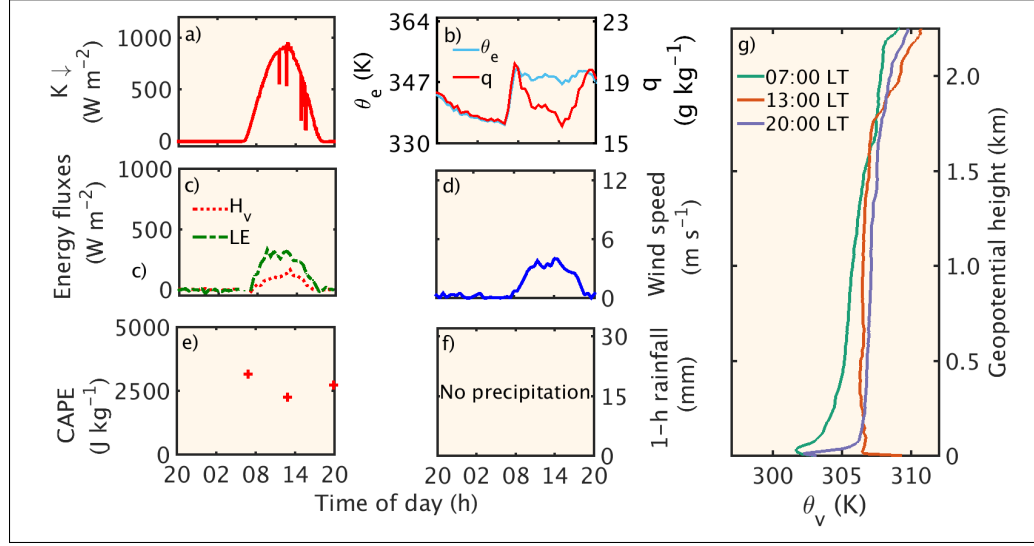| t (LT)	08:00	14:00
h_{ML} (m)	223	1150
$\langle \theta_v \rangle_{ML}$ (K)	296	301.2
$\langle q \rangle_{ML}$ (g kg^{-1})	15.8	16.4
Δq (g kg^{-1})	-0.2	-0.7
$\Delta \theta_v$ (K)	1.3	0.3
γ_{θ_v} (K km^{-1})	2.4	4.1
γ_q (g kg^{-1} km^{-1})	-4.3	-1.4
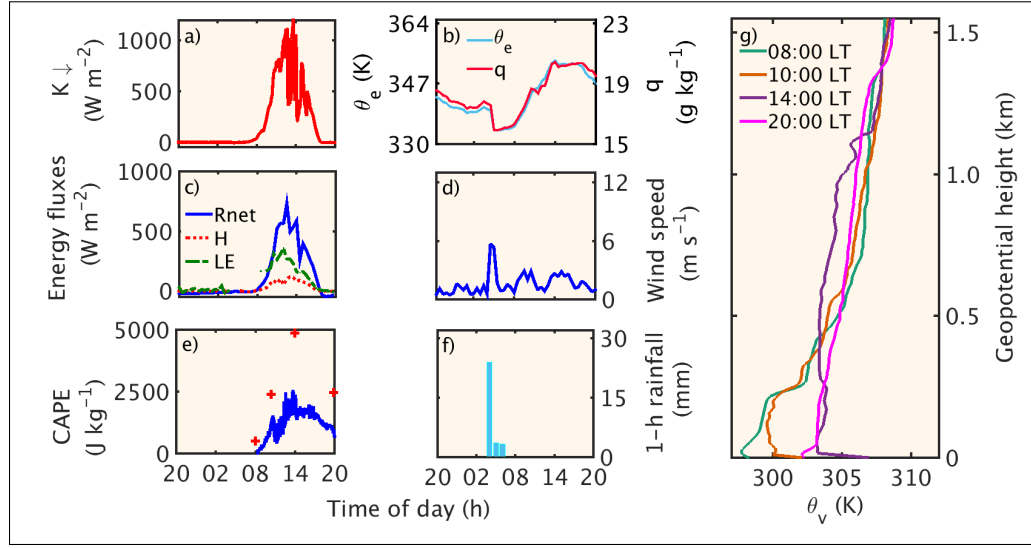
Figure 2.10: Case study of a disturbed day, 15 October 2014. Diurnal cycle of: (a) incoming solar radiation, (b)equivalent potential temperature (θ_e) and specific humidity (q), (c) net radiation (R_{net}), virtual sensible heat flux(H_v) and latent heat flux (LE), (d) wind speed, (e) convective available potential energy (red symbols: derived from soundings, solid line: measured), (f) precipitation, and profiles of (g) virtual potential temperature (θ_v).

The temperature inversion at the entrainment zone varied from 1.3 K (08:00 LT) to 0.3 K (14:00 LT). The capping inversion became weaker over the day, similarly to the undisturbed day. Also, the lapse rate above the mixed layer varied from 2.4 K km^{-1} (08:00 LT) to 4.1 K km^{-1} (14:00 LT). The mean virtual potential temperature of the CBL ($\langle\theta_v\rangle_{ML}$) varied from 296 K to 301.2 K and the mean specific humidity ($\langle q\rangle_{ML}$) varied from 15.8 to 16.4 g kg^{-1}, respectively at 08:00 and 14:00 LT (Figure 2.10g).

The storm passage, during the nighttime, caused an additional cooling in the lower layer of the troposphere which took time to warm up. Also, the cloudy conditions in the early morning decreased the incoming solar radiation, slowing the formation of a deep mixed layer. Which is in agreement with the observation made by Garstang et al. (1990) who says that early morning precipitation can delay the growth of the mixed layer.

Even though the passage of storms over the night can slow down the development of a deep mixed layer, the main impacts in its development can be seen when storms occur during the day. The passage of a MCS over the site of study on 09 November 2014, resulted in an accumulated rainfall of 43.6 mm (Figure 2.11f). The storm formation led to an increase in the wind speed of 10.6 m s^{-1} (Figure 2.11d).

The high CAPE (2895 J kg^{-1}) is another indicator of the strength of the storm (Figure 2.11e). During the passage of the storm, the equivalent potential temperature was reduced about 22 K and the specific

Table 2.4: Thermodynamic attributes for 09 November 2014, derived from the measurements at T3 site

t (LT)	08:00	14:00
h_{ML} (m)	64	312
$\langle\theta_v\rangle_{ML}$ (K)	300.6	297.3
$\langle q\rangle_{ML}$ (g kg^{-1})	19.0	16.4
Δq (g kg^{-1})	-0.2	-0.4
$\Delta\theta_v$ (K)	1.6	3.2
γ_{θ_v} (K km^{-1})	1.6	5.3
γ_q (g kg^{-1} km^{-1})	-1.7	-3.0

humidity by 5.76 g kg^{-1} (Figure 2.11b), due to the storm downdrafts carrying cold and dry air from aloft to the CBL. After the rainfall, the warming rate of the CBL was 0.78 K h^{-1}, almost half of the rate for 15Oct, and the humidification rate was four times smaller than on 15 October 2014, 0.18 g kg^{-1}. These warming and humidification rates are up to 7 times lower than the average for typical undisturbed days. The mean virtual potential temperature of the CBL ($\langle\theta_v\rangle_{ML}$), for this day, varied from 300.6 K to 297.3 K and the mean specific humidity ($\langle q\rangle_{ML}$) varied from 19.0 to 16.4 g kg^{-1}, respectively at 08:00 and 14:00 LT (Figure 2.11g), which quantifies the effect of cold and dry air brought from storm downdrafts to the ABL. The daily average solar radiation on 09 November 2014 was equivalent to 21% of the average for 15 October 2014, for example (Figure 2.11a), and virtual sensible heat flux (daily average of 15.4 W m^{-2}), resulted in weak surface heating. Consequently, low growth rates of the ML are observed, which attained only 50 m h^{-1}, with a ML depth of 312 m at 13:00 LT. This value represents approximately a quarter of typical values for undisturbed days. The temperature inversion strength at the top of the ML varied between 1.6 K (08:00 LT) and 3.2 K (14:00 LT). The passage of storms during the day also led to a more stable entrainment zone, limiting the growth of the CBL.
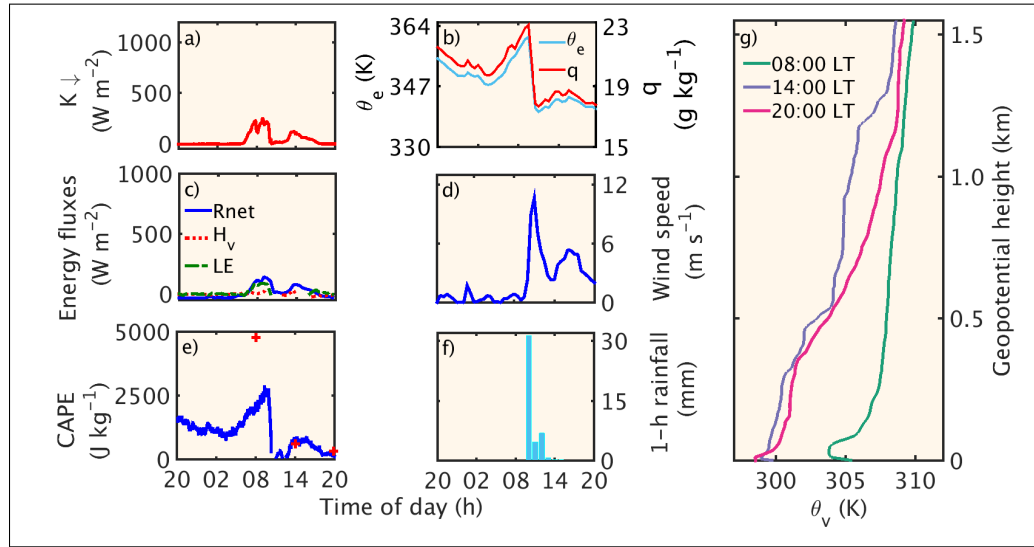
Figure 2.11: Case study of a disturbed day, 09 November 2014. Diurnal cycle of: (a) incoming solar radiation, (b)equivalent potential temperature (θ_e) and specific humidity (q), (c) net radiation (R_{net}), virtual sensible heat flux(H_v) and latent heat flux (LE), (d) wind speed, (e) convective available potential energy (red symbols: derived from soundings, solid line: measured), (f) precipitation, and profiles of (g) virtual potential temperature (θ_v).

2.5 Averaged convective boundary layer growth under undisturbed and disturbed conditions

From the data set obtained during the GoAmazon field campaign, an ensemble of 23 random undisturbed days were selected. Typical mixed layer depth observed for this ensemble was 199 ± 26 m at 08:00 LT

and 1088 ± 81 m at 14:00 LT. Within this ensemble, the difference between the dry and wet season mixed layer depth, on average, is less than 40 meters in the morning and less than 100 meters in the afternoon. The wet season shows a depth of 207 ± 32 m at 08:00 LT and growth rate of 148 m h^{-1}, on average (Figure 2.12a). A residual layer is observed at 20:00 LT, which attains 1387 ± 127 m, meaning that in the late afternoon, the mixed layer could be deeper than at 14:00 LT. However, due to the lack of information about the CBL between 14:00 and 20:00 LT, it is not possible to know the depth of the CBL in this period. For the dry season, a shallower CBL is observed at 08:00 LT (184 ± 47 m), with the same growth rate observed in the wet season (Figure 2.12). This may be related to the small ensemble size; but, regardless the ensemble size and the methods used to obtain the mixed layer depth, the present results are similar to results reported in previous studies (e.g., Fisch et al., 2004; Fitzjarrald and Garstang, 1981; Strong et al., 2005).
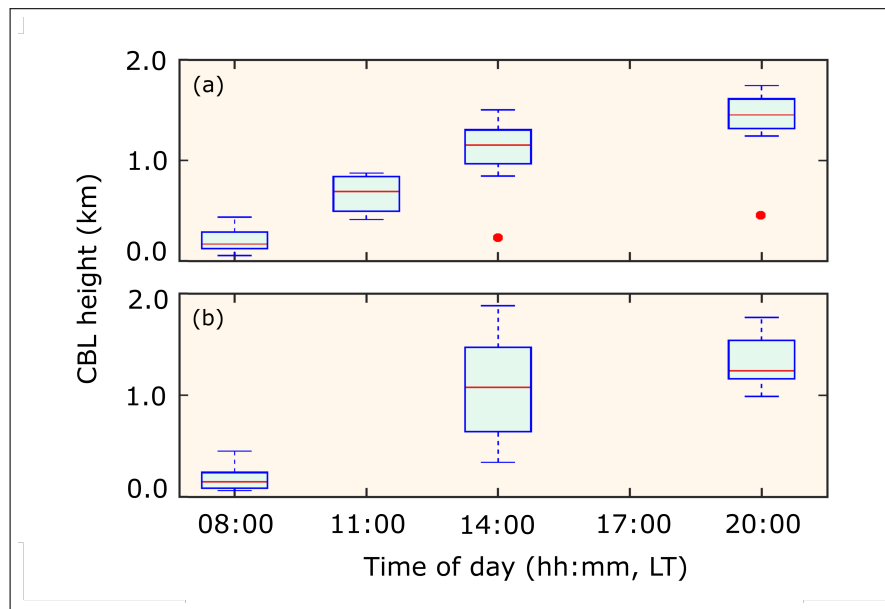
Figure 2.12: Convective boundary layer growth for undisturbed days. (a) Wet season and (b) Dry season. The box has 50% of the data and the redline indicates the median (25% of the data over the median and 25% under the median), the other quartiles are represented by the upper (25%) and lower (25%) whiskers. The red symbols are the outliers

Despite the large period of study, the lack of soundings in the afternoon limited the analysis of undisturbed days, and it is not possible to track the CBL depth after all precipitation events in this period. Also, the variable time when the precipitations occur leads to many possibilities on how fast the CBL can grow. However, despite such limitations, by taking an ensemble of 10 days with precipitation in the nighttime, and an ensemble of 27 days with precipitation during the daytime, we can see how long the mixed-layer takes to grow from the time of the precipitation, and how it was before the precipitation. The criteria for defining the ensemble was to consider only events when the rainfall rates exceeded 20 mm h^{-1}, which is a characteristic rainfall rate for MCSs over the site of study (Fuentes et al., 2016). For the nighttime period, the CBL in the previous day of the ensemble (6 to 20 hours before the rain event) was very variable, but

considerably deep (up to an average of 1067 m) (Figure 2.13a). About 8 hours after the precipitation, the ML reaches, on average, growth rates of 202.7 m h^{-1}, which is comparable to undisturbed days. For the days with daytime precipitation, a shallow ML is observed up to 5 hours before the rain event, with an average depth of 170 m (Figure 2.13b). However, the CBL depth was very variable after the passage of a storm. For some periods, growth rates were, on average, as high as 835 m h^{-1} (9 hours after the storm), and as low as 50 m h^{-1} (2 hours after the storm). It shows the high variability of the mixed-layer growth before and after the passage of mesoscale convective systems in the Amazon rainforest.
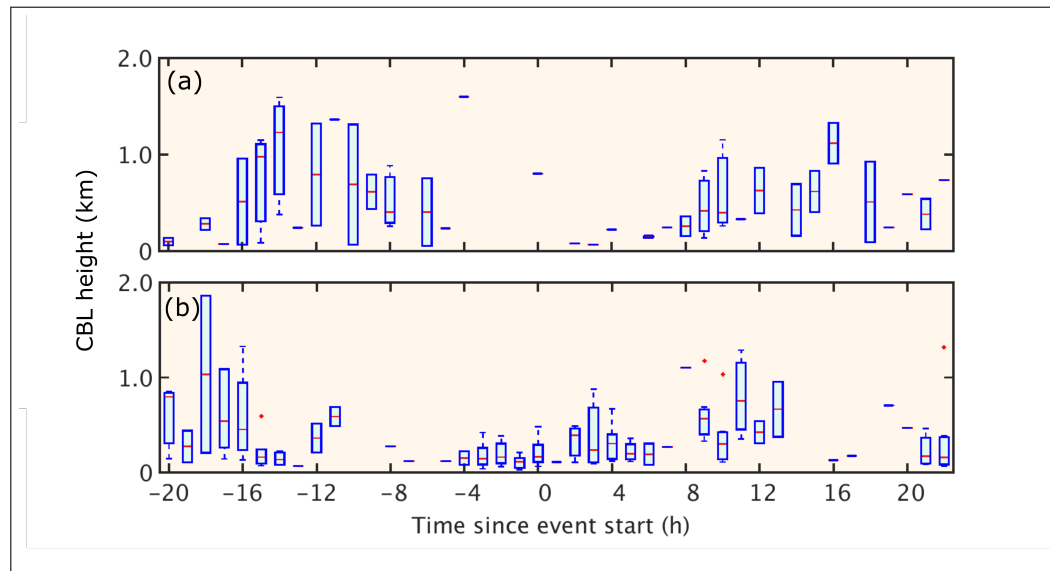
Figure 2.13: Convective boundary layer growth for disturbed days. (a) Nighttime occurrence of a MCS and (b) daytime occurrence of a MCS. The box has 50% of the data and the redline indicates the median (25% of the data over the median and 25% under the median), the other quartiles are represented by the upper (25%) and lower (25%) whiskers. The red symbols are the outliers

Some of the surface variables are summarized in Figure 2.14 regarding the time of the precipitation event, using the same ensemble of the Figure 2.13b, except when there was no measurement for a specific day or variable and the day was omitted from the ensemble. The averaged variables show a common feature prior to the precipitation event. The sensible heat flux, latent heat flux, equivalent potential temperature, specific humidity and convective available potential energy all decrease drastically at the moment antecedent the precipitation, and even after about 3 hours after the end of the rainfall do not return to its initial state. There are several reasons for that. Despite the preferential time of precipitation observed for mesoscale convective systems, there is still plenty of variabilities evolved regarding the onset and offset of the precipitation, which is observed in the variability of the measured data. It also implies that the precipitation event could be registered around, for example, 16:00 LT. Even if just after the precipitation there is a clear sky, it is not possible that the heat fluxes increase as much as in the middle of the day (e.g., 12:00 LT), and the same way, the temperature will not increase, then it is not a favorable condition for CBL growth. Thus, the goal here is to quantify by how much these variables are modified in disturbed days.

Thus, the sensible heat flux is reduced by an average of 38.0 W m^{-2} and latent heat flux by 223.0 W m^{-2} (Figure 2.14a). The diminish of solar radiation due to the increasing cloudiness prevents the warming of the lower layers of the atmosphere, causing the gradual decrease in the intensity of these variables. Interestingly the latent heat flux has a peak half-hour before the precipitation (from an average of 70.0 W m^{-2} to 223.0 W m^{-2}, Figure 2.14b), what is explained by the fact that there is an intense transport of moisture from the surface to the higher levels of the atmosphere at this moment. The averaged CAPE was approximately 1893.0 J kg^{-1} (Figure 2.14e) before the rainfall starts, which is a compatible value expected for the occurrence of storms in the Amazon rainforest. The specific humidity and the equivalent potential temperature increased, for these cases, respectively, by 1.27 g kg^{-1} and 5.2 K (Figure 2.14c,d, zoomed out in Figure 2.15). The importance of these variables is linked to the transport of moisture and temperature across the atmospheric boundary layer. The decrease in these variables is the result of the downdrafts associated to the storm passage, what brings dry and cold air from the layers above the convective boundary layer. Thus, these changes in moisture content and temperature at the surface are directly linked to the strength of the downdrafts, in contrast to the CAPE value that is related to the strength of the updraft, since it is the amount of energy available for convection.
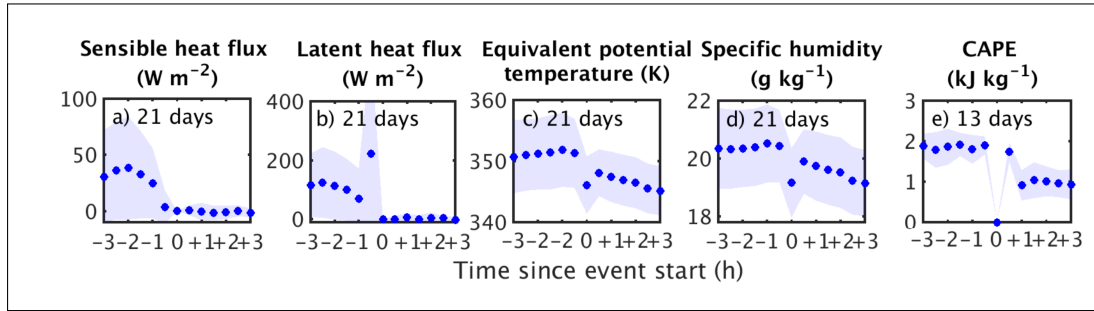
Figure 2.14: Variation of thermodynamic variables at surface for mesoscale convective systems passage (time 0): 3 hours before the system's passage (-3) up to 3 hours after (+3). (a) Sensible heat flux, (b) latent heat flux, (c) equivalent potential temperature, (d) specific humidity, and (e) convective available potential energy. The shadow represents the standard deviation of the data.
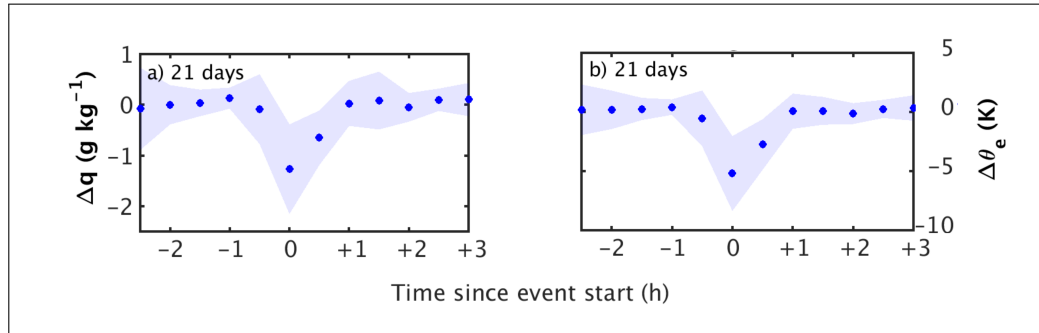
Figure 2.15: (a) Variation of specific humidity and (b) equivalent potential temperature with the time of precipitation event.The shadow represents the standard deviation of the data.

Regarding the diurnal pattern of the variables explored above, even with the different times of precipitating events, it is seen a similar pattern comparable in "shape" to undisturbed days, but different in intensity, as expected (Figure 2.17). While for sensible heat flux undisturbed days can have on average more than 100.0 W m^{-2} around noon, the disturbed days did not exceed the average of 55.0 W m^{-2} in the same period (Figure 2.16a). The latent heat flux, however, exhibited a slightly higher value for disturbed days than undisturbed days. The maximum observed during the dry season (wet season) for the undisturbed condition is the average of 268.0 W m^{-2} (253.5 W m^{-2}), and for the condition of mesoscale convective systems has recorded the average of 270.9 W m^{-2} (Figure 2.16b). It can be attributed to the more intense activity of transport of moisture in disturbed conditions, as mentioned previously for the analysis focused on the time of the precipitation. Equivalent potential temperature has a mean diurnal value of 346.7 K (Figure 2.16c), and the specific humidity, 19.4 g kg^{-1} (Figure 2.16d), and CAPE, 1107.0 J kg^{-1} (Fig. 2.16e). Compared to undisturbed conditions, equivalent potential temperature, specific humidity, and CAPE did not show a significant difference in daily averages.
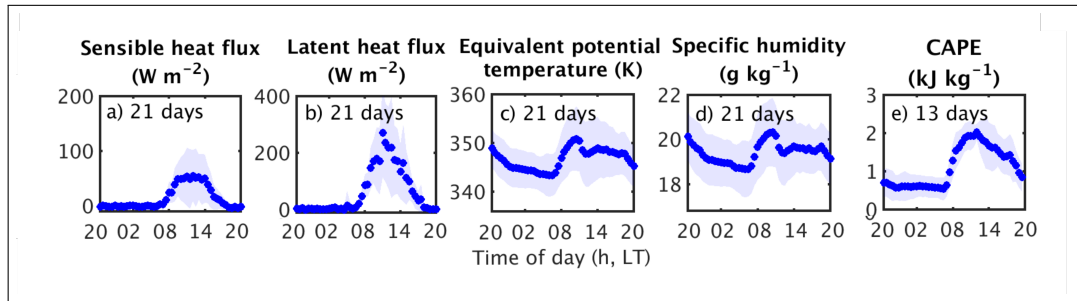
Figure 2.16: Diurnal variation of thermodynamic variables at surface for days when there is a MCS passage. (a) Sensible heat flux, (b) latent heat flux, (c) equivalent potential temperature, (d) specific humidity, and (e) convective available potential energy. The shadow represents the standard deviation of the data.

Some averaged variables were then estimated according to the time of the day. On average, the mixed layer reached 203 ($\pm$ 137) m at 07:30 LT, 1137 ($\pm$ 744) m at 10:00 LT, and 1085 ($\pm$ 700) m at 13:00 LT (Figure 2.17a). The other variables did not show a big variation over the day, remaining pretty much constant, however, with a big dispersion (Figure 2.17c-h). Some of these variables will be later used on modeling within this work.
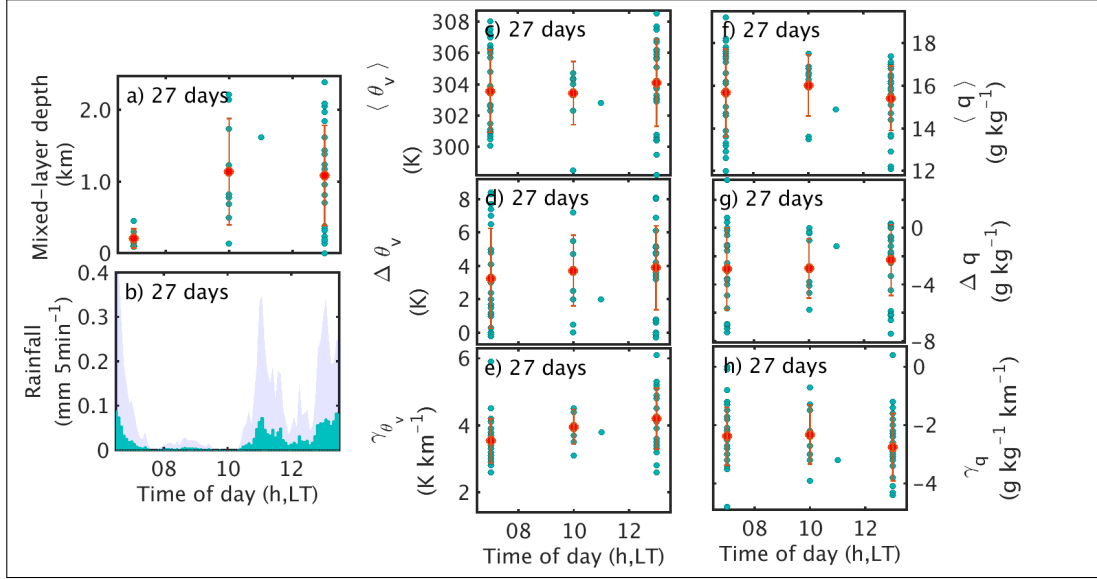
Figure 2.17: Thermodynamic attributes of the convective boundary layer (CBL) for the cases of MCS passage, for an ensemble of 27 days. (a) CBL depth, (b) 5-minute averaged rainfall rate, (c) mixed layer averaged virtual potential temperature, (d) strength of the virtual potential temperature inversion at the top of the CBL, (e) virtual potential temperature lapse rate above the CBL, (f) mixed layer averaged specific humidity, (g) strength of specific humidity variation at the top of the CBL, (h) specific humidity lapse rate above the CBL. The bars (a, c-h) and the shadow (b) are the standard deviation from the mean values.

A study made by Schiro and Neelin (2018) have a similar approach to study organized systems, such as mesoscale convective systems and unorganized systems. One of the differences between Schiro and Neelin (2018) study and the current results presented is the precipitation rate used to determine the events for the study, while Schiro and Neelin (2018) used 10 mm h^{-1}, the present study used 20 mm h^{-1}. Also, the days identified in this work, when mesoscale convective systems passed over the site of study, are not the same than the days presented by Schiro and Neelin (2018), due to the different methods used to determine MCSs. However, despite such differences, the results obtained for the conditions before and after the passage of storms are coherent. In addition, Schiro and Neelin (2018) did not focus on the changes in the convective boundary layer depth, which is the main contribution of the current work.

2.5.1 Modeling the convective boundary layer for disturbed days

This section will briefly show how a model responds to the conditions present in the atmospheric boundary layer for disturbed days, specifically for mesoscale convective systems. The physical model chosen to compare the growth of the convective boundary layer against the observations is a model proposed by McNaughton and Spriggs (1986), that assumes that the "*vegetation completely covers the ground and, then, the transpiration is the only important component of evaporation*".

McNaughton and Spriggs (1986) used two formulations to describe the entrainment process, which neglect the contribution of moisture to buoyancy and assumes that the height (h) times the difference of the virtual potential temperature at the surface and at the mixed layer is constant. Other implicit assumptions

are, for example, related to the turbulence, as homogeneity, stationary, and ergodicity. It results in a relationship for entrainment velocity (dh/dt) that is not dependent on wind (Eq. 2.10). This model is, therefore, a mixed-layer model based only on thermodynamic variables:

$$\frac{dh}{dt} = \frac{H_v}{\rho c_p h \gamma_v} \tag{2.10}$$

where the H_v is the virtual sensible heat flux (Eq. 2.7), h is the convective boundary layer depth, c_p is the specific air capacity at constant pressure, and γ_v is the virtual temperature inversion strength, given as:

$$\gamma_v = \gamma_\theta + 0.61 T \gamma_q \tag{2.11}$$

and γ_θ is given by Eq. 2.3 and γ_q by Eq. 2.4.

All the variables are obtained at the surface, except the temperature strength inversion, which is obtained from soundings. However, when the soundings are available, it is possible to obtain the CBL growth from the temperature profiles, through methods as the virtual potential temperature derivative, as explained in the methodology section, and there is no real need to model the CBL height. Then, to perform this simple model for the case studies it will be performed using the values of γ_v obtained from the soundings of each day and, a second comparison is using the averaged values obtained from 27 case studies, as in Figure 2.17, which are then interpolated (cubic spline) for each half hour from 07:00 to 14:00 LT. This second comparison will rely on knowing only the surface thermodynamic variables to predict the entrainment rates since the virtual potential temperature strength is prescribed as the averaged values when the occurrence of convective systems. Also, for comparison, four (4) additional estimates of the mixed layer height are incorporated here. The ARM (Atmospheric Radiation Measurement) - U.S. Department of Energy has also the data set for the height of the convective boundary layer estimated by different methods: the Liu-Liang method, the Heffter method, and the Bulk Richardson method for two thresholds (0.5 and 0.25). These methods are described by Sivaraman et al. (2013) and summarized in Appendix B.

The first hypothesis is that the model will reasonably predict the convective boundary layer growth when using the variables obtained for each case of study. However, as seen in Figure 2.18, the model overestimated the mixed layer growth for 09 November 2014, and underestimate it for two out of three estimates of the mixed layer height. There is also no preference of methodology to estimate the CBL height when comparing to the model prediction. For 15 October 2014, there is no relative error larger than 63%, except using the second derivative of virtual potential temperature method, when the relative error is as high as 120% when the model is compared to the observation. For the 09 November 2014 case, the relative error surpassed 1000% comparing the second derivative of virtual potential temperature against the model at 07:30 LT, while the best estimate was at 13:30 LT comparing the Bulk Richardson number (0.5), when the absolute error was only 18%.
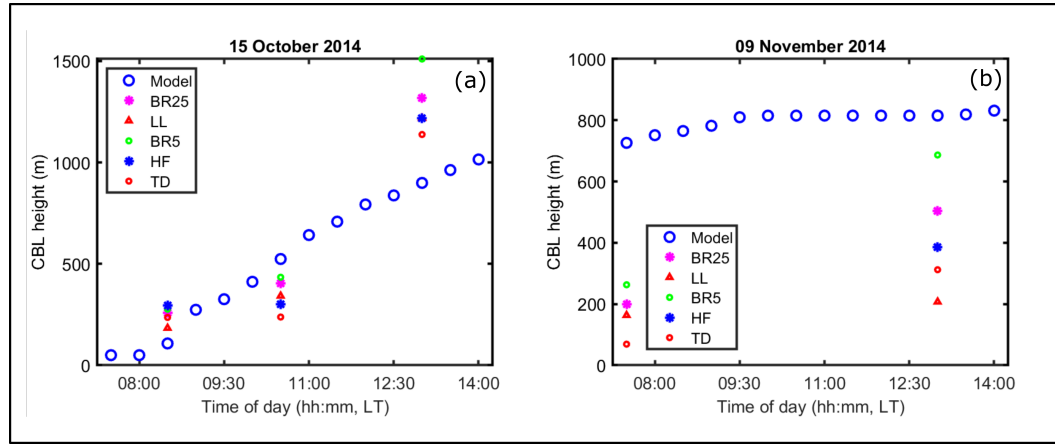
Figure 2.18: Convective boundary layer height using a mixed-layer model (McNaughton and Spriggs, 1986) for the case studies of mesoscale convective system: (a) 15 October 2014 and (b) 09 November 2014. BR25 is the Bulk Richardson method for a 0.25 threshold, LL is the Liu-Liang method, BR5 is the Bulk Richardson method for 0.5 threshold, HF is the Heffter method and TD is the virtual potential temperature derivative method.

A second comparison is made using the averaged values of the virtual temperature lapse rate (γ_v) applied to the case studies. The Figure 2.19 illustrates how, interestingly, the performance of the model for 09 November 2014 increased, showing relative errors as low as 4% for the case when the Bulk Richardson number (0.25) was used to estimate the CBL height.
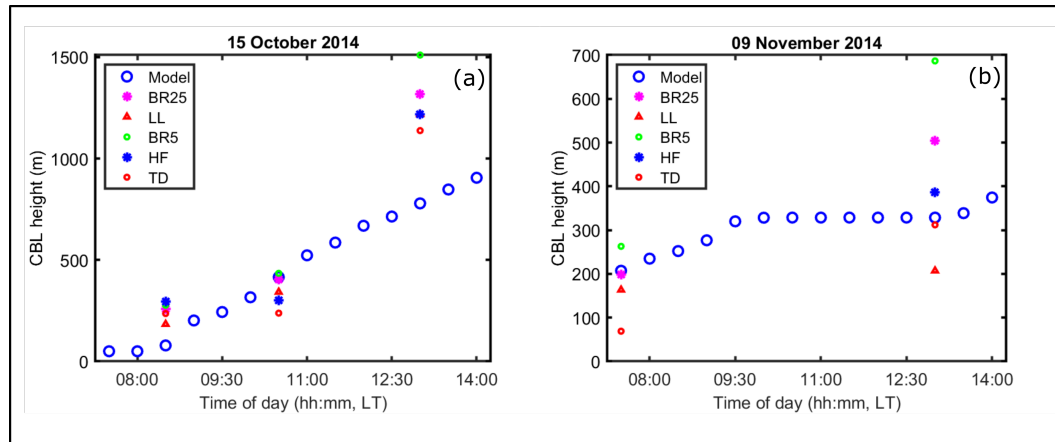
Figure 2.19: Convective boundary layer height using a mixed-layer model (McNaughton and Spriggs, 1986) for the case studies of mesoscale convective system: (a) 15 October 2014 and (b) 09 November 2014. BR25 is the Bulk Richardson method for a 0.25 threshold, LL is the Liu-Liang method, BR5 is the Bulk Richardson method for 0.5 threshold, HF is the Heffter method and TD is the virtual potential temperature derivative method.

Finally, the last comparison is made based on all averaged variables obtained from an ensemble of 27 days with precipitation characterized as mesoscale convective systems. The model is not capable of predicting the averaged mixed layer growth of the CBL (Figure 2.20), underestimating the height of the

CBL, with relative error ranging from 0.6 (13:00 LT) to 1.6 (10:30 LT). It makes sense in statistics terms. The non-multiplicativity property of non-independent variables states that $E[XY]$ is not necessarily equal to $E[X] \cdot E[Y]$, where $E[XY]$ is the expected value of two variables X times Y.
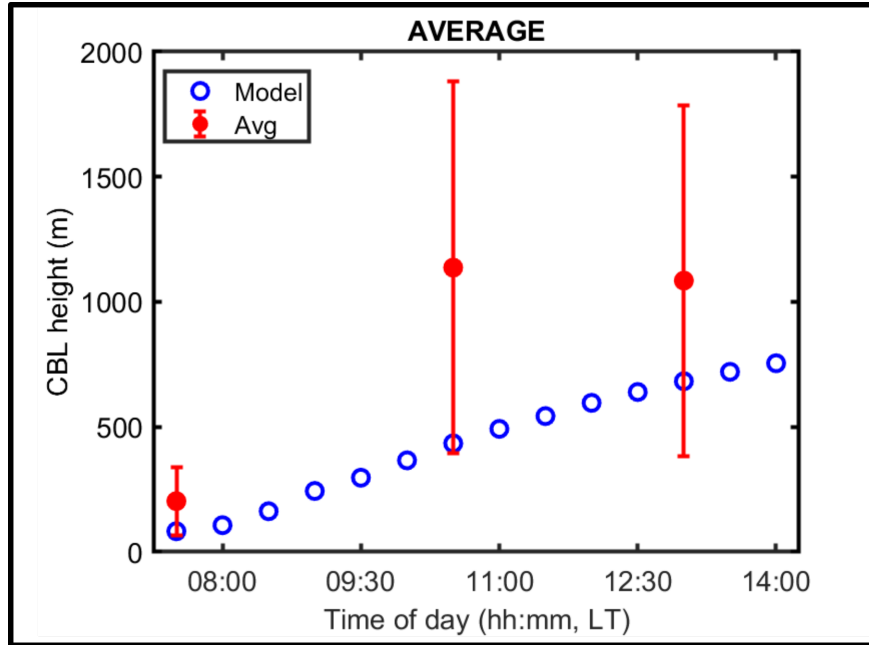
Figure 2.20: Convective boundary layer height using a mixed-layer model (McNaughton and Spriggs, 1986) for the average of 27 case studies of mesoscale convective system. The "avg" represents the averaged convective boundary layer height obtained from the case studies, and "model" is the result obtained from the model using the averaged conditions obtained from the case studies.

Thus, with this simple model, it is shown the necessity of integration of other variables to better describe the CBL development over the day. It was also shown that the averaged γ_v can be implemented to help to describe the mixed layer depth when there is a passage of a mesoscale convective system and there is the absence of such information. In addition, if using more than one averaged variable at once in this thermodynamic model can lead to high errors due to the dependence among virtual sensible heat flux, temperature, and the virtual potential temperature lapse rate.

2.6 Summary and Conclusions

The undisturbed case showed typical conditions of clear days, with high incoming solar radiation and high energy fluxes over the day. As a result, a deep ML was observed in the early afternoon with a large growth rate. In contrast, when there is a precipitation during the nighttime, the soundings revealed a shallow CBL in the morning and slower CBL growth rate. This difference is mainly due to the extra cooling in the surface, generated by the storm downdrafts and the cloudy conditions in the early morning. Despite its differences, the CBL depth is still comparable to the undisturbed condition. However, when the precipitation happened in the morning, the abrupt decrease in the equivalent potential temperature

and the specific humidity due to the storm downdrafts prevents the ML to grow as fast as in the previous cases. The strong inversion observed over the CBL limits the air aloft from entering the CBL, reducing the heating of this layer, and inhibiting its growth. A very simple thermodynamic model was applied for disturbed conditions, showing that the model does not completely capture the features of the mixed layer under disturbed conditions. However, it is not possible to affirm that all the convective boundary layer models have the same result, since models including dynamic effects, as the subsidence may have a better performance. The research questions addressed here are, then, summarized below.

> 1. What are the thermodynamic conditions (e.g., temperature and humidity) in the convective boundary layer preceding a mesoscale convective system?

The thermodynamic features of the convective boundary layer just before the passage of a MCS changed as follows:

- Sensible heat flux decreased, on average, by 38.4 ± 45.9 W m^{-2};

- Latent heat flux decreased, on average, by 223.0 ± 369.9 W m^{-2};

- Equivalent potential temperature decreased, on average, by 5.2 ± 6.2 K;

- Specific humidity decreased, on average, by 1.3 ± 1.3 g kg^{-1};

- Convective available potential energy decreased, on average, by 1890 ± 227 kJ kg^{-1}.

> 2. What are the thermodynamic conditions (e.g., temperature and humidity) in the convective boundary layer after the passage of a mesoscale convective system?

The thermodynamic features of the convective boundary layer just after the passage of a MCS changed as follows:

- Sensible heat flux increased, on average, by 0.8 ± 4.4 W m^{-2};

- Latent heat flux increased, on average, by 5.4 ± 13.0 W m^{-2};

- Equivalent potential temperature increased, on average, by 2.0 ± 1.1 K;

- Specific humidity increased, on average, by 0.7 ± 0.7 g kg^{-1};

- Convective available potential energy increased, on average, by 1731 ± 615 kJ kg^{-1}.

> 3. How do the thermodynamic changes in the convective boundary layer after the passage of a mesoscale convective system relates to the convective boundary layer growth rate?

The convective boundary layer had a variable growth after the passage of the mesoscale convective system. Its growth rates varied from 50 m h^{-1} to 150 m h^{-1}. The growth of the CBL is highly dependent on the time of the precipitation. When the precipitation occurred during the nighttime, the CBL had similar growth rates than the ones observed during undisturbed days. However, when the mesoscale convective storms passed by the site of study during the daytime, more variation was observed.

> 4. How do an atmospheric boundary layer model perform for disturbed days conditions, such as the days when there is a passage of mesoscale convective systems?

The mixed-layer model used in this work does not take into account atmospheric dynamics features, but rather it only considers thermodynamic drivers for the CBL growth. Thus, the model did not perform well to predict the CBL growth under disturbed conditions, such as the passage of mesoscale convective systems, and resulted in errors that surpassed 1000%. Also, when carefully observed, the virtual potential temperature profiles for the disturbed days, it is not very clear where is the depth of the mixed layer, and, in several days, it seems that there is the presence of more than one mixed-layer in the same profile. Thus, multi mixed layer models could be used to investigate entrainment rates in such environmental conditions, for example.

> Limitations

To get a large sample of days to study the conditions before and after the precipitation was a challenge, due to the different times when precipitation occurs and the lack of soundings that could describe in details the mixed-layer growth. To obtain a more consistent analysis, it is valuable to create ensembles encompassing more specific types of storm and time of precipitation. In addition, it is needed to evaluate the dynamics involved in the process of the CBL growth, which is another relevant component to be included in future works. However, this part of the work could provide some thermodynamic variables quantification regarding the passage of mesoscale convective systems over the Amazon rainforest.

Finally, this study provides a path to future investigations and experiments in this subject and presents some of the limitations encountered, also addressed in the next chapter, which will serve as a starting point for future studies with this data set.

Chapter 3

Why does it matter?

3.1 Introduction

This work has no meaning if it is not applied or is within a context. Even a simple result can indicate a path for new research topics and bring different questions, that are not answered yet. A simple thermodynamic characterization of the atmospheric boundary layer can improve the inputs of physical models, helping in forecast and climate predictions. Case studies can also be used to validate model results.

One key point for the understanding of the convective boundary layer processes relies in the cloud formation. In the Amazon rainforest, it has been one of the most recent topics of investigation in the meteorology field: to determine how pollutants brought from urban areas are changing the concentration of cloud condensation nuclei and how they are impacting the precipitation pattern in the Amazon rainforest. In the between, this presented work characterized some attributes of the convective boundary layer before and after the passage of mesoscale convective systems, to evaluate the current atmospheric state found in the Amazon rainforest. This chapter complements this work and has the goal to establish the connections among what is presented in the previous chapter and the environmental, social, and political context. Thus, it I will explore some of the research opportunities that can be derived from the characterization of the atmospheric boundary layer and can be studied in future works, connecting social, environmental and political issues. However, this chapter does not intend to be a literature review on each one of the discussed topics, rather encourage deeper thought in a more global context to reinforce the importance of research results.

3.2 Atmospheric research opportunities in the Amazon rainforest

This work investigated only a very aspect of the convective boundary layer: the diurnal variation of thermodynamic attributes under the passage of mesoscale convective systems. However, following this work, several approaches can be considered, and some of them as a result of the weaknesses found in Chapter 2.

3.2.1 Cold pool and its relation to the convective boundary layer growth

The impact of the cold pool generated after the passage of a storm was not investigated in the present work. However, cold pools play an important role in the structure of the atmospheric boundary layer and are likely to trigger new convection on its boundary. Cold pools initiate its formation once the evaporative cooling of the ABL happens through convective downdrafts, which creates a region of cold and dry air. Then, one of the weaknesses of the presented work is that we do not

Figure 3.1: Representation of a cold pool

know where the site of the study was localized within the cold pool, which limits the evaluation of the thermodynamic attributes after the passage of a storm. Thus, something to be further investigated is how the cold pools are triggering convection over the Amazon rainforest and how the localization of the site of study relative to the cold pool can change the results interpretation. At the present, it was not identified any comprehensive study that characterizes cold pools over the Amazonian region: as strength, size, and lifetime (Figure 3.1). The GoAmazon 2014/15 (Martin et al., 2017), which provided an extensive data set, can be a good opportunity to deepen knowledge on this topic, and further improve the understanding of the results presented in Chapter 2.

3.2.2 Subsidence effects

As important as the thermodynamic characterization, the dynamic characterization of the atmospheric boundary layer is needed to fully understand the atmospheric boundary layer development. Subsidence (sinking of air in a region of high pressure), for example, can inhibit the growth of the convective boundary layer. This is the case when the subsidence velocity is larger than the entrainment rate. However, determining the subsidence velocity at the top of the boundary layer is a little challenge, because it requires the calculation

Figure 3.2: Representation of subsidence over the atmospheric boundary layer

of the horizontal divergence of the wind field, which is not trivial to measure. But, dynamics attributes have to be considered to estimate the convective boundary layer development, and models need to take it into consideration to completely describe the atmospheric boundary layer. The model presented in Chapter 2, for example, do not represent subsidence, which can be one of the reasons for its very low performance. Then, integrating the results found in this work with a dynamic evaluation of the atmospheric boundary layer can improve physical models.

It was shown by Arias et al. (2011), from 1984 to 2007, a reduction in the cloudiness over the Amazon

rainforest that was consistent with large-scale circulation. The reduction in clouds showed an important impact on forest growth rates. Once there is an increase in the incoming solar radiation, the plants increase the photosynthetic activity, consequently increasing growth rates. In addition, it was observed an increase in subsidence, and the reduction of moisture transport to the upper troposphere, that will contribute to the observed decrease in the formation of high clouds. But, the study made by Arias et al. (2011) did not evaluate the relation between the increase in pollutants in the atmosphere - in the Amazon basin - and its effects in reducing or increasing cloudiness. Thus, again, the GoAmazon 2014/15 experiment (Martin et al., 2017) is an opportunity to understand better such relations, and the characterization of the thermodynamic state of the atmosphere, as shown in this work (Chapter 2) will provide complementary information to better explain the causes and consequences of changes in cloudiness over the rainforest.

Other aspects of the dynamics of the atmospheric boundary layer in the Amazon rainforest were explored in Appendix C.

3.2.3 Diverse precipitation events and different wind regimes

Mesoscale convective systems are not the only kind of precipitation observed over the Amazon rainforest. Unorganized systems have to be evaluated as well. Schiro and Neelin (2018) developed a similar work than the one described here (Chapter 2), but also looking at the thermodynamic patterns observed in the passage of unorganized systems. However, Schiro and Neelin (2018) did not describe the effects of the convective boundary layer growth, which could complement the work. In this current work, in the Appendix B, it is shown additional evaluation performed for cases of local (formed) precipitation. Precipitation under different wind regimes, as westerly or easterly, can also be evaluated taking the advantage of the GoAmazon 2014/15 (Martin et al., 2017) data set.

Then, converging these evaluations under different weather conditions - based all on the same data set - will allow the creation of a big picture of all the thermodynamic and dynamic modifications that rainfall can bring, and provide a consistent framework for modeling the atmospheric boundary layer in the Amazon basin.

3.2.4 Spatial representativity of results

Also not considered in this work is the spatial representativity of the results. This topic is closely related to the lack of information, in Chapter 2, about the cold pool characterization and the overall representativity of any study in the Tropics. The location of the site of study within the cold pool, as mentioned before, can play a role in the determination of the thermodynamic characteristics of the convective boundary layer. Thus, correlations between the distance from the center (or the boundary) of the cold pool to the site of study and meteorological variables can be established, increasing the cohesion of the results.

The overall representativity refers to understand what is the level of generalization one can make using the results from this work in space, and also time. The Amazon rainforest has an immense area and it is suffering from degradation over the years, which can imply in a not unique pattern overall its extension. Perhaps, in the boundaries of the rainforest, where deforestation is more intense, the characterization

described in Chapter 2 may be useless to describe the atmospheric boundary layer. Then, it is suggested that, when using the results found in this work, the site location is taken into consideration [1].

3.3 Impacts: a link between society and environmental issues

3.3.1 Effects of pollution in the CBL growth

The GoAmazon 2014/15 (Martin et al., 2017) aims to study, among other subjects, the cloud formation under polluted and pristine environments in the Amazon rainforest. The air pollution over the Amazon rainforest is a great concern, since big cities are within this ecosystem, altering considerably the air quality in the surrounded regions. The pollutants emitted in Manaus (Brazil), for example, can travel long distances within the forest, as observed in the measurements obtained in one of the sites of studies (e.g., T3 is 70 km far from Manaus). And, pollutants can interfere in the cloud formation: inhibiting or enhancing it. Overall, it is observed an increase in precipitation events in regions downwind some cities (Arya et al., 1999). Fan et al. (2018) recently showed this enhancement of precipitation in originally pristine environments in the Amazon rainforest. The increasing concentration of ultra-fine aerosol particles (less than 50 nanometers) lower supersaturation of clouds, and in addition to the cloud condensation nuclei (e.g., more than 50 nanometers) leads to more convection (Fan et al., 2018).

If it is confirmed that the pollutants that reach the site of study enhance cloud formation, and assuming that either rainfall rates or frequency of precipitation also increases, physical models may be prepared to absorb such changes to make better predictions. Also, under these assumptions, the thermodynamic patterns observed in the case studies showed in Chapter 2 may be seen more frequently in the future. On the other hand, if the opposite is observed, one can measure the extension of the impact of drought events, for example.

Overall, it is well known some of the direct effects of air pollution. For example, (Arya et al., 1999) in the book "*Air pollution meteorology and dispersion*" presents a summary on the effects of air pollution on human health, e.g., accidental releases, chronic exposure, extreme air pollution episodes; effects on vegetation and animals, e.g., injury or damage of plant species, reduction in the growth rates of forests, changes in maturity of leaves, changes in susceptibility to pests; domestic animals, e.g., deaths and illness; effects on materials and structures, e.g., corrosion of metals, chemical erosion of buildings, discoloration or fading of fabrics, vulnerability of rubber to high concentrations of ozone; atmospheric effects, e.g., visibility reduction, radiative effects, fog formation and precipitation, acid deposition, stratospheric ozone depletion; climate, e.g., global warming or cooling. Thus, again, improving how models can predict the convective boundary layer under precipitation events can be a key to simulate scenarios, more consistently, under the presence of pollutants.

---

[1]Despite the results for the convective boundary layer growth for undisturbed conditions are in agreement with previous works (e.g., Fisch et al., 2004), it does not necessarily mean that the disturbed conditions are the same as well.

3.3.2 Social impacts due to changes in precipitation patterns

It is not hard to relate some of the impacts of changes in precipitation pattern to the peoples' life. Excessive rain can cause flooding, destroying houses, and affecting diverse activities as horticulture, hunting, fishing, logging, and gold prospecting (Fisher, 2000). Lack of precipitation causes drought: killing plants and lowering the level of water bodies. And there is no major reason why researchers are interested in learning the environmental states and its alterations: because it affects directly how we, human beings, live. So, understanding the convective boundary layer under different conditions allow scientists to perform physical models to predict impacts, and then help to prevent it or manage adverse situations.

> Some of the indigenous communities depend on horticulture. Thus, practices as *"[...] clearing, planting, and harvesting are pegged to the alternating seasons. [...] Given the relatively flat relief of the landscape, even a slight increase in rainfall causes streams and rivers to overflow their banks and flood the surrounding forest. Gullies become streams; hollows become lakes. Cracked, hardened earth transforms in a muddy morass." Fisher (2000)*
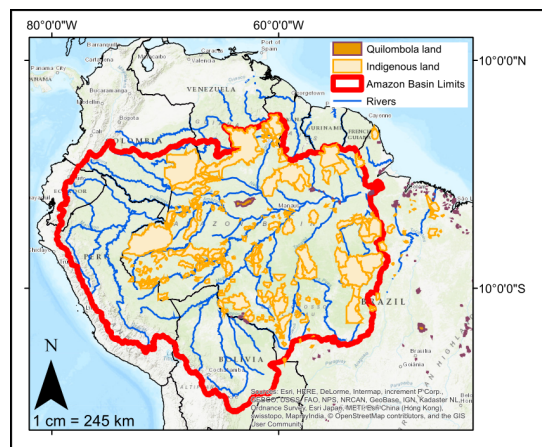
Figure 3.3: Amazon basin: indigenous and quilombola lands. Map created on ArcGis using data from: World Wildlife (WWF) and ArcGis feature service by carusogeo

In the Amazon rainforest, particularly, indigenous and quilombolas [2] are being directly affected by deforestation and its consequences (Figure 3.3 shows the indigenous and quilombola areas remaining until 2015). Logging is invading the Amazon rainforest endangering the fauna, flora, and native cultures. A recent issue of the National Geographic (Wallace et al., 2018), for example, explores how some tribes in the Amazon are struggling to preserve its traditions and culture under the threat caused by illegal activities in the rainforest as logging, and the lack of good policies and laws and environmental monitoring to protect these fragile communities. Then, adding these threats to climate changes, the social impact will be even more significant. It reinforces the necessity in integrating research results as the ones in this work to the scientific community and to the external community. It is the only path to help to protect vulnerable cultures.

---

[2]Quilombola communities are inhabited by descendants of African slaves, that preserve their culture, values, and religion

3.3.2.1 Biotic pump, transport of moisture

It is not only indigenous and quilombola communities that will suffer from the alterations in the Amazon rainforest climate. As mentioned in Chapter 1, the Amazon rainforest has a very tight atmospheric structure that allows it to keep what is known as the "biotic pump". To encourage this thought it will be proposed two scenarios. The first is if the uncontrolled deforestation keeps growing: the amount of moisture transported from the land surface to the atmosphere will be drastically reduced. It means that will be less water vapor available in the atmosphere to condensate and precipitate, consequently making the rainforest (or parts of it) a region of high pressure, and it will reduce the pressure gradient observed between the forest and the ocean, that is what sustains the biotic pump (Figure 3.4).
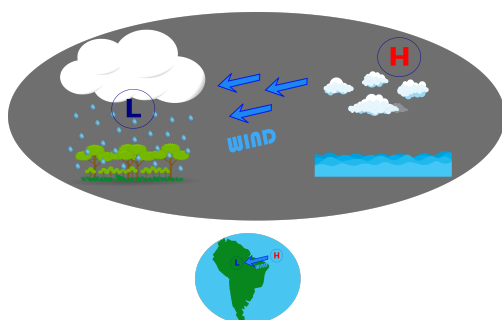
Figure 3.4: Schematic illustration of the biotic pump

In the case this gradient pressure is, in fact, reduced, less moisture from the ocean will reach the forest, reducing, even more, the precipitation over the forest, and perhaps increasing burning events. Thus, the final consequence can be more drought episodes, which can lead at some point, to the desertification of this region. A second scenario could be the enhancement of precipitation due to the increase of pollutants in the pristine environment. If the pollutants brought from big cities are favoring cloud formation and precipitation the pressure gradient can increase, which will make the forest rainier. Only these two scenarios are shown, but endless scenarios can be drawn. The major idea is that, because the rainforest is one of the most important contributors to the transport of moisture to the other regions in Brazil, as the southeast and south, either desertification or humidification of the forest will also impact large centers (Figure 3.5).

If the desertification or humidification happens, it will be also observed in the rest of the country. The social impacts in both scenarios can be disastrous, in the whole country. Brazil has an economy largely based on agriculture, which will for sure be impacted by such climate changes. Also, the cities cannot endure extreme events such as drought, that directly affect the water supply, neither extreme precipitation events that can cause flooding for several days - also compromising water quality and displacing families from their houses.
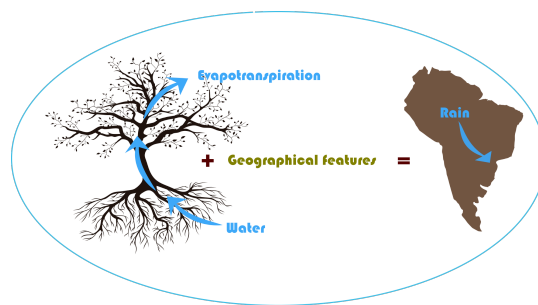
Figure 3.5: Schematic illustration of the moisture transport from the forest to the other regions in Brazil

3.3.2.2 Implications of deforestation

However, to test all these hypotheses, more studies have to be conducted, and the results may be reported to stimulate political changes and to inform the population. Then, this presented work, especially Chapter 2, despite its simplicity, is contributing to filling out some gaps in the understanding of the atmospheric processes.

The deep interest to comprehend the atmospheric boundary layer processes in the Amazon rainforest is linked to the efforts to reduce degradation and prevent climate change. Once processes can be understood and can be implemented in models, the scientists have a powerful tool to support environmental policies and protect the environment.

Figure 3.6: Amazon basin: remaining forested area until 2010. Map created on ArcGis using data from: World Wildlife (WWF)

As presented in Fisch et al. (2004), the convective boundary layer grows significantly different in the dry season when comparing a pasture site and a forested site. Thus, if the deforestation does not stop, it is very likely that patterns observed in a pasture for the convective boundary layer growth will be seen more often over the rainforest, changing how clouds are formed.

The Figure 3.6 shows the remaining forested areas in the Amazon basin in 2010. A reduction in deforestation rates in Brazil dropped above 70% from 2000 to 2012, which was a result of an "*an extensive network of indigenous lands and protected areas across the Amazon*" (Boucher, 2014). Unfortunately, after the Brazilian court decides to review the legislation in 2012, a new "forest code" was applied, aggregating some economic advances in Brazil, sustained by this new "smooth" legislation that allowed agricultural and cattle raising in regions previously protected. It was largely reported in the news as a tragic change [3] [4]. The World Wild Life reports that the deforestation increased by 29% between 2015 and 2016, and a declining after this period, but it was not quantitatively reported [5].

3.3.2.3 Health issues

> "*Unfortunately, we do not fully understand how ecosystem services (such as human health benefits) could be secured by conserving natural capital.*" Bauch et al. (2015)

Bauch et al. (2015) evaluated the relation between climate factors as temperature and rainfall with

---

[3] https://news.mongabay.com/2018/07/deforestation-skyrockets-in-the-amazon-rainforest/
[4] The Guardian: https://goo.gl/oXrNqW
[5] https://www.worldwildlife.org/stories/protecting-progress-in-the-brazilian-amazon

some diseases commonly found in the Amazon rainforest, like malaria, acute respiratory infections (ARI), diarrhea, and dengue [6]. Malaria, ARI, and diarrhea where found negatively correlated for temperature and rainfall during the dry season, and for temperature in the rainy season. For the precipitation, during the rainy season, it was positively correlated for these three diseases. Dengue showed a different pattern being the opposite of it. It was positively correlated for temperature and rainfall during the dry season, and for temperature in the rainy season, and negatively correlated to the rainfall in the rainy season.

Not only diseases are correlated to climate factors, but deaths are also reported as highly correlated to fire emissions due to deforestation. Reddington et al. (2015) correlated the fire emissions due to deforestation during non-drought years in the Amazon rainforest, between 2002 and 2011, with the adult mortality caused by "*cardiopulmonary disease and lung cancer due to exposure to PM2.5 [7] from fires*". This study showed that the reduction in the deforestation in Brazil can reduce drastically the premature adult mortality.

> *"[...] reductions in Brazils deforestation rates have caused reduced fire emissions resulting in improved air quality with positive impacts on human health."* Reddington et al. (2015)

Both studies show the importance of climate factors directly or indirectly. Changes in patterns of precipitation can increase the incidence of certain diseases and fire emissions. Deforestation can increase drought events and consequently increase biomass burning. However, it can also increase cloud condensation nuclei and enhance convection. Thus, it adds to the reasons why it is needed to understand all the relations among pollutants and cloud formation, to be able to identify what is the balance and the prevailing factors that can contribute to irreversible alterations in the Amazon basin (and the World) climate, and then prevent future consequences due to land alteration.

3.4 Political issues

The Amazon rainforest protection is directly related to the politics that define preservation areas, establish an environmental legislation, and monitor endangered areas. Because the majority of the rainforest is within Brazil, there is a special concern with the environmental policies in this country.

Currently, there are several guidelines released in 2008 that are compiled in the document entitled "The Sustainable Amazon Plan (PAS)" [8]. These guidelines aim a sustainable development of the Amazon, the appreciation of the cultural and environmental diversity of the Amazon, to promote the cooperation among the federal, state, and county governments, to amplify the regional infrastructure, to ensure the territorial rights for local communities (indigenous and quilombola), to fight the illegal deforesting, to promote the utilization of degraded areas and reforest degraded areas, to promote scientific studies, among

---

[6] The work explores other diseases as AIDS, arthritis, and leukemia, which do not show correlation with climate factors

[7] PM2.5: particulate matter with a diameter of fewer than 2.5 micrometers

[8] Material in Portuguese: `http://www.casacivil.gov.br/.arquivos/110106-MI-PlanoAmazoniaSustentavel-PAS.pdf`

others.

Despite the current guidelines for The Sustainable Amazon Plan (PAS), changes in the legislation that occurred in 2012, made the "forest code" [9] more susceptible to a misguided interpretation. There is a specific change in the "forest code" which allows that the proposed land regularization can be used as a tool for deforestation. In simple words, people can (clear a forest region), occupy the land, and claim for regularization. The alteration in the "forest code" was also accompanied by government reduction of costs in the environmental protection sector, making the small communities and the forest even more vulnerable.

In the current scenario, Brazil is facing a big political issue. The ongoing of the environmental concerns are being barely discussed in the debates for the elections. The most popular candidate does not even mention the environment in its government plan; the second most popular, which is supported by the previous president that reduced deforestation, show many concerns and highlight in his government plan the compromise with environmental education, and even cite an appreciation with the Amazon rainforest[10]. However, the future is unreliable, and environmentalists and researchers have to be persistent toward improvements in the environmental legislation.

3.5   Final considerations

On the overall, this work is a very basic characterization of the thermodynamics of the convective boundary layer in the Amazon rainforest. Many weaknesses were highlighted in this chapter, in order to provide suggestions and motivation for future works.

The Amazon rainforest is a precious nature's gift but it has been neglect by politicians who do not care about environmental degradation. Our mission as scientists is to explore nature to come up with facts and solutions for human acts against it.

In addition, all research is made to amplify the scientific knowledge in a specific area, but unfortunately, not all countries and/or cultures give the relevance that science deserves. The Brazilian science, for example, is degrading, as the Amazon rainforest is. The investments in Science were reduced from R\$10 billion (2010) to R\$4.8 billion (2017) [11][12]. It drastically reduced the research on all sectors. This chapter summarized some important issues related to the study of the convective boundary layer and its implications in different fields. Neglecting or reducing the source to keep investigations causes a deceleration in the attempt to prevent negative impacts from the human actions. Thus, again, more than mere results or a mere characterization of a very specific topic, this chapter had the intention to provoke a deeper thought about the relevance of research. More than a scientific motivation or well-elaborated research questions, researchers should connect their topics to all implications it can have for every living being. It would help, also, to better communicate the importance of scientific results to the community and push the government to take effective actions.

---

[9]Material in Portuguese http://www.planalto.gov.br/ccivil_03/_Ato2011-2014/2012/Lei/L12651.htm

[10]Material in Portuguese: http://www.tse.jus.br/eleicoes/eleicoes-2018/propostas-de-candidatos

[11]Currency by October 2018: US\$1 = R\$3.71

[12]Material in Portuguese: https://epocanegocios.globo.com/Brasil/noticia/2018/04/ao-cortar-investimentos-em-ciencia-brasil-assassina-o-futuro.html

Thus, again, more than presenting a characterization of the convective boundary layer under the passage of mesoscale convective systems, which is a very specific subject, this chapter proposed a reflection on how we see research results, and some of the issues faced to try to protect our ecosystems. And, the last thought:

> *"Can we marshal the resources necessary to secure the gains weve made and chart a new path forward?"* WWF – World Wildlife [a]
>
> ────────────────────
> [a]`https://www.worldwildlife.org/stories/protecting-progress-in-the-brazilian-amazon`
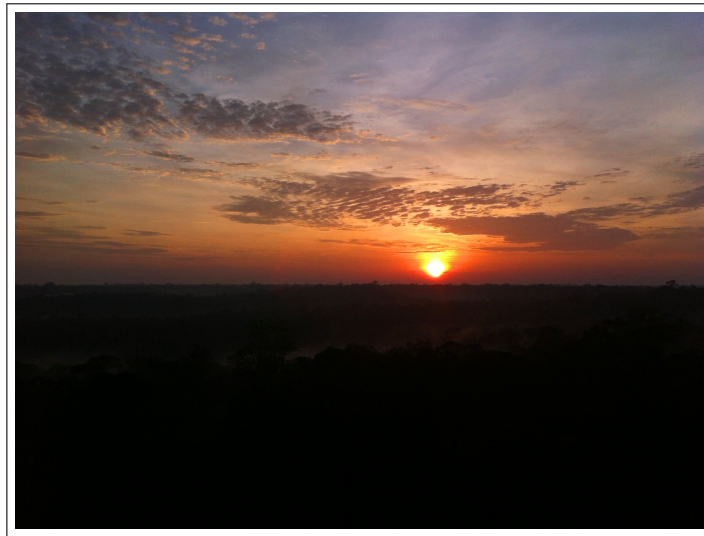
Figure 3.7: Sunrise in the Amazon rainforest (ZF2 site). Picture taken during the GoAmazon 14/2015 from personal archive.

Complementary equations

A.1 Thermodynamic variables

Potential temperature (Stull, 1988)

$$\theta \cong T \left(\frac{P_0}{P_z} \right)^{0.286}$$ (A.1)

, where T is the temperature (measured) in Kelvin, P_0, is the pressure of reference (1000 mb), and P_z is the pressure level (measured) at the altitude z.

Virtual potential temperature

$$\theta_v = \theta(1.0 + 0.61q)$$ (A.2)

where θ is the potential temperature and q is the specific humidity.

Specific humidity

$$q = \frac{m_v}{m_v + m_d} = \varepsilon \frac{e}{P - 0.378e}$$ (A.3)

, where m_v is the mass of water vapor, m_d, is the mass of dry air, $\varepsilon = 0.622$ is the ratio of the molecular weight of water vapor to the molecular weight of dry air, P are the air pressure and e is the vapor pressure.

Vapor pressure

$$e = e_s \cdot RH$$ (A.4)

, where e_s is the saturation vapor pressure and RH, is the relative humidity (measured).

Saturation vapor pressure: Teten's equation

$$e_s = 610[Pa] \exp \left(\frac{17.27T}{237.4 + T} \right)$$ (A.5)

where the temperature T is in Celcius.

Equivalent potential temperature

$$\theta_e \cong \theta + \frac{L_v}{c_p r} \tag{A.6}$$

, where θ is the potential temperature, L_v, is the latent heat of vaporization, c_p is the specific heat capacity of the air at constant pressure, and r is the water vapor mixing ratio.

Water vapor mixing ratio

$$r = \frac{m_v}{m_d} = \varepsilon \frac{e}{P - e} \tag{A.7}$$

, where m_v is the mass of water vapor, m_d, is the mass of dry air, $\varepsilon = 0.622$ is the ratio of the molecular weight of water vapor to the molecular weight of dry air, P are the air pressure, and e is the vapor pressure.

A.2 Convective boundary layer height (Sivaraman et al., 2013)

Liu-Liang Method

$$h_{ML} = \theta_k - \theta_1 \geq 0.5K \tag{A.8}$$

then, the convective boundary layer height is defined as the first level k where the difference of potential temperature θ at this level and level 1 is larger than 0.5 K, for land surfaces. A second criterion has to be meet in this method. The gradient of the potential temperature with height has to be larger than 4.0 K/km.

Bulk Richardson method

$$Ri_b = \left(\frac{gz}{\theta_{v0}} \right) \left(\frac{\theta_v - \theta_{v0}}{u_z^2 + v_z^2} \right) \tag{A.9}$$

where g is the acceleration due to gravity, θ_v is the virtual potential temperature, u is the zonal component of the wind and v is the meridional component of the wind. Subscripts z and 0 refers, respectively, to the level of the measurement and the surface measurement.

The height of the convective boundary layer is determined when $Ri_b > 0.25$ or, according a second criteria, $Ri_b > 0.5$.

Complementary case studies

B.1 Case studies for diverse precipitation regime

The previous cases showed how mesoscale convective systems are disrupting the thermodynamic attributes of the mixed layer. The selected cases had a clear pattern of precipitation defined by an intense precipitation followed for several hours of a stratiform rain. The current case study is for a day when is registered the passage of a squall line. The total of precipitation on 09 May 2014 was 23.9 mm, and the largest accumulated precipitation at 09:00 LT (Figure B.1f). The maximum incoming solar radiation was 232.2 W m^{-2} at 09:30 LT. Just before the time of the most intense rainfall rate (09:00 LT), the equivalent potential temperature decreased 4.9 K and the specific humidity, 1.31 g kg^{-1} (Figure B.1b). Maximum wind speed for this day was 4.1 m s^{-1}.

Table B.1: Thermodynamic attributes for 09 May 2014, derived from the measurements at T3 site

t (LT)	07:00	13:00
h_{ML} (m)	244	287
$\langle \theta_v \rangle_{ML}$ (K)	301.8	300.5
$\langle q \rangle_{ML}$ (g kg^{-1})	18.5	17.5
Δq (g kg^{-1})	0.2	-0.4
$\Delta \theta_v$ (K)	0.9	1.3
γ_{θ_v} (K km^{-1})	3.8	4.9
γ_q (g kg^{-1} km^{-1})	-4.6	-4.0

The passage of a squall line did not allow a deep and fast mixed-layer growth. In the morning (07:00 LT) the mixed-layer was estimated as 244 m deep. Despite the mixed-layer being well developed at this time, the estimated depth at 13:00 LT is 287 m, representing a growth rate of 7.2 m h^{-1}.
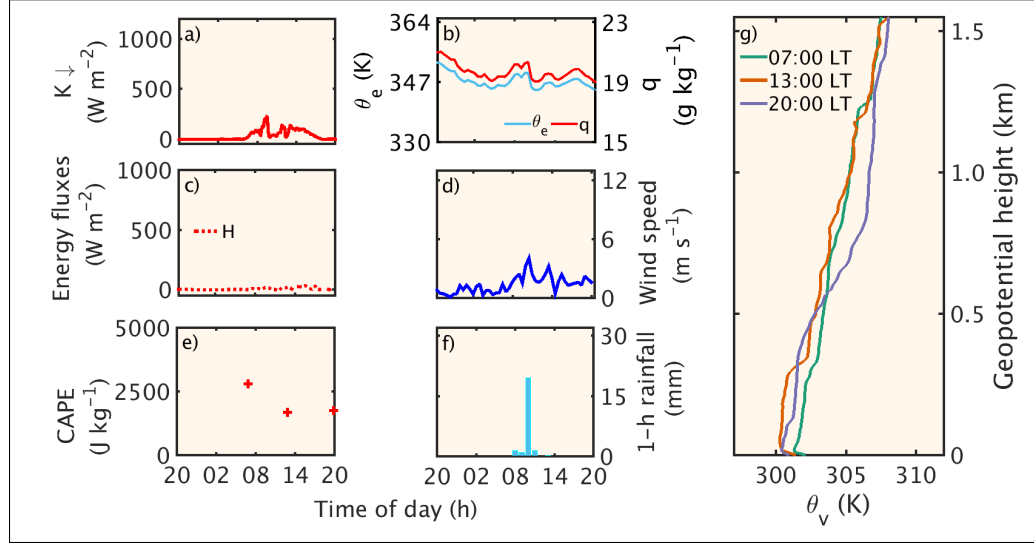
Figure B.1: Case study of a disturbed day, 09 May 2014. Diurnal cycle of: (a) incoming solar radiation, (b)equivalent potential temperature (θ_e) and specific humidity (q), (c) net radiation (R_{net}), virtual sensible heat flux(H_v) and latent heat flux (LE), (d) wind speed, (e) convective available potential energy (red symbols: derived from soundings, solid line: measured), (f) precipitation, and profiles of (g) virtual potential temperature (θ_v).

.

Another case study is presented to show the impacts of a local formed precipitation. On 16 August 2014, the satellite images show a very localized precipitation over the site of study. The total of accumulated precipitation was 17.32 mm, with the maximum accumulated rainfall registered at 09:00 LT (Figure B.2f), with wind speed at the surface reaching 6.7 m s^{-1}. The maximum solar incoming radiation was at 10:00 LT, 882.1 W m^{-2} (Figure B.2a). A second maximum is observed at 15:00 LT, 304.3 W m^{-2} (Figure B.2a). By the time of the strongest rainfall episode (around 09:00 LT), the equivalent temperature decreased 16.8 K and the specific humidity, 4.17 g kg^{-1}. The layer-average virtual potential temperature at the first morning sounding (07:00 LT) was 300.0 K and the layer-averaged specific humidity, 16.8 g kg^{-1}. The cold and dry air brought to the lowest layers of the atmosphere made these values decrease, as seen in the soundings launched at 13:00 LT, when the layer-averaged virtual potential temperature was 297.6 K, and the layer-averaged specific humidity, 15.1 g kg^{-1}. The strength of the virtual potential temperature inversion at the top of the mixed layer at 07:00 LT was 1.1 K, and at 13:00 LT, 4.2 K.

The mixed-layer was very shallow over the day, growing from 42.2 m (07:00 LT) up to 74.4 m (13:00 LT). The layer-averaged virtual potential temperature varied from 300 K (07:00 LT) to 297.6 K (13:00

Table B.2: Thermodynamic attributes for 16 August 2014, derived from the measurements at T3 site

t (LT)	07:00	13:00
h_{ML} (m)	42.2	74.4
$\langle \theta_v \rangle_{ML}$ (K)	300.0	297.6
$\langle q \rangle_{ML}$ (g kg^{-1})	16.8	15.1
Δq (g kg^{-1})	0.6	-0.1
$\Delta \theta_v$ (K)	1.1	4.2
γ_{θ_v} (K km^{-1})	4.7	5.2
γ_q (g kg^{-1} km^{-1})	-8.0	-2.2

LT), and the layer-averaged specific humidity was also reduced from 16.8 to 15.1 g kg^{-1}.
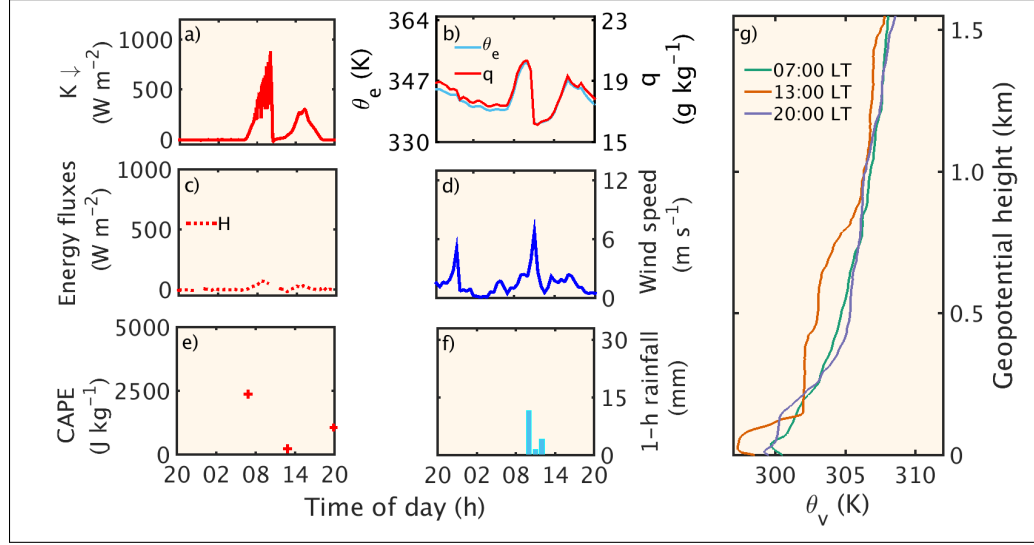
Figure B.2: Case study of a disturbed day, 16 August 2014. Diurnal cycle of: (a) incoming solar radiation, (b)equivalent potential temperature (θ_e) and specific humidity (q), (c) net radiation (R_{net}), virtual sensible heat flux(H_v) and latent heat flux (*LE*), (d) wind speed, (e) convective available potential energy (red symbols: derived from soundings, solid line: measured), (f) precipitation, and profiles of (g) virtual potential temperature (θ_v).

B.2 Averaged attributes

Surface averaged variables are summarized in Figure B.3 regarding the time of the precipitation event, for an ensemble of 19 days, except when there was no measurement for a specific day or variable and the day was omitted from the ensemble. As in the mesoscale convective system's analysis, the surface variables decrease drastically by the time of the precipitation. Thus, the sensible heat flux is reduced by an average of 38.0 W m^{-2} and latent heat flux by 223.0 W m^{-2}. As in the mesoscale convective cases, the increased cloud cover reduced the solar radiation and consequently the warming of the lower layers of the atmosphere. The latent heat flux has a peak one hour before the precipitation, but not as significant as the peak observed in the MCS's cases, from an average of 105.1 W m^{-2} to 129.1.0 W m^{-2}). The averaged CAPE was approximately 1554.0 kJ kg^{-1} before the rainfall starts, again smaller than for the MCS's cases. The specific humidity and the equivalent potential temperature reduced, respectively, by 0.96 g kg^{-1} and 4.1 K (Figure B.3). Then, higher sensible heat flux coupled to smaller perturbations in the ABL after a precipitation event when compared to the MCS situation, tell us that the CBL should be deeper for regional precipitation.
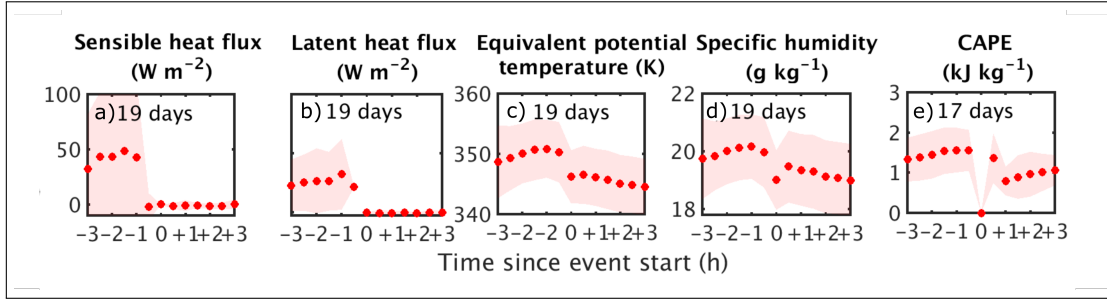
Figure B.3: Variation of thermodynamic variables at surface for squall line passage(time 0): 3 hours before the systems passage (-3) up to 3 hours after (+3). (a) Sensible heat flux, (b) latentheat flux, (c) equivalent potential temperature, (d) specific humidity, and (e) convective available potentialenergy. The shadow represents the standard deviation of the data

But, before moving on the analysis of the CBL height, let's take a look at the diurnal variation of these variables. When there is the occurrence of regional precipitation, the daily mean sensible heat flux is 15.3 $\pm$ 23.0 w m^{-2} (Figure B.4a); latent heat flux, 57.3 $\pm$ 74.7 W m^{-2} (Figure B.4b); equivalent potential temperature, 346.1 $\pm$ 3.3 K (Figure B.4c); the specific humidity, 19.2 $\pm$ 0.7 W m^{-2} (Figure B.4d); and, CAPE, 1053.0 $\pm$ 371.7 J kg^{-1} (Figure B.4e). In fact, the surface energy fluxes are higher for the regional events of precipitation, and the CAPE is lower. Which makes sense, since the intensity of this kind of precipitation is lower than the MCS cases.
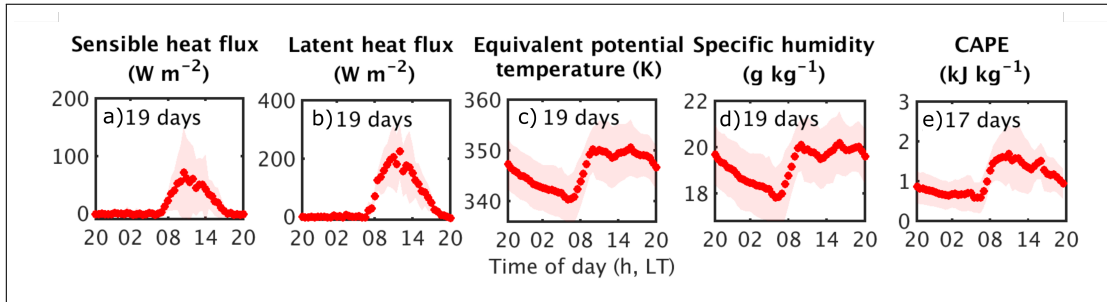
Figure B.4: Diurnal variation of thermodynamic variables at surface for squall line passage. (a) Sensible heat flux, (b) latent heat flux, (c) equivalent potential temperature, (d) specific humidity, and (e) convective available potential energy. The shadow represents the standard deviation of the data

Thus, the variation of the convective boundary layer depth over the day for regional precipitation is, in fact, larger than for mesoscale convective systems. In the early morning, the CBL is, on average, 19% shallower in the regional cases (164.1 $\pm$ 90.2 m) than in the MCS's cases. However, it grows up to an average of 1885.0 $\pm$ 671.1 m, which is about 40% deeper than in MCS. But, it is followed by a reduction in its thickness to 812.2 $\pm$ 690.8 m.
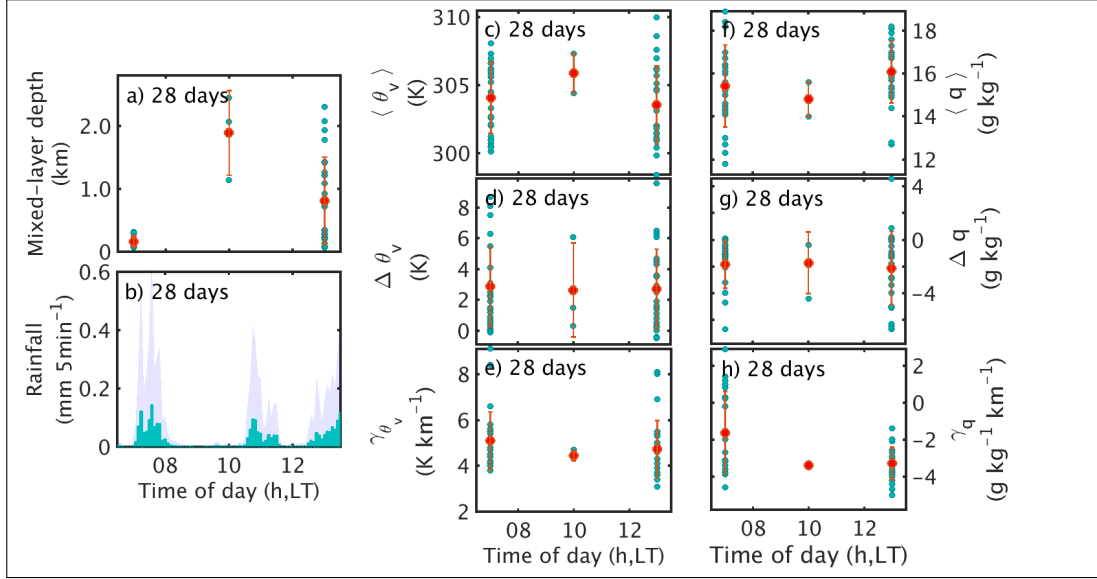
Figure B.5: Convective boundary layer (CBL) attributes for regional systems, for an ensemble of 28 days. (a) CBL depth, (b) 5-minute averaged rainfall rate, (c) mixed layer averaged virtual potential temperature, (d) strength of the temperature inversion at the top of the CBL, (e) virtual potential temperature lapse rate above the CBL, (f) mixed layer averaged specific humidity, (g) strength of specific humidity variation at the top of the CBL, (h) specific humidity lapse rate above the CBL. The bars and the shadow are the standard deviations from the mean values.

B.2.1 Modeling the CBL

Using the same model described in Section 2.5.1, the two case studies for regional precipitation are analyzed.

The Figure B.6 shows the performance of the model compared to the estimates of the convective boundary layer height. For both days, the method of the second derivative is not in agreement with the estimates of the different methods, provided by the Atmospheric Radiometric Measurements (ARM). Also, the model does not capture the growth of the CBL for any of the estimates. Only for the early morning for 16 August 2014, the model was capable to closer predict the CBL height for the Liu-Liang and Bulk Richardson (0.25) methods.
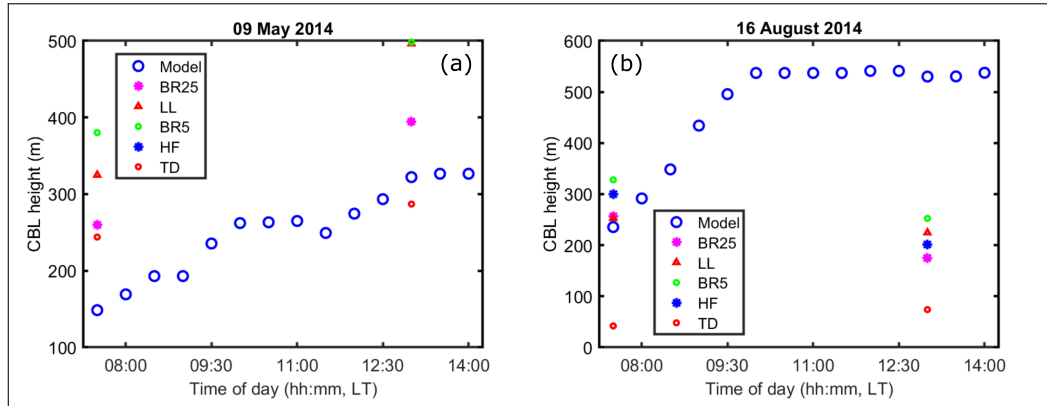
Figure B.6: Convective boundary layer height using a mixed-layer model McNaughton and Spriggs (1986) for the case studies of regional precipitation: (a) 09 May 2014 and (b) 16 August 2014. BR25 is the Bulk Richardson method for a 0.25 threshold, LL is the Liu-Liang method, BR5 is the Bulk Richardson method for 0.5 threshold, HF is the Heffter method and TD is the virtual potential temperature derivative method.

The Figure B.7 represents the model performance using the averaged values of γ_θ and γ_q to calculate the γ_v. All the others variables are the same than in the Figure B.6. Using the averaged lapse rate, the model had the worst performance, with increased errors of up to 50%.
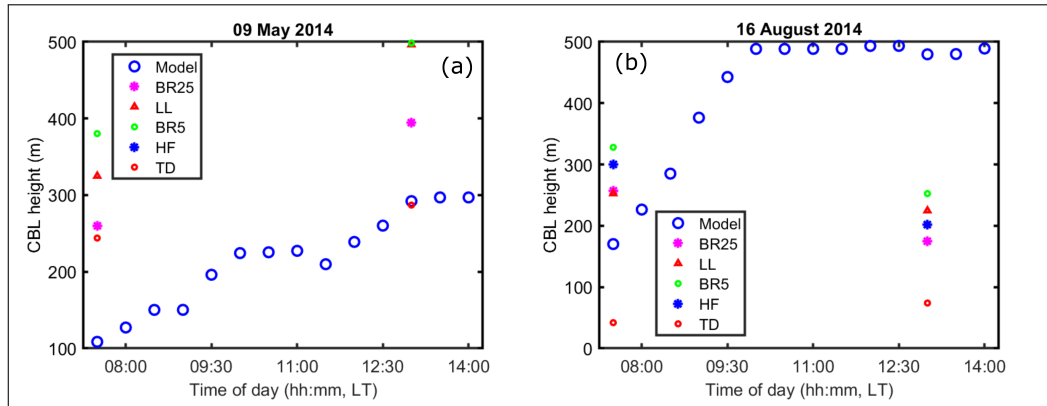
Figure B.7: Convective boundary layer height using a mixed-layer model McNaughton and Spriggs (1986) for the case studies of regional precipitation, using the averaged values og γ_v: (a) 09 May 2014 and (b) 16 August 2014. BR25 is the Bulk Richardson method for a 0.25 threshold, LL is the Liu-Liang method, BR5 is the Bulk Richardson method for 0.5 threshold, HF is the Heffter method and TD is the virtual potential temperature derivative method.

B.3   Summary

This complementary section showed by how many thermodynamic variables in the convective boundary layer are impacted by the passage of regional/local precipitating systems. Overall the changes in the initial conditions of the CBL are smaller than for cases when a mesoscale convective system passed over the site

of study. Also, the CBL was capable to grow deeper for such conditions, which can be an indicator that the strongest the precipitation, more time is needed for the mixed layer grow again.

The mixed-layer model did not perform well for the case studies, neither for the mesoscale convective system nor the regional precipitation. It was already expected, since the model does not capture the dynamic effects in the CBL, such as the subsidence after the passage of storms. It can be one of the reasons why the model overestimates in the majority of the cases the depth of the mixed layer in the afternoon. The subsidence suppresses the convective boundary layer growth, and if included in the physical model it may reduce the errors.

Appendix C

The performance of exponential and hyperbolic models of wind speed profile within an Amazon forest canopy

C.1 Introduction

Transport of mass, momentum, and energy experienced by the rainforest can affect global scale, for example, impacting atmospheric deep convection (Fuentes et al., 2016). The importance of studying the Amazon rainforest is due to its significance for the Earth's climate. For example, the rainforest emits many hydrocarbons (e.g., isoprene, sesquiterpenes), that react with ozone and nitrate radicals, leading to the formation of secondary aerosols. These aerosols can be transported from the lower layers and result in cloud condensation nuclei (CCN), increasing the precipitation. These compound emissions are related to canopy features, for example, foliage temperature, soil moisture and incident photosynthetically active radiation. However, the transport of these scalars is related to the turbulence. Moreover, to characterize the turbulent mixing within the forest, one requirement is to determine the wind speed profiles over vegetated surfaces. Other applications related to transfer of scalars (e.g., spores, pollen, contaminants, aerosol) and wind flow are associated with agriculture, forestry, and atmospheric circulation (Massman, 1997). And to study momentum transfer inside and above plant canopies we need to determine the turbulent diffusivity, which in turn can be obtained by the wind velocity profile and the drag force see (Raupach, 1988). For example, Massman and Weil (1999) developed a closure model of turbulence statistics using the parameterizations of wind speed profile given by Massman (1997), and Finnigan et al. (2015) used the log-law, Yi et al. (2005) and Inoue (1963) used wind flow models to study turbulence in complex canopies.

In the absence of data, a wind flow model can fulfill the requirement to estimate momentum transport. The wind flow within canopies does not follow the exponential profile dependent only on the surface characteristics. The top of the canopy behaves like a surface where the flow passes by, and the wind flow below the top of the trees is driven by the canopy architecture (e.g., leaf area density). For tall canopies, like the rainforest, the wind speed profile has an inflection point just above the canopy with a strong wind shear that is not well described by models designed for short canopies (e.g., corn). There are several models to describe the wind flow within and above plant canopies (see Landsberg and James, 1971; Massman, 1997; Raupach and Thom, 1981; Raupach, 1988, 1994; Shaw, 1977; Yi, 2008; Souza et al., 2016; Santana et al., 2017), either analytical or empirical. Raupach (1988) describes an exponential model with a single parameter related to the leaf area index (LAI). Massman (1997) developed a model taking into account foliage features (drag coefficient, drag area index, leaf density, shelter factor) and a parameterization for the friction velocity. Yi (2008) proposed to include a parameter multiplying the exponential model, which includes the drag coefficient. Other models have been developed (e.g., Landsberg and James, 1971), but with very few studies related to the rainforest canopy (Souza et al., 2016). Shaw (1977) and Yi (2008) discuss the importance of the s-shaped wind profile in forest canopies. The s-shaped wind profile is a result of two maximums in the wind profile. The first maximum is at the top of the canopy and, the secondary, at the region where the trunks are located, where the spaces between the trunks allow a faster wind flow. (Katul et al., 2004) studied canopy turbulence for different canopy structures (e.g., rice, corn, pine, boreal forest) and found that a common issue that models did not reproduce well was the secondary maximum of the wind speed. The most recent models including these features are described by Souza et al. (2016) and Santana et al. (2017). Both models are based on the previous model by Raupach et al. (1996) and Yi (2008), but including specific parameterization for the Amazon rainforest.

The objective of this study is to determine the best approach for the wind flow within a rainforest canopy. To accomplish this goal, five wind flow models will be performed for two distinct case studies: (i) one day of the dry season, and (ii) one day of the wet season. The canopy studied is part of the experimental site called ZF2, located in the Amazon rainforest (Brazil). The data from this field campaign are going to be used to verify the model's accuracy. A well-characterized wind profile can help to improve turbulence parameterization, chemistry models, and transport models.

C.2 Methodology

A field campaign was performed at the Cuieiras Biological Reserve (-2.60191° latitude, -60.2093° longitude). It is located at 60 km north-northwest of the city of Manaus (Brazil). This campaign is part of GoAmazon project, described in details by Martin et al. (2017). The site is covered by the rainforest, whose canopy is 30 to 40 meters tall. For this study, the height adopted is 35 meters.

A 50-meter tower was deployed to investigate the turbulence and chemistry within and above the canopy. Measurements were taken from 04 April 2014 to January 2015. Several measurements took place at the site of study, described by Fuentes et al. (2016), that allow calculating the exchanges of momentum, sensible heat flux, latent heat flux, and carbon dioxide flux densities. For the scope of this work, it is going to be used the wind speed data provided by seven sonic anemometers deployed in a tower within the plant

canopy (model CSAT3, Campbell Scientific, Inc., Logan, Utah). The sonic anemometer provides data for zonal (u), meridional (v), and vertical (w) components of the wind, measured at a frequency of 20-Hz. They are displaced at heights of 7.0 m, 13.5 m, 18.4 m, 22.1 m, 24.5 m, 31.6 m, 34.9 m. The manual of the CSAT3 recommends that the instrument should face the prevailing wind direction, to avoid the interference of the other parts of the equipment (hardware). The prevailing wind direction at the site is from the northeast. All the equipment were deployed facing east.

It is going to be used the daily average wind speed (average over 24 hours) and hourly average for six distinct periods of the day: 00:00 LT, 04:00 LT, 08:00 LT, 12:00 LT, 16:00 LT, and 20:00 LT, to represent the temporal evolution of the wind profiles within the canopy.

To estimate the wind speed within the plant canopies we need to know the canopy structure. Previous studies reported leaf area index (LAI) for this site ranging from 5.7 to 7.3 m^2 m^{-2}, (see Santana et al., 2017; Freire et al., 2017) for more details. The value adopted here is LAI=6.0.

C.2.1 The wind flow models

Several models have been developed to describe the wind flow within and above plant canopies (Landsberg and James, 1971; Massman, 1997; Raupach, 1988, 1994; Shaw, 1977; Yi, 2008; Souza et al., 2016; Santana et al., 2017). In this study, five models will be performed to compare their accuracy and reliability to the measured data at the ZF2. The models were chosen based on their simplicity to describe the flow in the rainforest canopy.

To compare the models performance to the measurements will be calculated the root-mean square error (RMSE= $\left(\Sigma_{i=1}^{n} (x_0 - x)^2 / n \right)^{1/2}$), where x is the measured value and x_0 is the estimated value by the models.

C.2.1.1 Raupach (1988)

Raupach (1988) is an empirical exponential wind profile model (Eq. (C.1)), where $\overline{u}(z)$ is the wind speed at height z and $\overline{u}(h)$ is the wind speed at the top of the canopy h. This model has a single parameter (λ) related to the leaf area index as an attenuation coefficient. Raupach (1988) presents the values of the λ coefficient obtained for several crops with experimental values. Based on the present values, and using an exponential fit for the data provided, the value obtained for the rainforest was $\lambda = 3.2$.

$$\overline{u}(z)/\overline{u}(h) = \exp\left[-\lambda\left(1 - z/h\right)\right] \tag{C.1}$$

This model is a good approximation for the upper part of the wind profile within plant canopies.

C.2.1.2 Massman (1997)

This one-dimensional model uses parameterization for the friction velocity (u_*) normalized by wind speed at the top of the canopy ($u(h)$) to determine z_0/h and d/h as a function of drag area index and foliage distribution (Eq. (C.2)); where $-n$ is function of the drag coefficient, the leaf area index, and three coefficients ($c_1 = 0.320$, $c_2 = 0.264$ and $c_3 = 1.51$), $\zeta(z)$ is the cumulative drag area, and $C_d(z)$ is the

foliage drag coefficient. For this study was adopted a constant drag coefficient ($C_d = 0.2$), and a constant cumulative leaf drag area per unit plantform area ($\zeta = C_d \cdot LAI$). The parameterization of the friction velocity is basically a linear combination of the limits when the drag area index ($\zeta(h)$) goes to zero then $u_*/u(h)$ goes to $\sqrt{C_s}$, and when $\zeta(h)$ goes to infinite then $u_*/u(h) = 0.3$ (Massman, 1997) (Equation (C.3)).

$$u(z)/u(h) = \exp\left[-n\left(1 - \zeta(z)/\zeta(h)\right)\right], \text{and} \tag{C.2}$$

$$u_*/u(h) = c_1 - c_2 \exp\left[-c_3 \zeta(h)\right], \tag{C.3}$$

C.2.1.3   Raupach et al. (1996) and Yi (2008)

Taking into account the different canopy structure of short and tall canopies, Raupach et al. (1996) and Yi (2008) proposed a model including a hyperbolic tangent function to better describe the s-shape characteristic of the wind profile within the forest canopy (Eq. (C.4)):

$$u(z)/u(h) = \tanh\left[\beta + \gamma \cdot \exp\left(-LAI\left(1 - \frac{z}{h_i}\right)\right)\right] \tag{C.4}$$

where h_i is the height of the inflection point, and β and γ are empirical parameters. However, they are related to the physical features of the forests. The parameter β affects the bottom part of the canopy, which is necessary to describe the secondary maximum of the wind speed. The parameter γ is related to the upper part of the canopy and does not interfere with the profile near the ground. The parameters adopted for these parameters are $\beta = 0.1$ and $\gamma = 1.973$. Both parameters were based on the adjustments made by Santana et al. (2017), described in the following section. Some authors found that the inflection point and γ change over the course of the day (see Júnior et al. (2013); Souza et al. (2016)). The lowest values of h_i and γ are found between 11:00 and 13:00 LT and the highest values are in the morning (06:00 LT) and the evening (17:00 LT). However, for this study, both variables are considered constants.

C.2.1.4   Souza et al. (2016)

To provide a realistic model to describe the wind speed profile in the Amazon plant canopy, Souza et al. (2016) proposed an empirical-analytic method that includes the features of the rainforest (Eq. (C.5)). The main advantage of this model, according to Souza et al. (2016), is the estimate of a realist vertical wind profile for a limited amount of data. This formulation incorporates the vertical structure of the forest canopy and some aerodynamic characteristics of the coupling between the flows above and within the canopy (Souza et al., 2016).

$$\bar{u}(z)/\bar{u}(h) = \left\{ \left[\frac{-1 + \exp(\mu z)}{\exp(\omega z)}\right] \alpha \tanh\left[\beta + \gamma \times \exp\left(-LAI\left(1 - \frac{z}{h_i}\right)\right)\right]\right\} \tag{C.5}$$

where μ, α, β, γ and ω are fit parameters. Santana et al. (2017) suggested that $\mu = 1.016$, $\alpha = 0.7275$, $\beta = 0.1583$, $\gamma = 1.973$ and $\omega = 1.0$ are good parameters for the wind flow in the Amazon rain forest.

C.2.1.5 Santana et al. (2017)

Santana et al. (2017) modified the model developed by Souza et al. (2016) to obtain a more simplified version and to fit the data for five study sites in the Amazon rainforest. This version of the model is reduced to two empirical parameters, for the following values: $\mu = 1.012$ and $\beta = 0.1$.

$$\bar{u}(z)/\bar{u}(h) = \left\{ \left[\frac{-1 + \exp(\mu z)}{\exp(z)} \right] \tanh \left[\beta + \exp \left(-LAI \left(1 - \frac{z}{h} \right) \right) \right] \right\} \tag{C.6}$$

C.3 Results and discussion

For this study is presented two case studies. The first one is a random day during the dry season. The dry season in the Amazon has less precipitating days, high atmospheric pressure and large incoming solar radiation; the wet season has more precipitating days and cloudiness periods, lower atmospheric pressure and higher water vapor content. Despite these differences, the models present a similar performance for both days used as study cases for the wind speed average over 24 hours, but in another hand, when we keep the same parameterization and analyze the hourly averaged wind flow for different periods over the day, there are significant differences in the performance of the models (Table C.1).

Table C.1: Root-mean square error of the presented models for wind flow within canopy for the study cases: wet season (30 October 2014) and dry season (25 July 2014).

	00:00	04:00	08:00	12:00	16:00	20:00	24–h
Wet Season							
Raupach (1988)	0.14	0.12	0.10	0.22	0.11	0.12	0.13
Massman (1997)	0.08	0.12	0.16	0.31	0.19	0.15	0.05
Raupach et al. (1996) and Yi (2008)	0.17	0.14	0.08	0.20	0.09	0.12	0.15
Souza et al. (2016)	0.18	0.15	0.09	0.20	0.10	0.12	0.17
Santana et al. (2017)	0.18	0.16	0.11	0.23	0.13	0.13	0.16
Dry Season							
Raupach (1988)	0.13	0.13	0.15	0.11	0.10	0.11	0.12
Massman (1997)	0.13	0.14	0.24	0.17	0.16	0.10	0.08
Raupach et al. (1996) and Yi (2008)	0.14	0.14	0.12	0.10	0.09	0.15	0.14
Souza et al. (2016)	0.15	0.15	0.11	0.11	0.10	0.15	0.15
Santana et al. (2017)	0.16	0.16	0.15	0.13	0.12	0.13	0.14

The case study representing the wet season corresponds to 30 October 2014 (Figure C.1(a)). This day is described by Fuentes et al. (2016), where the emphasis was to describe the characteristics of the mixing ratio of trace gases and how it is related to the turbulence characteristics, based on the measurements obtained in the same campaign for the data used here. The case study representing a day in the dry season

is 25 July 2014 (Figure C.1(b)), which was randomly selected.

C.3.1 Wind flow models compared to 24-hours average

For the 24-hours average, the exponential model by Raupach (1988) represented fairly well the wind speed in the region of the trunks and near the upper part of the canopy. However, the region with the highest leaf area density is not described. The main reason is that the model follows an exponential profile, which does not allow to reproduce the characteristics-shape. A secondary reason is that the parameter λ was estimated based on the reported data from Raupach (1988), and the fit adopted to represent the rainforest canopy may not be adequate. The model represented the dry season better (RMSE $=0.12$) than the wet season (RMSE $= 0.13$).

The model developed by Massman (1997) is the model that best describes the wind profiles within the plant canopy. This model fits better to the upper part of the canopy, including the region with the highest leaf area density ($h/z > 0.5$), because it includes coefficients that take into account the drag coefficient. In other words, it accounts for the resistance of the leaves against the wind flow, allowing the model to reproduce the lower wind velocities according to the leaf area index. However, it does not capture the second maximum of the wind speed in the region $z/h < 0.5$. It is due to the inability of the model to reproduce the s-shape because this model is also based on the exponential profile. Differently, of the previous model, it described better the wet season (RMSE$= 0.05$) than the dry season (RMSE$= 0.08$).

With the contributions made by Raupach et al. (1996) and Yi (2008), the inclusion of the hyperbolic function allows to capture the signature of the s-shape of the wind profile, but mainly above the canopy (not shown). For the chosen parameters it showed a performance worse than the two previous models, with RMSE $=0.15$ for the wet season and RMSE$=0.14$ for the dry season. A better adjustment of the parameters can improve the model response.

The models described by Souza et al. (2016) and Santana et al. (2017) showed similar performance to the Raupach et al. (1996) and Yi (2008) (Table C.1). The explanation for this behavior is that the parameters are not appropriate for the cases study provided. Looking to the results reported by Souza et al. (2016) and Santana et al. (2017) it is seen that within the canopy the models are not describing the second maximum of the wind velocity, which is an important feature of the wind flow within tall canopies.
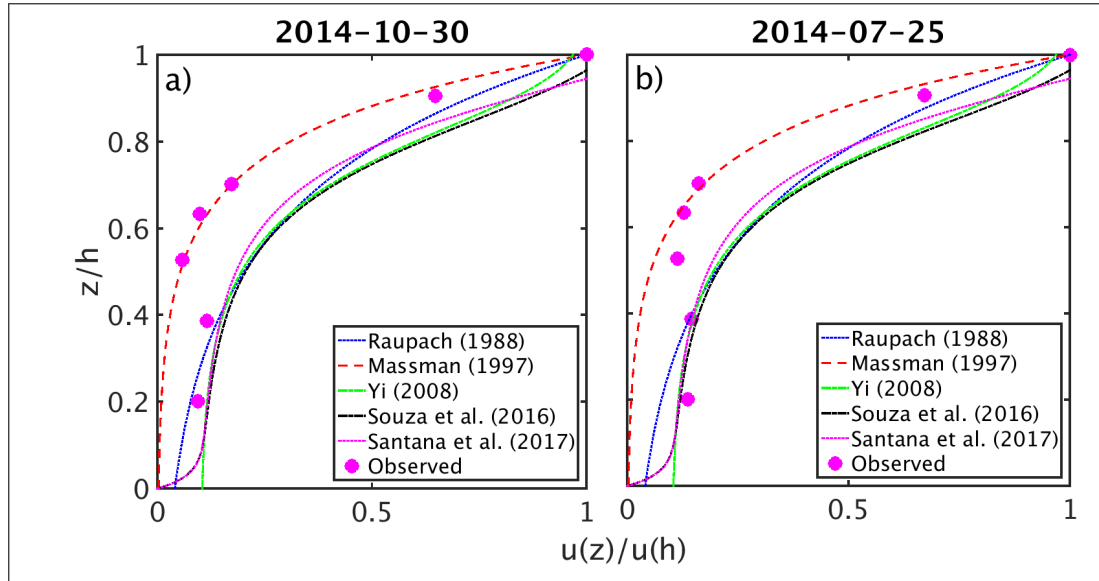
Figure C.1: The observed mean vertical wind profile (24–hour average) compared to exponential and hyperbolic models for (a) wet season (30 October 2014) and (b) dry season (25 July 2014).

C.3.2 Wind flow models compared to distinct periods of the day

Here, we will compare the same models and parameterizations described in the methodology against the 1–hour average wind flow profiles for six periods of the day: 00:00 LT, 04:00 LT, 08:00 LT, 12:00 LT, 16:00 LT, and 20:00 LT. The Table C.1 summarize the root-mean-square error for all the cases presented in this paper.

For the wet season (Figure C.2), (Massman, 1997) best describes the wind flow at 00:00 LT and 04:00 LT. The following hours are fairly well describe by both Raupach et al. (1996) and Yi (2008), and Souza et al. (2016). At 12:00 LT, is identified the worst performance of the models (RMSE > 0.20).

For the dry season (Figure C.3), Raupach (1988) and Massman (1997) reproduced better the wind flow within the canopy for 00:00 LT, 04:00 LT, and 20:00 LT. At 08:00 LT, the best profile was from Souza et al. (2016). And at 12:00 and 16:00 LT, Raupach et al. (1996) and Yi (2008) were more suitable to the data.
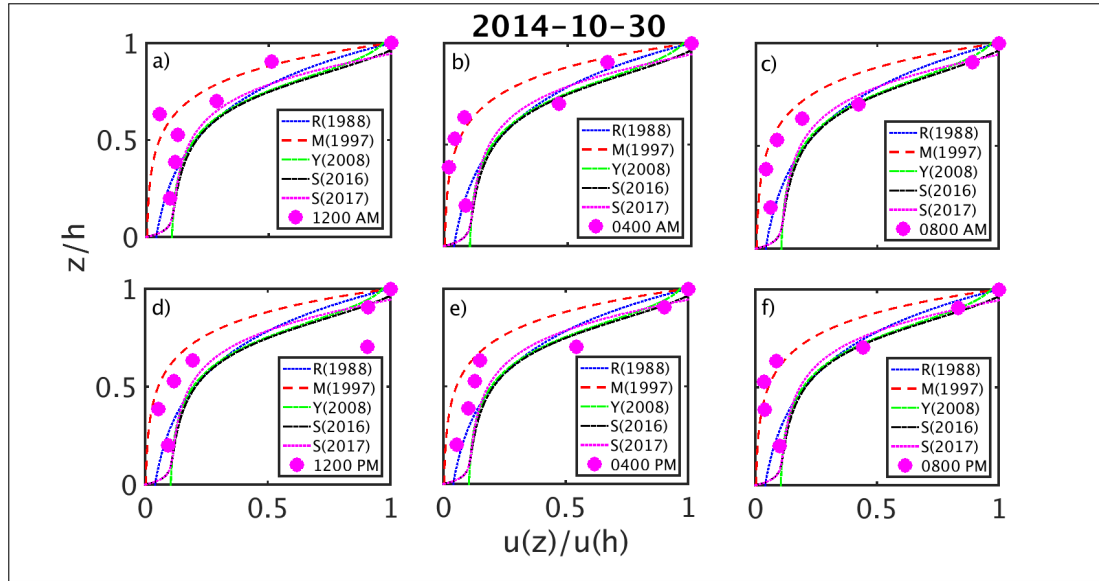
Figure C.2: The observed vertical wind profile (1-hour average), for 30 October 2014, compared with exponential and hyperbolic models for different periods of the day: (a)00:00 LT, (b) 04:00 LT, (c) 08:00 LT, (d) 12:00 LT, (e) 16:00 LT, (f) 20:00 LT
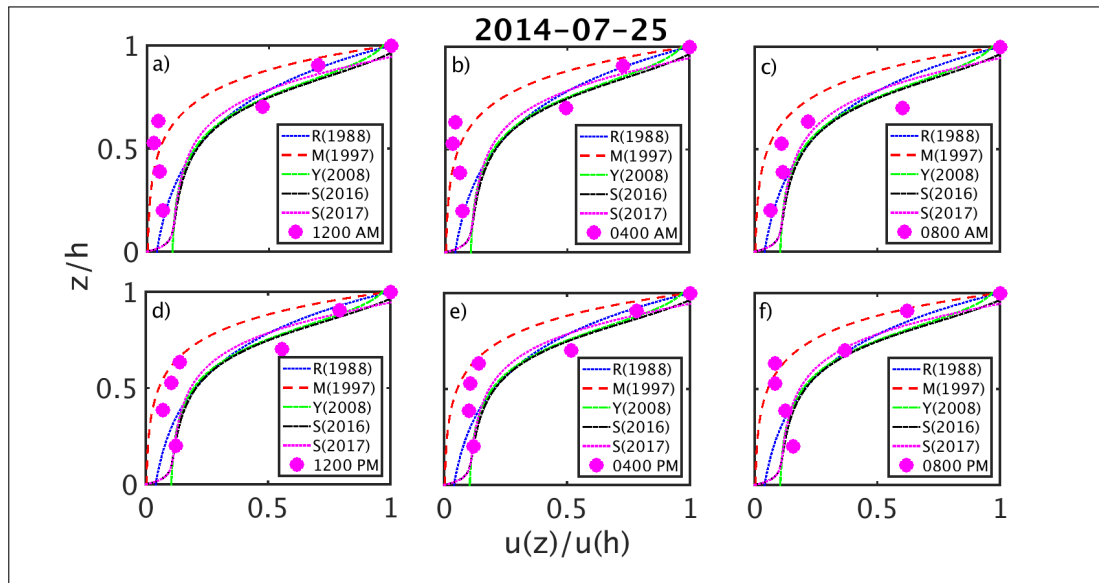
Figure C.3: The observed vertical wind profile (1-hour average), for 07 July 2014, compared with exponential and hyperbolic models for different periods of the day: (a)00:00 LT, (b) 04:00 LT, (c) 08:00 LT, (d) 12:00 LT, (e) 16:00 LT, (f) 20:00 LT.

On overall, for the described parameterization, there is no preferable model to represent the wind flow for different periods of the day. The model by Raupach (1988) and Massman (1997) showed better performance when the wind speed was lower compared to the other periods of the day. Santana et al.

(2017) did not represent well any of the wind flow profiles.

C.4 Conclusions

Obtain a reliable wind flow profile within the forest canopy is necessary to estimate better the transport of momentum. There are several applications for this study, including better parameterization of the turbulent diffusion coefficient.

There was no significant difference between the wind profile for the wet and dry season, for the cases study. The largest variation of $u(z)/u(h)$ was 6% of difference for the value observed near 20 meters.

Despite the fact that the exponential models do not reproduce the s-shape characteristic of the wind velocity observed within the rainforest canopy, they had a better performance than the hyperbolic models. The model from Massman (1997) was the best model, providing the most reliable estimate for the wind flow in the region where the leaf area density is large. However, new parameterizations have to be performed to make a better judgment related to the hyperbolic models.

Any of these models can fairly represent the wind speed profile within the rainforest canopy, for 24-hours average, for the same parameters and coefficients described in this study. A better performance of some models is related to more reliable inputs, e.g. leaf area index and drag coefficient. An ideal approach could be using the models for specific layers of the canopy. Applying a model for the lower part of the canopy and a secondary model for the upper part could be a better solution when one wants to reproduce the features related to the second maximum of the wind profile.

The results for the hourly average have to be improved changing the parameters for the models. We showed that is necessary to b careful when adopting wind speed profile models. The diurnal variation of the profiles within the canopy can lead to significant errors in the estimate if we adopt the same parameterization for the 24–hour average wind profiles. Júnior et al. (2013) and Souza et al. (2016) shows how the parameter γ and the inflection point changes over the day for a forest. Then, new simulations have to be performed to evaluate the diurnal variations of the wind speed flow.

Bibliography

Ahmed, F., and J. D. Neelin, 2018: Reverse engineering the tropical precipitation–buoyancy relationship. *Journal of the Atmospheric Sciences*, **75 (5)**, 1587–1608.

Andreae, M., and Coauthors, 2002: Biogeochemical cycling of carbon, water, energy, trace gases, and aerosols in amazonia: The lba-eustach experiments. *Journal of Geophysical Research: Atmospheres*, **107 (D20)**, LBA–33.

Andreae, M. O., and P. J. Crutzen, 1997: Atmospheric aerosols: Biogeochemical sources and role in atmospheric chemistry. *Science*, **276 (5315)**, 1052–1058.

Arias, P. A., R. Fu, C. D. Hoyos, W. Li, and L. Zhou, 2011: Changes in cloudiness over the amazon rainforests during the last two decades: diagnostic and potential causes. *Climate Dynamics*, **37 (5-6)**, 1151–1164.

Arya, S. P., and Coauthors, 1999: *Air pollution meteorology and dispersion*, Vol. 310. Oxford University Press New York.

Bauch, S. C., A. M. Birkenbach, S. K. Pattanayak, and E. O. Sills, 2015: Public health impacts of ecosystem change in the brazilian amazon. *Proceedings of the National Academy of Sciences*, 201406495.

Betts, A., G. Fisch, C. Von Randow, M. Silva Dias, J. Cohen, R. Da Silva, and D. Fitzjarrald, 2009a: The amazonian boundary layer and mesoscale circulations. *Amazonia and Global Change. Washington, DC: AGU*.

Betts, A. K., 1992: Fife atmospheric boundary layer budget methods. *J. Geophys. Res.*, **97 (D17)**, 18 523–18 531.

Betts, A. K., G. Fisch, C. V. Randow, M. A. F. S. Dias, J. C. P. Cohen, R. D. Silva, and D. R. Fitzjarrald, 2009b: The amazonian boundary layer and mesoscale circulations. *Amazonia and Global Change*, 163–181.

Betts, A. K., J. D. Fuentes, M. Garstang, and J. H. Ball, 2002a: Surface diurnal cycle and boundary layer structure over rondônia during the rainy season. *Journal of Geophysical Research: Atmospheres*, **107 (D20)**, LBA–32.

Betts, A. K., J. D. Fuentes, M. Garstang, and J. H. Ball, 2002b: Surface diurnal cycle and boundary layer structure over rondônia during the rainy season. *J. Geophys. Res.*, **107 (D20)**.

Betts, A. K., L. V. Gatti, A. M. Cordova, M. A. S. Dias, and J. D. Fuentes, 2002c: Transport of ozone to the surface by convective downdrafts at night. *Journal of Geophysical Research: Atmospheres*, **107 (D20)**, LBA–13.

Betts, A. K., and C. Jakob, 2002: Evaluation of the diurnal cycle of precipitation, surface thermodynamics, and surface fluxes in the ecmwf model using lba data. *Journal of Geophysical Research: Atmospheres*, **107 (D20)**, LBA–12.

Betts, A. K., and P. Viterbo, 2005: Land-surface, boundary layer, and cloud-field coupling over the southwestern amazon in era-40. *Journal of Geophysical Research: Atmospheres*, **110 (D14)**.

Boucher, D., 2014: How brazil has dramatically reduced tropical deforestation. *Solutions Journal*, **5 (2)**, 66–75.

Cecchini, M. A., and Coauthors, 2017: Sensitivities of amazonian clouds to aerosols and updraft speed. *Atmospheric Chemistry and Physics*, **17 (16)**, 10 037–10 050.

Collow, A. B. M., M. A. Miller, and L. C. Trabachino, 2016: Cloudiness over the amazon rainforest: Meteorology and thermodynamics. *Journal of Geophysical Research: Atmospheres*, **121 (13)**, 7990–8005.

Culf, A., G. Fisch, Y. Malhi, and C. Nobre, 1997: The influence of the atmospheric boundary layer on carbon dioxide concentrations over a tropical forest. *Agricultural and forest meteorology*, **85 (3-4)**, 149–158.

da Costa Galvão, J. A., and G. Fisch, 2000: Análise do balanço de energia em áreas de floresta e de pastagem na amazônia. *Rev. Brasileira de Meteorol.*, **15**, 25–38.

de Arellano, J. V. G., C. C. van Heerwaarden, B. J. H. van Stratum, and K. van den Dries, 2015: *Atmospheric boundary layer: Integrating air chemistry and land interactions*. Cambridge University Press, 265 pp.

Dias, M. S., and Coauthors, 2002: Cloud and rain processes in a biosphere-atmosphere interaction context in the amazon region. *Journal of Geophysical Research: Atmospheres*, **107 (D20)**, LBA–39.

Dias-Junior, C. Q., N. L. Dias, J. D. Fuentes, and M. Chamecki, 2017: Convective storms and non-classical low-level jets during high ozone level episodes in the amazon region: An arm/goamazon case study. *Atmospheric environment*, **155**, 199–209.

Fan, J., and Coauthors, 2018: Substantial convection and precipitation enhancements by ultrafine aerosol particles. *Science*, **359 (6374)**, 411–418.

Finnigan, J., I. Harman, A. Ross, and S. Belcher, 2015: First-order turbulence closure for modelling complex canopy flows. *Quart. J. Roy. Meteor. Soc.*, **141 (692)**, 2907–2916.

Fisch, G., J. Tota, L. Machado, M. S. Dias, R. d. F. Lyra, C. Nobre, A. Dolman, and J. Gash, 2004: The convective boundary layer over pasture and forest in amazonia. *Theoretical and Applied Climatology*, **78 (1-3)**, 47–59.

Fisher, W. H., 2000: *Rain forest exchanges*. Smithsonian Inst Press, 80–96 pp.

Fitzjarrald, D. R., and M. Garstang, 1981: Vertical structure of the tropical boundary layer. *Mon. Wea. Rev.*, **109 (7)**, 1512–1526.

Fitzjarrald, D. R., K. E. Moore, O. M. Cabral, J. Scolar, A. O. Manzi, and L. D. de Abreu Sá, 1990: Daytime turbulent exchange between the amazon forest and the atmosphere. *Journal of Geophysical Research: Atmospheres*, **95 (D10)**, 16 825–16 838.

Fraund, M., and Coauthors, 2017: Elemental mixing state of aerosol particles collected in central amazonia during goamazon2014/15. *Atmosphere*, **8 (9)**, 173.

Freire, L., and Coauthors, 2017: Turbulent mixing and removal of ozone within an amazon rainforest canopy. *Journal of Geophysical Research: Atmospheres*, **122 (5)**, 2791–2811.

Fu, R., B. Zhu, and R. E. Dickinson, 1999: How do atmosphere and land surface influence seasonal changes of convection in the tropical amazon? *Journal of Climate*, **12 (5)**, 1306–1321.

Fuentes, J. D., and Coauthors, 2016: Linking meteorology, turbulence, and air chemistry in the amazon rain forest. *Bulletin of the American Meteorological Society*, **97 (12)**, 2329–2342.

Garstang, M., 1987: Atmospheric surface and boundary layers of the amazon basin (final report).

Garstang, M., and D. R. Fitzjarrald, 1999: *Observations of surface to atmosphere interactions in the tropics*. Oxford University Press, USA.

Garstang, M., and Coauthors, 1990: The amazon boundary-layer experiment (able 2b): A meteorological perspective. *Bulletin of the American Meteorological Society*, **71 (1)**, 19–32.

Gash, J., and C. Nobre, 1997: Climatic effects of amazonian deforestation: Some results from abracos. *Bulletin of the American Meteorological Society*, **78 (5)**, 823–830.

Gerken, T., and Coauthors, 2016: Downward transport of ozone rich air and implications for atmospheric chemistry in the amazon rainforest. *Atmospheric Environment*, **124**, 64–76.

Giangrande, S. E., and Coauthors, 2017: Cloud characteristics, thermodynamic controls and radiative impacts during the observations and modeling of the green ocean amazon (goamazon2014/5) experiment. *Atmospheric Chemistry and Physics*, **17 (23)**, 14 519–14 541.

Gloor, M., and Coauthors, 2015: Recent amazon climate as background for possible ongoing and future changes of amazon humid forests. *Global Biogeochemical Cycles*, **29 (9)**, 1384–1399.

Goulding, M., R. Barthem, E. J. G. Ferreira, and R. Duenas, 2003: *The Smithsonian atlas of the Amazon*. Smithsonian Books Washington.

Greco, S., and Coauthors, 1990: Rainfall and surface kinematic conditions over central amazonia during able 2b. *J. Geophys. Res.: Atmospheres*, **95 (D10)**, 17 001–17 014.

Gu, D., and Coauthors, 2017: Airborne observations reveal elevational gradient in tropical forest isoprene emissions. *Nature communications*, **8**, 15 541.

Harriss, R., and Coauthors, 1990: The amazon boundary layer experiment: wet season 1987. *Journal of Geophysical Research: Atmospheres*, **95 (D10)**, 16 721–16 736.

Houze Jr, R. A., 2004: Mesoscale convective systems. *Reviews of Geophysics*, **42 (4)**.

IBGE, C., 2010: Retrieved from: ¡ http://www. censo2010. ibge. gov. br/¿. **23**.

Inoue, E., 1963: On the turbulent structure of airflow within. *Journal of the Meteorological Society of Japan. Ser. II*, **41 (6)**, 317–326.

Jiménez-Muñoz, J. C., C. Mattar, J. Barichivich, A. Santamaría-Artigas, K. Takahashi, Y. Malhi, J. A. Sobrino, and G. Van Der Schrier, 2016: Record-breaking warming and extreme drought in the amazon rainforest during the course of el niño 2015–2016. *Scientific reports*, **6**, 33 130.

Júnior, C. Q. D., L. D. Sa, V. B. Pachêco, and C. M. de Souza, 2013: Coherent structures detected in the unstable atmospheric surface layer above the amazon forest. *J. Wind Eng. Ind. Aerodyn.*, **115**, 1–8.

Katul, G. G., L. Mahrt, D. Poggi, and C. Sanz, 2004: One-and two-equation models for canopy turbulence. *Boundary-Layer Meteorol.*, **113 (1)**, 81–109.

Kuo, Y.-H., K. A. Schiro, and J. D. Neelin, 2018: Convective transition statistics over tropical oceans for climate model diagnostics: Observational baseline. *Journal of the Atmospheric Sciences*, **75 (5)**, 1553–1570.

Landsberg, J. J., and G. B. James, 1971: Wind profiles in plant canopies: studies on an analytical model. *Journal of Applied Ecology*, **8 (3)**, 729–741.

Liu, Y., and Coauthors, 2018: Isoprene photo-oxidation products quantify the effect of pollution on hydroxyl radicals over amazonia. *Science advances*, **4 (4)**, 2547.

Machado, L. A., and Coauthors, 2018: Overview: Precipitation characteristics and sensitivities to environmental conditions during goamazon2014/5 and acridicon-chuva. *Atmospheric Chemistry and Physics*, **18 (9)**, 6461–6482.

Marengo, J. A., G. Fisch, C. Morales, I. Vendrame, and P. C. Dias, 2004: Diurnal variability of rainfall in southwest amazonia during the lba-trmm field campaign of the austral summer of 1999. *Acta amazonica*, **34 (4)**, 593–603.

Marengo, J. A., G. F. Fisch, L. M. Alves, N. V. Sousa, R. Fu, and Y. Zhuang, 2017: Meteorological context of the onset and end of the rainy season in central amazonia during the goamazon2014/5. *Atmospheric Chemistry and Physics*, **17 (12)**, 7671.

Martin, C. L., D. Fitzjarrald, M. Garstang, A. P. Oliveira, S. Greco, and E. Browell, 1988: Structure and growth of the mixing layer over the amazonian rain forest. *Journal of Geophysical Research: Atmospheres*, **93 (D2)**, 1361–1375.

Martin, S., and Coauthors, 2017: The green ocean amazon experiment (goamazon2014/5) observes pollution affecting gases, aerosols, clouds, and rainfall over the rain forest. *Bulletin of the American Meteorological Society*, **98 (5)**, 981–997.

Martin, S. T., and Coauthors, 2010: Sources and properties of amazonian aerosol particles. *Reviews of Geophysics*, **48 (2)**.

Massman, W., and J. Weil, 1999: An analytical one-dimensional second-order closure model of turbulence statistics and the lagrangian time scale within and above plant canopies of arbitrary structure. *Boundary-Layer Meteor.*, **91 (1)**, 81–107.

Massman, W. J., 1997: An analytical one-dimensional model of momentum transfer by vegetation of arbitrary structure. *Boundary-Layer Meteor.*, **83 (3)**, 407–421.

Mather, J. H., and J. W. Voyles, 2013: The arm climate research facility: A review of structure and capabilities. *Bull. Am. Meteorol. Soc.*, **94 (3)**, 377–392.

McNaughton, K. G., and T. W. Spriggs, 1986: A mixed-layer model for regional evaporation. *Boundary-Layer Meteorology*, **34 (3)**, 243–262.

Nobre, C., D. Wickland, and P. Kabat, 1996a: The large scale biosphere-atmosphere experiment in amazonia (lba). *Concise Experimental Plan. INPE, C. Paulista, SP, Brazil*.

Nobre, C. A., H. R. d. R. G. Fisch, R. F. da F. Lyra, E. P. da Rocha, A. C. L. da Costa, and V. N. Ubarana, 1996b: 24 observations of the atmospheric boundary layer in rondonia. *Amazonian Deforestation and Climate*, J. H. C. Gash, C. A. Nobre, J. M. Roberts, and R. L. Victoria, Eds., John Wiley, 413–424.

Nobre, C. A., P. J. Sellers, and J. Shukla, 1991: Amazonian deforestation and regional climate change. *Journal of climate*, **4 (10)**, 957–988.

Pöhlker, C., and Coauthors, 2012: Biogenic potassium salt particles as seeds for secondary organic aerosol in the amazon. *Science*, **337 (6098)**, 1075–1078.

Pöhlker, M. L., and Coauthors, 2016: Long-term observations of cloud condensation nuclei in the amazon rain forest–part 1: Aerosol size distribution, hygroscopicity, and new model parametrizations for ccn prediction. *Atmospheric Chemistry and Physics*, **16 (24)**, 15 709–15 740.

Poveda, G., L. Jaramillo, and L. F. Vallejo, 2014: Seasonal precipitation patterns along pathways of south american low-level jets and aerial rivers. *Water Resources Research*, **50 (1)**, 98–118.

Randow, C. V., and Coauthors, 2004: Comparative measurements and seasonal variations in energy and carbon exchange over forest and pasture in south west amazonia. *Theor. Appl. Climatol.*, **78 (1)**, 5–26.

Raupach, M. R., 1988: Canopy transport processes. *Flow and transport in the natural environment: advances and applications*, Springer, 95–127.

Raupach, M. R., 1994: Simplified expressions for vegetation roughness length and zero-plane displacement as functions of canopy height and area index. *Boundary-Layer Meteor.*, **71 (1)**, 211–216.

Raupach, M. R., J. J. Finnigan, and Y. Brunet, 1996: Coherent eddies and turbulence in vegetation canopies: the mixing-layer analogy. *Boundary-Layer Meteorology 25th Anniversary Volume, 1970–1995*, 351–382.

Raupach, M. R., and A. S. Thom, 1981: Turbulence in and above plant canopies. *Annual Review of Fluid Mechanics*, **13 (1)**, 97–129.

Rayner, K. N., and I. D. Watson, 1991: Operational prediction of daytime mixed layer heights for dispersion modelling. *Atmospheric Environment. Part A. General Topics*, **25 (8)**, 1427–1436.

Reddington, C., E. Butt, D. Ridley, P. Artaxo, W. Morgan, H. Coe, and D. Spracklen, 2015: Air quality and human health improvements from reductions in deforestation-related fire in brazil. *Nature Geoscience*, **8 (10)**, 768.

Rehbein, A., T. Ambrizzi, and C. R. Mechoso, 2018: Mesoscale convective systems over the amazon basin. part i: climatological aspects. *International Journal of Climatology*, **38 (1)**, 215–229.

Roberts, G. C., M. O. Andreae, J. Zhou, and P. Artaxo, 2001: Cloud condensation nuclei in the amazon basin:marine conditions over a continent? *Geophysical research letters*, **28 (14)**, 2807–2810.

Sá, S. S. d., and Coauthors, 2017: Influence of urban pollution on the production of organic particulate matter from isoprene epoxydiols in central amazonia. *Atmospheric Chemistry and Physics*, **17 (11)**, 6611–6629.

Salati, E., and J. Marques, 1984: Climatology of the amazon region. *The Amazon*, Springer, 85–126.

Santana, R. A. S., C. Q. Dias-Júnior, R. S. Vale, J. Tóta, and D. R. Fitzjarrald, 2017: Observing and modeling the vertical wind profile at multiple sites in and above the amazon rain forest canopy. *Adv. in Meteor.*, **2017**, 1–8.

Schiro, K. A., F. Ahmed, S. E. Giangrande, and J. D. Neelin, 2018: Goamazon2014/5 campaign points to deep-inflow approach to deep convection across scales. *Proceedings of the National Academy of Sciences*, **115 (18)**, 4577–4582.

Schiro, K. A., and J. D. Neelin, 2018: Tropical continental downdraft characteristics: mesoscale systems versus unorganized convection. *Atmos Chem Phys*, **18**, 1997–2010.

Shaw, R. H., 1977: Secondary wind speed maxima inside plant canopies. *J. Appl. Meteor.*, **16 (5)**, 514–521.

Sivaraman, C., S. McFarlane, E. Chapman, M. Jensen, T. Toto, S. Liu, and M. Fischer, 2013: Planetary boundary layer (pbl) height value added product (vap): Radiosonde retrievals. *Department of Energy Office of Science Atmospheric Radiation Measurement (ARM) Program (United States)*.

Song, F., and G. J. Zhang, 2017: Improving trigger functions for convective parameterization schemes using goamazon observations. *Journal of Climate*, **30 (21)**, 8711–8726.

Souza, C. M., C. Q. Dias-Júnior, J. Tóta, and L. D. de A. Sá, 2016: An empirical-analytical model of the vertical wind speed profile above and within an amazon forest site. *Meteor. Applic.*, **23 (1)**, 158–164.

Strong, C., J. Fuentes, M. Garstang, and A. Betts, 2005: Daytime cycle of low-level clouds and the tropical convective boundary layer in southwestern amazonia. *Journal of Applied Meteorology*, **44 (10)**, 1607–1619.

Stull, R. B., 1988: *An introduction to boundary layer meteorology*. Springer Science & Business Media.

Suframa, 2003: Superintendência, da zona franca de manaus. *Proposta para o Programa de Desenvolvimento Sustentável para a Área de Atuação da SUFRAMA. Manaus*.

Tanaka, L. d. S., P. Satyamurty, and L. Machado, 2014: Diurnal variation of precipitation in central amazon basin. *International Journal of Climatology*, **34 (13)**, 3574–3584.

Tennekes, H., and A. Driedonks, 1981: Basic entrainment equations for the atmospheric boundary layer. *Boundary-Layer Meteorology*, **20 (4)**, 515–531.

Thalman, R., and Coauthors, 2017: Ccn activity and organic hygroscopicity of aerosols downwind of an urban region in central amazonia: seasonal and diel variations and impact of anthropogenic emissions. *Atmospheric Chemistry and Physics*, **17 (19)**, 11 779–11 801.

Trapp, R. J., 2013: *Mesoscale-convective Processes in the Atmosphere*. Cambridge University Press.

Wallace, S., C. Fagan, and C. H. James, 2018: Last tribes of amazon – threatened by the outside world. *National Geographic*, National Geographic, 42–71.

Wang, J., and Coauthors, 2009: Impact of deforestation in the amazon basin on cloud climatology. *Proceedings of the National Academy of Sciences*, pnas–0810156 106.

Wendisch, M., and Coauthors, 2016: Acridicon–chuva campaign: Studying tropical deep convective clouds and precipitation over amazonia using the new german research aircraft halo. *Bulletin of the American Meteorological Society*, **97 (10)**, 1885–1908.

Wright, J. S., R. Fu, J. R. Worden, S. Chakraborty, N. E. Clinton, C. Risi, Y. Sun, and L. Yin, 2017: Rainforest-initiated wet season onset over the southern amazon. *Proceedings of the National Academy of Sciences*, **114 (32)**, 8481–8486.

Yi, C., 2008: Momentum transfer within canopies. *J. Appl. Meteor. and Climat.*, **47 (1)**, 262–275.

Yi, C., R. K. Monson, Z. Zhai, D. E. Anderson, B. Lamb, G. Allwine, A. A. Turnipseed, and S. P. Burns, 2005: Modeling and measuring the nocturnal drainage flow in a high-elevation, subalpine forest with complex terrain. *J. of Geophys. Res.: Atmospheres*, **110 (D22)**.

Zhuang, Y., R. Fu, and H. Wang, 2018: How do environmental conditions influence vertical buoyancy structure and shallow-to-deep convection transition across different climate regimes? *Journal of the Atmospheric Sciences*, **75 (6)**, 1909–1932.

Zimmerman, P., J. Greenberg, and C. Westberg, 1988: Measurements of atmospheric hydrocarbons and biogenic emission fluxes in the amazon boundary layer. *Journal of Geophysical Research: Atmospheres*, **93 (D2)**, 1407–1416.